ORNL/TM-10841
ENDF-347

ornl

OAK RIDGE NATIONAL LABORATORY

MARTIN MARIETTA

^{58}Ni + *n* Transmission, Differential Elastic Scattering and Capture Measurements and Analysis from 5 to 813 KeV

C. M. Perey
F. G. Perey
J. A. Harvey
N. W. Hill
N. M. Larson
R. L. Macklin

OPERATED BY
MARTIN MARIETTA ENERGY SYSTEMS, INC.
FOR THE UNITED STATES
DEPARTMENT OF ENERGY

Printed in the United States of America. Available from
National Technical Information Service
U.S. Department of Commerce
5285 Port Royal Road, Springfield, Virginia 22161
NTIS price codes—Printed Copy: A06; Microfiche A01

ORNL/TM-10841
ENDF-347

Engineering Physics and Mathematics Division

^{58}Ni + n TRANSMISSION, DIFFERENTIAL ELASTIC SCATTERING AND CAPTURE MEASUREMENTS AND ANALYSIS FROM 5 TO 813 KeV

C. M. Perey, F. G. Perey, J. A. Harvey,
N. W. Hill,* N. M. Larson,** and R. L. Macklin

*Instrumentation and Controls Division
**Computing and Telecommunications Division

DATE PUBLISHED — September 1988

Prepared for the
Office of Energy Research
Nuclear Physics

Prepared by the
OAK RIDGE NATIONAL LABORATORY
Oak Ridge, Tennessee 37831
operated by
MARTIN MARIETTA ENERGY SYSTEMS, INC.
for the
U.S. DEPARTMENT OF ENERGY
under contract DE-AC05-84OR21400

CONTENTS

ACKNOWLEDGMENTS

The authors thank P. G. Young of Los Alamos National Laboratory for performing the average capture cross-section calculations and R. R. Spencer for providing the code to calculate the correlation coefficient between the neutron and radiation resonance widths. They are pleased to acknowledge many useful discussions with and constructive suggestions from the reviewers of this report, D. C. Larson and R. R. Winters. They are grateful to S. R. Damewood for her invaluable technical know-how in the typing and presentation of this report. This research was sponsored by the Office of Energy Research, Nuclear Physics, U. S. Department of Energy, under Contract No. DE-AC05-84OR21400 with Martin Marietta Energy Systems, Inc.

ABSTRACT

High-resolution neutron measurements for ^{58}Ni-enriched targets were made at the Oak Ridge Electron Linear Accelerator (ORELA) from 100 eV to ≈20 MeV in transmission, from 10 keV to 5 MeV in differential elastic scattering, and from 2.5 keV to 5 MeV in capture. The transmission data were analyzed from 10 to 813 keV with the multilevel R-matrix code SAMMY which uses Bayes' theorem for the fitting process. This code provides energies and neutron widths of the resonances inside the 10- to 813-keV region as well as a possible parameterization for resonances external to that region to describe the smooth cross section from 10 to 813 keV. The differential elastic data at different scattering angles were compared to theoretical calculations from 30 to 813 keV using an R-matrix code based on the Blatt-Biedenharn formalism. Various combinations of spin and parity were tried to predict cross sections for the well defined $\ell > 0$ resonances, and comparison with the data then provided spin and parity assignments for most of these resonances. The capture data were analyzed from 5 to 450 keV with a least-squares fitting code using the Breit-Wigner formula. In this energy region 30% more resonances were observed in the capture data than in the transmission data.

From 5 to 813 keV, 477 resonances are reported. The reduced widths of the 62 s-wave resonances follow the Porter-Thomas distribution and their nearest neighbor spacings agree with the Wigner distribution. The average s-wave level spacing is equal to 13.6 ± 0.5 keV and the s-wave strength function to $(3.1 \pm 0.6) \times 10^{-4}$. The staircase plot of the s-wave reduced level widths and the plot of the Lorentz-weighted strength function show only a slight possibility of doorway states. The level densities calculated with the Fermi-gas model for $\ell = 0$ and $\ell > 0$ resonances are compared with the cumulative number of observed resonances. The average radiation widths were deduced from resonances analyzed in the three data sets below 450 keV. The mean values of the distributions of the radiation widths are equal to 2.3 eV for the s-wave resonances, 0.77 eV for the p-wave resonances, and 1.3 eV for the d-wave resonances and the standard deviations are 1.7 eV, 0.33 eV, and 0.5 eV respectively. The correlation coefficient between the s-wave reduced neutron widths and radiation widths is equal to 0.66 ± 0.11. The average capture cross section as a function of the neutron incident energy is compared to prediction based on the tail of the giant electric dipole resonance.

1. INTRODUCTION

The cross sections of structural materials in the iron region are important in reactor applications because of the stainless steels that are used. The ENDF/B-V evaluation (DIV79) of the nickel resonance parameters is based on measurements taken prior to 1971 and is identical to ENDB/B-IV and ENDF/B-III versions.

High-resolution neutron measurements were performed at ORELA in the resonance region. In previous publications (PER82, PER83) the resonance parameters obtained from the simultaneous analyses of the transmission and capture data for ^{60}Ni were reported. In the present work, in addition to the transmission and capture, the differential elastic scattering was also measured for ^{58}Ni and the three types of data were analyzed simultaneously.

The parameters given in this publication supersede the preliminary results reported earlier (PER77, PER85). The analysis, up to 650 keV, of the transmission data taken at the 78-m flight path (PER85) had been done with a single channel radius of 6.5 f. The data above 180 keV were properly fitted only if an extra energy dependent background correction (in addition to the usual corrections) was applied to the data. Since such a background correction was not previously observed in ORELA transmission measurements we decided to repeat the measurements but with a 200-m flight path rather than with one of 78 m. These new data, which have much improved resolution (see Fig. 1), are in complete agreement with the earlier data. The difficulties encountered in the previous analysis (PER85), i.e., the need to introduce an arbitrary background correction, can be removed by using a different channel radius for the p-wave channel than for the s- and d-wave channels.

The experimental procedures used in each of the three measurements are described in Sect. 2 with discussions of the various background and deadtime corrections. In Sect. 3 the analysis methods are given in detail.

The results of the analysis are presented in Sect. 4 and compared with previous works in Sect. 5. The results and the behavior of the average resonance parameters are discussed in Sect. 6.

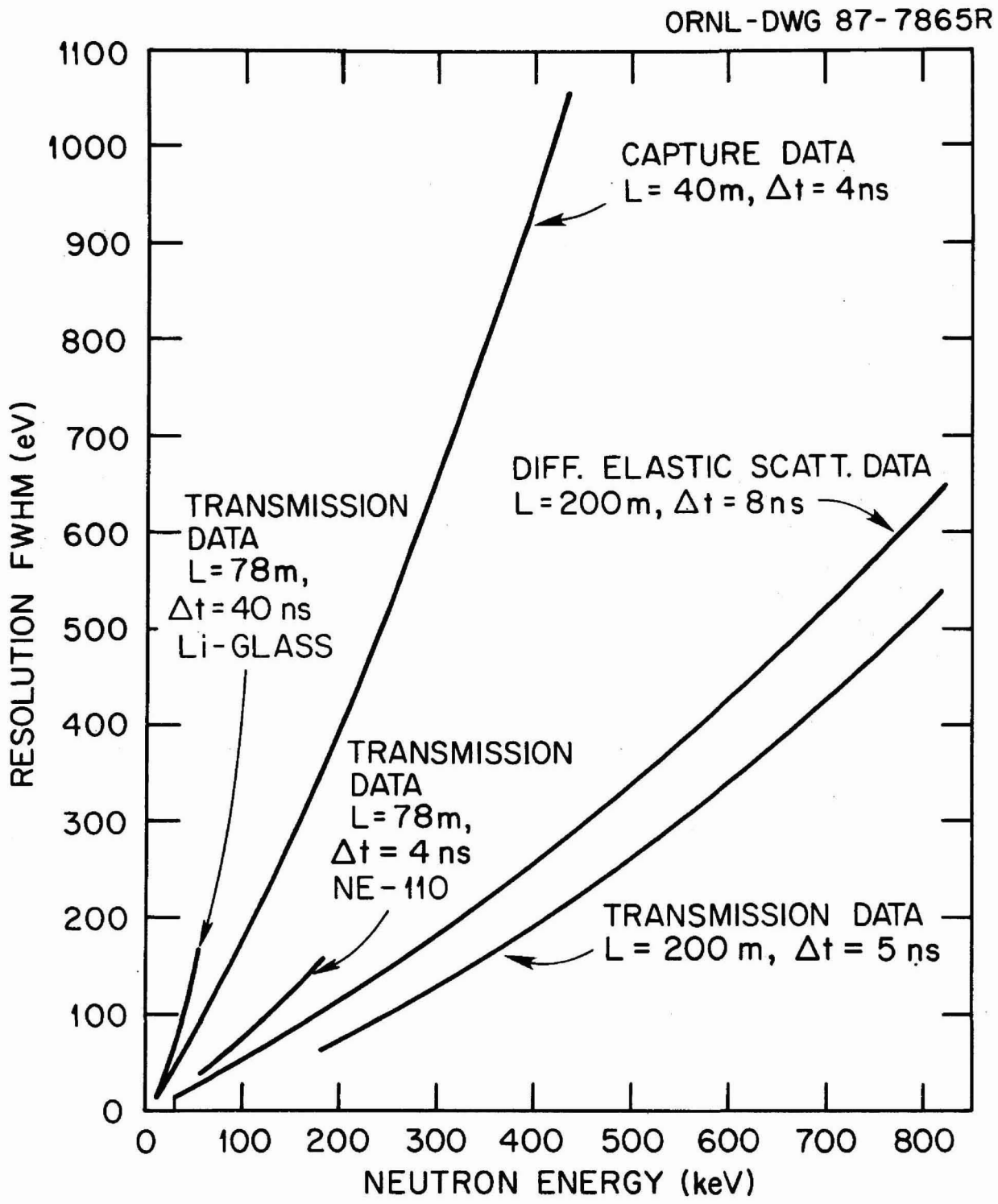

Fig. 1. The effective Gaussian resolution (FWHM) is shown as a function of the neutron incident energy for the five experimental configurations in the regions where the data were analyzed.

2. DATA ACQUISITION AND DATA PROCESSING

2.1 TRANSMISSION MEASUREMENTS

2.1.1 Data Acquisition

The transmission measurements were made by the time-of-flight technique using neutron pulses from the ORELA water-moderated tantalum target. Collimators were utilized to focus primarily on moderated or unmoderated neutrons from the target, depending on the measurement. Two measurements were made with a 78.217 ± 0.004 m flight path with two different neutron detectors using only water-moderated neutrons. The transmission measurement with a 201.578 ± 0.005 m flight path used mainly unmoderated neutrons produced in the tantalum target.

The measurements with moderated neutrons using a 78-m flight distance were made on two samples weighing 49.98 and 4.997 grams with thicknesses of 0.0764 and 0.00770 atoms/b of nickel enriched to 99.93% in ^{58}Ni.

For the energy region from 100 eV to 200 keV, transmission data were acquired using a 1.3-cm-thick, 11-cm-diameter, ^{6}Li glass scintillator mounted on a RCA 4522 photomultiplier tube. The electron beam burst was 40 ns wide, producing a beam power on the target of 50 kW at 800 Hz. At low energies, the energy resolution is determined by the moderator and by the detector thickness while at high energies the 40-ns burst width determines the resolution. The moderation length is less than 25 mm (COC83) for neutrons below 30 keV. Two filters were inserted in the beam at 5 m: a 1-g/cm^2 ^{10}B filter ($1/e$ transmission at approximately 1 keV) to eliminate low-energy neutrons due to preceding bursts, and a 0.6-cm-thick lead filter to reduce the gamma flash intensity. Transmission data from 4 to 1500 keV were obtained using a 2-cm-thick, 7.5-cm-diameter NE-110 proton recoil scintillator mounted on a RCA 4522 photomultiplier. The electron beam burst was 4 ns wide, producing a beam power of 8 kW at 1000 Hz. The energy resolution obtained with this NE-110 scintillator was determined by the moderation time at lower energies and the 4-ns burst width at higher energies. Two filters were again inserted in the neutron beam at 5 m; a 1-g/cm^2 ^{10}B filter and a 0.6-cm-thick ^{238}U filter. For these transmission measurements, the detectors were gated off during the gamma flash and the succeeding ≈ 5 μs to eliminate possible extraneous events due to phototube afterpulsing.

The 200-m transmission measurement was made with an "effective" sample enrichment of 99.99% ^{58}Ni achieved by the use of a 0.005-cm-thick foil of natural nickel in the open beam to compensate for the ^{60}Ni in the 52.40 grams of nickel enriched to 99.93% in ^{58}Ni; the sample thickness was 0.172 atoms/b. A 2.5-cm-thick, 5.2×8.9 cm NE-110 scintillator mounted between two RCA 8854 photomultipliers was used as the neutron detector. The neutron beam was collimated to pass only

through the scintillator. The electron beam burst was 5-ns wide producing a beam power of 6 kW at 800 Hz. The measurements covered the energy region from 100 keV to 20 MeV. The energy resolution in percent was determined mainly by the burst width and is given approximately by 0.07 $[E(MeV)]^{1/2}$. Two filters were inserted in the beam at 5 m: a 0.3-g/cm^2 ^{10}B filter to reduce overlap neutrons and 4.4 cm of uranium to reduce the intensity of gamma rays from the tantalum target.

Data were acquired using an EG&G time digitizer and stored in one of the ORELA Data Acquisition Computers (BET69).

2.1.2 Data Reduction

The data were first corrected for the deadtime (1104 ns) of the digitizer and then corrected for the backgrounds.

For the 78-m transmission data taken with the ^{6}Li glass detector the maximum deadtime corrections were 15% with the open beam, 10% with the thick (0.0764 atoms/b) sample in and 14% with the thin (0.00770 atoms/b) sample in. With the NE-110 detector these corrections were 23% with the open beam, 18% with the thick sample in and 22% with the thin sample in. For the 200-m data the maximum deadtime corrections were 10% with the open beam and 6% with the sample in.

During the transmission measurements using water-moderated neutrons, three sources of backgrounds were monitored: (1) a background arising from 2.2-MeV gamma rays produced by neutron capture in the water moderator of the target; (2) a time and beam independent room background; and (3) a background produced from neutrons scattered by the detector which, with the NE-110 detector, arises mainly from a 478-keV gamma ray from the $^{10}B(n,\alpha\gamma)$ reaction produced from the absorption of scattered neutrons by the boron in the Pyrex face of the photomultiplier. For the 78-m transmission data taken with the ^{6}Li glass detector the background corrections were less than 3% of the open beam counting rate. To aid in the determination of these backgrounds and to optimize the signal-to-background ratio for the NE-110 detector, four separate pulse-height spectra were recorded. The contribution of all of these backgrounds was less than 1% over the energy region where the data were analyzed. Additional details on corrections for these backgrounds are given in Refs. LAR76 and LAR83. The 200-m transmission data were corrected only for a constant background (determined at long times) since there was little neutron capture in the narrow water-cooling channels in the tantalum target and little background from 478-keV gamma rays with this two-photomultiplier detector. This constant background is less than 0.3% above 180 keV.

Transmission data covering the energy range from 100 eV to 20 MeV were sent to Brookhaven National Data Center.

2.2 DIFFERENTIAL ELASTIC SCATTERING MEASUREMENTS

2.2.1 Data Acquisition

The scattering measurement was also done with the time-of-flight technique using neutron pulses from the ORELA water-moderated tantalum target. The flight path was 200.192 ± 0.014 m, and a collimator allowed both unmoderated and moderated neutrons to reach the sample.

The scattering measurement was made using 52.45 grams of Ni powder enriched to 99.93% in ^{58}Ni contained in a 5.14-gram hollow cylindrical container (5.85-cm high, 3.30-cm outside diameter, and 2.30-cm inside diameter) made from 0.005-cm-thick natural nickel foil which resulted in an effective enrichment of 97.0% in ^{58}Ni. The ^{58}Ni cylinder was suspended at the center of a 183-cm-diameter scattering chamber which was evacuated and isolated from the flight-path beam tube by means of a 0.025-cm Mylar entrance window.

The scattering data were obtained with a 0.3-g/cm^2 ^{10}B filter to eliminate low-energy neutrons associated with the previous burst, and with two filters of ^{238}U to reduce the intensity of the gamma flash from the target. One ^{238}U filter (0.5 cm thick) covered the whole collimator, the other (2.5 cm thick) shadowed only the tantalum part of the target. The measurements covered the energy region from approximately 10 keV to 5 MeV. The electron beam burst width was 8 nsec resulting in an energy resolution at higher energies of approximately 0.11 $[E(MeV)]^{1/2}$ percent.

Six neutron detectors were located 19.1 cm from the center of the chamber at angles of 39°, 55°, 90°, 120°, 140°, and 160° from the direction of the incident neutron beam. Each neutron detector consisted of a 7.62-cm-long by 4.32-cm-diam cylinder of NE-110 which was viewed at each end by RCA 8850 photomultiplier tubes. Additional details of the experimental arrangement for these scattering measurements can be found in reference HOR86.

The threshold for each phototube was set below the single photoelectron level, and a fast coincidence between the two tubes of each detector was required to define an event. The summed anode signals were split into two pulse-height windows and a 4500 channel time-of-flight (TOF) spectrum was taken for each window. The lower window was from threshold to about 14 photoelectrons, which corresponds to 160 keV proton energy for this detector. The upper window was for summed pulses greater than 14 photoelectrons. The two TOF spectra for a detector had equal counts at about 300 keV neutron energy. The efficiencies of the six detectors are quite similar since the thresholds and the two windows were set as described above. Details on the calculated efficiencies for these two-phototube detectors are given in reference HIL85.

The fast outputs of the six detectors were multiplexed to provide the stop signal and to set a four-bit tag generator of an EG&G clock. The system was designed so

that each detector could record a maximum of only one event from each accelerator burst (i.e., 800 s^{-1}). The data had to be corrected for deadtime which was caused predominantly by detection of the gamma flash scattered by the sample. A second EG&G time digitizer was modified so as to provide a seven-bit tag generator, and this was operated in parallel with the other time digitizer but with considerably fewer TOF channels. This allowed direct measurement of the gamma-flash events recorded by each detector, i.e., singly or in any multiple coincidence.

Data were also taken with one of the detectors placed in the direct beam to measure the product of the flux and the detector efficiency as a function of neutron energy.

2.2.2 Data Reduction

All spectra were normalized by means of a neutron monitor detector. After correcting for deadtime and a constant room background, the scattering spectra were divided by the spectrum from the in-beam detector to remove the energy dependence of the incident flux and detector efficiency. The data were not corrected for multiple scattering in the sample but were corrected for geometrical factors to deduce an absolute differential cross section within ≈15%.

2.3 CAPTURE MEASUREMENTS

2.3.1 Data Acquisition

The water-moderated tantalum target was used for measurements of prompt capture gamma ray energy as a function of neutron time-of-flight. The accelerator delivered pulses of electrons 1000 times a second with a time spread of 4 ns, full width at half maximum, and energies up to 180 MeV. Bremsstrahlung from the resultant electron-photon cascades freed neutrons from some of the tantalum nuclei with kinetic energies in a broad range centered near 700 keV. Many of those neutrons were slowed by elastic collisions in a disc-shaped region filled with water centered on the tantalum. Moderated and scattered neutrons from the water region passed through copper collimators to the capture cross-section apparatus 40.12 m away while the direct neutrons and gamma rays from the tantalum were intercepted by a shadow bar. A diagram with isometric sketches of significant subsections has been published (MAC83). Neutrons with energies below about 10 eV were removed from the collimated neutron beam by a ^{10}B filter. The neutron flux was monitored by a thin, 0.5 mm, ^{6}Li-glass scintillator 447 mm ahead of the sample (MAC71).

Thin and thick 99.935% enriched ^{58}Ni metal samples were used for the capture measurements. The sample size was 25.4 mm by 50.8 mm, nearly filling the collimated beam cross section. The samples, with thicknesses of 0.0038 at/b and 0.0382 at/b, were hung in thin mylar bags between two fluorocarbon liquid scintillator cells

for prompt gamma-ray detection (MAC71A). They faced and were fully illuminated by the ORELA pulsed neutron beam.

Pulse heights from the scintillators were measured as a function of neutron time-of-flight in a 56320-ns time range corresponding to energies from 2.6 keV to 2500 keV. Forty two hours of beam time were used for the thin sample measurement and 21.9 hours for the thick sample measurement. A pulse height bias of 153 keV was used. Detector efficiencies were calibrated by the saturated resonance method using the strong 4.9-eV resonance in ^{197}Au (MAC79) and monitored for stability with long-lived packaged radiation sources before, between, and after the enriched ^{58}Ni neutron capture measurements. The detectors showed a steady decrease of gain of 0.19% per day over the 12 days encompassing the ^{58}Ni and other measurements. The gain shift was interpolated to the midpoint of each sample measurement or calibration and a correction applied, precise to the nearest 0.4%. The standard deviation of the gold resonance calibrations in early 1975 was 0.7%, but they were analyzed by hand (PER77). Reanalysis of 16 later calibrations with the least squares program (MAC79) showed a (1.99 ± 0.81)% bias in the earlier method and this has been corrected in processing the nickel data.

2.3.2 Data Reduction

The primary two dimensional time-of-flight and prompt gamma-ray energy yield data were further processed (MAC71A) by correcting for electronic deadtime losses which increased as a function of time-of-flight to maxima of 5.1% for the thin sample and 9.0% for the faster counting thick sample. The scintillator background due to cosmic rays, uranium, thorium, and potassium in the local environment was about 48 c/s. Accelerator-induced radioactivities with half-lives longer than microseconds increased this background rate to 69 c/s for the thin sample and 79 c/s for the thick one as measured during each measurement by a 65536-ns time gate just preceding each fresh burst of neutrons. For comparison, the average detector count rate during the 56320-ns time-of-flight data gate was 313 c/s for the thin sample and 1461 c/s for the thick sample.

Backgrounds induced by beam neutrons at short times were measured in auxiliary measurements. With the beam in vacuum at the sample position one background component attributable to collimator and lithium glass scattering, decreased with time after the neutron pulse but was proportional to the fast neutron intensity, so it could be scaled to the monitor count for each experiment. Expressed in units of ^{58}Ni capture cross section, it decreased from 25 mb near 10 keV to 2.5 mb near 1000 keV for the thin Ni sample and from 3 mb to 0.3 mb for the thick Ni sample over the same energy range. Another background component was due to neutrons scattered by a sample itself into the detector and housing. A ^{208}Pb sample was used to evaluate this background since it gives little energy loss on scattering a neutron and has few resonances. The background component measured with it could be scaled to monitor counts and the scattering probability of a capture sample

and also shifted and broadened in energy to match the elastic scattering vs angle relations appropriate to the atomic mass (A) of a sample. Expressed again in units of the ^{58}Ni cross section this background component ranged from 9 mb to 1.2 mb for the thin Ni sample and from 8.4 mb to 1.1 mb for the thick Ni sample in the energy range where these data were analyzed.

Gamma-ray energy loss in the sample was calculated as 1.9% for the thin Ni sample and 8.9% for the thick Ni sample by a numerical integration code which includes the sample and detector geometry explicitly. This code was extensively checked against a Monte-Carlo code in France (LER75). Both of these calculations were based on the prompt gamma-ray spectrum produced by thermal neutron capture. For particular resonances there may be harder spectra dominated by gamma rays from 6 MeV to 9 MeV for which the energy loss corrections would be smaller.

2.3.3 Data Uncertainties

Known sources of uncertainty in the experimental work have been tabulated (BEE84) and combine to ~4% at the 68% probability level. While the gold-saturated resonance calibration has been checked against other elements with softer capture gamma-ray spectra such as holmium, silver, and uranium to about 1%, discrepancies of the order of 16% are observed for the 1.15-keV resonance of ^{56}Fe (MAC87) which has a very hard spectrum. Recent investigations (GAY88, PER88, SOW88) have revealed that this discrepancy is due to an incorrect weighting function for high-energy gamma rays. We do not have sufficient information on the spectra of the resonances of ^{58}Ni to perform a correction to the capture data due to the incorrect weighting function used. It is however likely that the capture data for some of the resonances are systematically too high, possibly by as much as 16%. Correlated uncertainties associated with flux-monitor calibration above 40 keV increase slowly with energy to 3.5% at 1400 keV (MAC84). The 153-keV pulse height bias was adequate for all the ^{58}Ni capture cross-section data as the threshold for the first inelastic gamma ray is 1480 keV.

3. DATA ANALYSIS

3.1 ENERGY SCALE

The absolute energy scale adopted in this analysis is the energy scale of the transmission measurements at the 200-m flight path station performed in July 1985. This choice is justified by new accurate laser measurements of the ORELA flight path lengths done in 1984 (LAR85). The uncertainties of the effective flight path lengths versus energy are discussed in detail in Ref. LAR84.

The energy scale of the transmission data below 180 keV, measured at the 80-m flight path, was adjusted to be consistent with the 200-m data. The relation between the two energy scales was determined through an overlapping region 120 keV wide centered at 190 keV where 12 $\ell > 0$ resonances could be clearly identified in both data sets.

The adjustment of the energy scale of the capture data from 5 to 450 keV was based on the correspondence found between the energy parameters of 59 resonances clearly seen simultaneously in the capture and transmission data from 10 to 400 keV.

The energy scale of the differential elastic-scattering data was found to be consistent with the energy scale of the 200-m transmission data.

3.2 TRANSMISSION DATA ANALYSIS

The transmission data were analyzed with the multilevel R-matrix Reich-Moore (REI58) formalism code SAMMY (LAR80). SAMMY is a constrained least-squares code which uses Bayes' theorem for the fitting process. In this work the code SAMMY was used to analyze only the transmission data since it does not yet include corrections for multiple scattering in the capture data.

The ^{58}Ni analysis documented in this report is similar to an analysis of ^{60}Ni reported in Ref. PER83, which should be consulted for more details. By using Bayes' equations, various data sets can be analyzed sequentially to yield a result equivalent to the simultaneous analysis of these data sets.

Three data sets were analyzed between 10 and 813 keV (see Table 1). From 10 to 180 keV the transmission data analyzed were those obtained with a 78-m flight path using an enriched ^{58}Ni sample with a thickness of 0.0764 at/b. In this energy range two different detectors and two neutron beam burst widths were used. Below 53 keV the data from a ^{6}Li glass detector taken with a burst width of 40 ns were used, and above 53 keV we used the data from a NE-110 detector taken with a burst width of 4 ns. Above 180 keV and up to 813 keV the more recent measurements taken with a 200-m flight path and a 5-ns beam burst width were analyzed. In this later experiment the sample thickness was 0.1724 at/b and a two-phototube NE-110

detector was used. The effective Gaussian resolution, full width at half maximum (FWHM), for the three experimental configurations used in the regions given above is shown in Fig. 1 as a function of the neutron incident energy. An exponential tail was added to the Gaussian resolution below 180 keV to account for the water moderator, which was used as neutron source in this region.

Table 1. Analyzed Data

Energy range (keV)	Flight path (m)	Burst width (ns)	Average Sample thickness (at/b)	Detector
Analyzed transmission data				
10 to 53	78.217 ± 0.004	40	0.0764 ± 0.0004	^{6}Li glass
53 to 180	78.217 ± 0.004	4	0.0764 ± 0.0004	NE-110
180 to 813	201.578 ± 0.005	5	0.172 ± 0.001	NE-110
Analyzed differential elastic scattering data				
30 to 813	200.192 ± 0.014	8	0.033 ± 0.001	NE-110
Analyzed capture data				
5 to 22	40.122 ± 0.004	4	0.00383 ± 0.00002	C_6F_6
22 to 450	40.122 ± 0.004	4	0.0382 ± 0.0002	C_6F_6

As discussed earlier in this report, when the transmission analysis is extended above 200 keV a single channel radius is inadequate to describe the transmission data. Some authors chose to use an energy-dependent radius (Refs. SYM78 and KIK85). We found that the transmission data could be analyzed with energy-independent radii if a much smaller radius is used for p-wave than for s- and d-wave resonances. These two radii were adjusted by the code along with 457 resonance parameters.

The transmission data from 10 to 813 keV are well described with 425 resonances of which two are negative energy resonances and three are above the analyzed region. These five external resonances do not correspond to actual resonances in ^{58}Ni but were used to describe accurately the smooth cross section in the region analyzed; therefore, these resonances must be included for the correct description of the data in this energy region. Since no transmission data below 10 keV were

fitted in obtaining the resonance parameters of Table 2, these parameters may not describe correctly the ^{58}Ni cross sections below 10 keV. As explained below, in Section 6.7, the known thermal capture cross section was used in determining the radiation widths of the negative energy resonances; consequently, the capture cross sections below the 6.9-keV resonance may be described accurately by these parameters. Calculations performed with the parameters of Table 2 give a 28.8-b thermal scattering cross section, whereas the accepted value is 25.3±0.4 b (MUG81). Therefore, we conclude that the scattering cross sections below 10 keV are not correctly described by these parameters.

Capture data were analyzed simultaneously with the transmission data up to 450 keV. All the resonances seen in the transmission data were also seen in the capture data, but 61 resonances analyzed in the capture data had too small a neutron width to be detected in transmission; however, these resonances were included in the transmission calculation to verify that the neutron widths assigned to these resonances are consistent with the transmission data.

All resonances showing the characteristic potential interference pattern of s-waves were assigned as s-waves. The differential elastic-scattering data were used to assign the spin and parity of $\ell > 0$ resonances whose neutron widths were large enough for them to be observed in the elastic scattering data (see Section 3.3). Below 450 keV, where the capture data were also analyzed, the resonances not seen in transmission data or seen in transmission data but not clearly seen in differential elastic scattering data, had their spin and parity assigned from the value of $g\Gamma_\gamma$ (p-wave if $g\Gamma_\gamma < 2$ eV and d-wave if $g\Gamma_\gamma > 2$ eV). These assignments are uncertain since, as shown in Section 6.5, the radiation width distribution for each ℓ value has a large standard deviation. However, in the case of four resonances (at 176.14, 242.36, 285.38 and 298.09 keV), seen very clearly in the capture data but which are very weak in the transmission data, an s-wave assignment gives the best agreement with the transmission data. Therefore, these four small resonances are assigned as s-waves but this assignment is uncertain. Above 450 keV most of the weak resonances were arbitrarily assigned as $p_{1/2}$. The results of this analysis are given in Table 2.

3.3 DIFFERENTIAL ELASTIC SCATTERING DATA ANALYSIS

The elastic-scattering measurements were used as the principal tool to determine the spin and parity of the $\ell > 0$ resonances. The theoretical calculations of the cross section at different scattering angles were compared with the experimental data. Various combinations of spins and parities were tested. The combination of spin and parity which yielded the best agreement with the data was adopted.

The theoretical cross sections were calculated as a function of the neutron incident energy with the R-matrix code RFUNCR (PER83A) which is based on the Blatt-Biedenharn formalism (BLA52). Doppler broadening and experimental resolution are taken into account in an approximate fashion: both effects are lumped

Table 2. Resonance parameters for ^{58}Ni + n from 6 to 813 keV

The transmission data analysis was performed with the following two channel radii:
R1 = 6.304 ± 0.010 fm for the $\ell = 0$ and $\ell = 2$ resonances.
R2 = 4.234 ± 0.008 fm for the $\ell = 1$ resonances.

The two negative energy resonances and the three s-wave resonances above 820 keV describe the smooth cross section in the analyzed region and are an integral part of the parameter file. The uncertainties are the statistical uncertainties given by the codes SAMMY and LSFIT except where note 3 is indicated.

	E_0 (keV)	Γ_n (eV)	$g\Gamma_n\Gamma_\gamma/\Gamma$ (eV)	Γ_γ (eV)	ℓ^a	J^a	Notes
1	−61.37 ± 1.09	4.39E+4 ± 3.E+2		(2.0)	0	0.5	1
2	−4.40	820. ± 39.		(1.4)	0	0.5	1
3	6.9064 ± 0.0002	0.025	0.024 ± 0.001	0.50	(1	0.5)	2
4	12.641 ± 0.001	0.032	0.030 ± 0.002	0.50	(1	0.5)	2
5	13.317 ± 0.001	7.43 ± 0.05	0.72 ± 0.01	0.79 ± 0.01	(1	0.5)	
6	13.638 ± 0.001	1.07 ± 0.03	0.68 ± 0.01.	0.49 ± 0.01	(1	1.5)	
7	15.310 ± 0.003	1332.1 ± 2.6	0.97 ± 0.30	0.97 ± 0.30	0	0.5	3
8	17.232 ± 0.002	0.032	0.030 ± 0.004	0.50	(1	0.5)	2
9	19.010 ± 0.001	0.090	0.077 ± 0.004	0.50	(1	0.5)	2
10	20.024 ± 0.001[b]	1.39 ± 0.12	0.29 ± 0.01	0.37 ± 0.01	(1	0.5)	
11	21.144 ± 0.001[b]	2.12 ± 0.12	0.76 ± 0.01	0.46 ± 0.01	(1	1.5)	
12	24.762 ± 0.001	0.018	0.018 ± 0.001	0.50	(1	0.5)	2
13	26.069 ± 0.001	0.21	0.35 ± 0.01	1.00	(1	1.5)	2
14	26.643 ± 0.001[b]	1.46	0.96 ± 0.01	0.72 ± 0.01	(1	1.5)	
15	27.63 ± 0.01	0.039	0.036 ± 0.003	0.50	(1	0.5)	2
16	32.268 ± 0.001[b]	0.30	0.46 ± 0.01	1.00	(1	1.5)	
17	32.397 ± 0.001	17.61 ± 0.28	1.48 ± 0.02	1.62 ± 0.02	1	0.5	
18	34.242 ± 0.001[b]	0.80	0.77 ± 0.01	0.74 ± 0.02	1	(1.5)	
19	35.070 ± 0.001	0.021	0.020 ± 0.005	0.50	(1	0.5)	2
20	36.133 ± 0.001	17.78 ± 0.28	1.57 ± 0.02	1.72 ± 0.03	0	0.5	
21	39.552 ± 0.001[b]	0.55	0.78 ± 0.01	1.35 ± 0.02	(2	1.5)	
22	44.013 ± 0.001	0.17	0.138 ± 0.004	0.70	(1	0.5)	2
23	47.901 ± 0.001[b]	4.52 ± 0.30	1.38 ± 0.02	0.81 ± 0.01	1	1.5	
24	51.906 ± 0.001[b]	0.40	0.95 ± 0.01	1.50 ± 0.02	(2	2.5)	
25	52.226 ± 0.001[b]	1.0	1.10 ± 0.01	1.23 ± 0.02	2	(1.5)	
26	54.790 ± 0.004	0.67	0.29 ± 0.01	0.50	(1	0.5)	2
27	58.700 ± 0.005[b]	0.80	0.71 ± 0.02	0.64 ± 0.03	(1	1.5)	
28	60.150 ± 0.001	16.46 ± 0.35	0.86 ± 0.02	0.44 ± 0.01	1	1.5	
29	61.791 ± 0.001	17.2 ± 0.7	1.68 ± 0.03	1.87 ± 0.04	1	0.5	
30	63.295 ± 0.004	3711. ± 6.	3.5 ± 0.7	3.5 ± 0.7	0	0.5	3
31	66.473 ± 0.002	0.70	0.71 ± 0.02	0.72 ± 0.04	(1	1.5)	2
32	68.673 ± 0.005	0.62	0.28 ± 0.02	0.50	(1	0.5)	2
33	69.917 ± 0.002[b]	7.3 ± 0.6	0.62 ± 0.02	0.68 ± 0.02	1	(0.5)	

Table 2. (continued)

	E_0 (keV)	Γ_n (eV)	$g\Gamma_n\Gamma_\gamma/\Gamma$ (eV)	Γ_γ (eV)	ℓ^a	J^a	Notes
34	78.087 ± 0.005	0.49	0.25 ± 0.14	0.50	(1	0.5)	2
35	81.326 ± 0.003[b]	1.0	1.29 ± 0.03	1.80 ± 0.10	(2	1.5)	
36	82.877 ± 0.001	41.5 ± 0.6	2.66 ± 0.04	1.38 ± 0.02	1	1.5	
37	83.391 ± 0.003[b]	4.0	0.90 ± 0.02	1.16 ± 0.04	0	0.5	
38	83.845 ± 0.002	31.0 ± 0.9	0.25	0.25	1	0.5	
39	83.917 ± 0.005[b]	2.3	1.39 ± 0.02	1.00 ± 0.02	(2	1.5)	
40	84.878 ± 0.006	0.40	0.20 ± 0.01	0.40	(1	0.5)	2
41	89.984 ± 0.001[b]	4.54 ± 0.36	0.75 ± 0.01	0.41 ± 0.01	1	(1.5)	
42	92.725 ± 0.004	0.49	0.25 ± 0.01	0.50	(1	0.5)	2
43	95.680 ± 0.002	0.65	1.47 ± 0.03	2.00	(2	2.5)	2
44	96.978 ± 0.002	0.60	0.64 ± 0.02	0.69 ± 0.03	(1	1.5)	2
45	97.604 ± 0.003	20.0 ± 0.9	0.43 ± 0.02	0.44 ± 0.02	1	0.5	
46	101.42 ± 0.01[b]	2.89 ± 0.20	1.28 ± 0.03	0.50 ± 0.01	2	(2.5)	
47	105.443 ± 0.004	9.5 ± 0.5	2.49 ± 0.03	1.43 ± 0.02	2	(1.5)	
48	107.12 ± 0.01[b]	1.0	0.31 ± 0.03	0.45	(1	0.5)	
49	107.760 ± 0.002[b]	2.85	1.72 ± 0.04	1.23 ± 0.04	2	(1.5)	
50	108.343 ± 0.002	1074.6 ± 3.9	4.8 ± 0.3	4.8 ± 0.3	0	0.5	3
51	110.750 ± 0.004[b]	4.0	0.96 ± 0.04	0.55 ± 0.03	(1	1.5)	
52	111.490 ± 0.005[b]	1.0	0.85 ± 0.04	0.74 ± 0.06	(1	1.5)	
53	116.82 ± 0.02	0.22	0.15 ± 0.02	0.50	(1	0.5)	2
54	117.879 ± 0.004	8.2 ± 0.5	1.15 ± 0.04	0.62 ± 0.02	1	1.5	
55	119.800 ± 0.003[b]	2.6	2.94 ± 0.04	1.57 ± 0.04	2	(2.5)	
56	121.07 ± 0.02	0.70	0.29 ± 0.03	0.50	(1	0.5)	2
57	121.424 ± 0.004	7.9 ± 0.6	1.71 ± 0.04	0.96 ± 0.03	2	(1.5)	
58	124.001 ± 0.002	458.3 ± 2.6	1.56 ± 0.15	1.56 ± 0.15	0	0.5	3
59	124.060 ± 0.006[b]	1.5	1.31 ± 0.05	1.16 ± 0.08	(2	1.5)	
60	125.320 ± 0.005[b]	1.7	2.64 ± 0.04	1.83 ± 0.06	2	(2.5)	
61	129.970 ± 0.004	12.7 ± 0.6	0.78 ± 0.02	0.40 ± 0.01	1	1.5	
62	132.840 ± 0.004	1.0	0.79 ± 0.02	0.66 ± 0.03	(1	1.5)	2
63	133.700 ± 0.003[b]	9.1 ± 0.5	1.94 ± 0.04	1.09 ± 0.02	1	1.5	
64	136.640 ± 0.003[b]	2.1	1.48 ± 0.06	1.13 ± 0.07	(2	1.5)	
65	137.606 ± 0.003	2034. ± 8.	2.9 ± 0.8	2.9 ± 0.8	0	0.5	3
66	137.85 ± 0.05	0.40	0.22 ± 0.04	0.50	(1	0.5)	2
67	140.000 ± 0.005[b]	2.1	0.91 ± 0.05	0.58 ± 0.05	(1	1.5)	
68	140.288 ± 0.004	3054. ± 10.	0.9 ± 0.6	0.9 ± 0.6	0	0.5	3
69	140.76 ± 0.04	0.40	0.22 ± 0.04	0.50	(1	0.5)	2
70	141.888 ± 0.006	32.6 ± 1.8	0.55 ± 0.05	0.56 ± 0.05	1	0.5	
71	142.430 ± 0.003	1.33	1.86 ± 0.07	1.16 ± 0.07	(2	2.5)	2
72	143.13 ± 0.03	0.30	0.19 ± 0.06	0.50	(1	0.5)	2
73	145.245 ± 0.002	84.3 ± 1.2	3.57 ± 0.10	1.83 ± 0.05	1	1.5	

Table 2. (continued)

	E_0 (keV)	Γ_n (eV)	$g\Gamma_n\Gamma_\gamma/\Gamma$ (eV)	Γ_γ (eV)	ℓ^a	J^a	Notes
74	148.810 ± 0.002[c]	78.5 ± 1.0	0.99 ± 0.05	0.50 ± 0.02	1	1.5	
75	149.170 ± 0.006[b]	1.8	1.29 ± 0.04	1.00 ± 0.05	2	(1.5)	
76	151.370 ± 0.007[b]	22.2 ± 1.2	1.05 ± 0.04	1.10 ± 0.05	1	0.5	
77	155.44 ± 0.03	0.70	0.29 ± 0.03	0.50	(1	0.5)	2
78	156.988 ± 0.003	36.1 ± 1.1	1.40 ± 0.06	0.71 ± 0.03	1	1.5	
79	158.088 ± 0.007	5191. ± 12.	3.3 ± 0.8	3.3 ± 0.8	0	0.5	3
80	159.860 ± 0.006[b]	5.2	2.13 ± 0.06	1.34 ± 0.05	2	(1.5)	
81	161.287 ± 0.006	13.9 ± 0.8	3.20 ± 0.07	1.16 ± 0.03	2	(2.5)	
82	161.95	0.43	0.23 ± 0.03	0.50	(1	0.5)	2
83	166.083 ± 0.005	48.5 ± 1.9	0.36 ± 0.05	0.37 ± 0.05	1	0.5	
84	167.090 ± 0.005[c]	13.7 ± 0.8	2.17 ± 0.06	1.18 ± 0.04	2	(1.5)	
85	168.61 ± 0.01[b]	8.25	1.44 ± 0.07	0.79 ± 0.05	1	1.5	
86	168.949 ± 0.002	413.6 ± 3.6	1.3 ± 0.2	1.3 ± 0.2	0	0.5	3
87	172.530 ± 0.006[b]	5.3 ± 0.5	2.77 ± 0.07	1.12 ± 0.03	2	(2.5)	
88	175.233 ± 0.003	47.6 ± 1.1	1.47 ± 0.07	0.75 ± 0.04	1	1.5	
89	176.14 ± 0.03	4.8	0.51 ± 0.05	0.56 ± 0.06	(0	0.5)	2
90	180.655 ± 0.001	17.8 ± 0.7	1.24 ± 0.05	0.64 ± 0.03	2	(1.5)	
91	181.299 ± 0.002	21.5 ± 1.0	0.69 ± 0.04	0.71 ± 0.04	1	0.5	
92	183.940 ± 0.004[c]	6.0 ± 0.4	1.78 ± 0.05	1.04 ± 0.04	2	(1.5)	
93	184.606 ± 0.001	106.2 ± 1.1	1.61 ± 0.06	0.81 ± 0.03	1	1.5	
94	185.500 ± 0.004[c]	2.3	2.33 ± 0.05	1.17 ± 0.05	2	(2.5)	
95	185.996 ± 0.001	24.6 ± 0.7	1.19 ± 0.05	0.61 ± 0.03	1	1.5	
96	186.86 ± 0.04	0.80	0.31 ± 0.04	0.50	(1	0.5)	2
97	187.68 ± 0.03	0.70	0.37 ± 0.04	0.78 ± 0.08	(1	0.5)	2
98	189.41 ± 0.01[b]	1.44	1.40 ± 0.06	1.36 ± 0.11	(2	1.5)	
99	191.48 ± 0.01[b]	8.2 ± 0.5	1.63 ± 0.07	0.90 ± 0.05	2	(1.5)	
100	191.896 ± 0.004	2465. ± 8.	3.3 ± 0.5	3.3 ± 0.5	0	0.5	3
101	192.65 ± 0.06	0.57	0.27 ± 0.05	0.50	(1	0.5)	2
102	194.01 ± 0.02	1.0	0.79 ± 0.05	0.66 ± 0.07	(1	1.5)	2
103	196.346 ± 0.003	8.1 ± 0.6	0.91 ± 0.06	0.49 ± 0.03	1	1.5	
104	198.162 ± 0.002	8.99 ± 0.40	4.56 ± 0.10	1.83 ± 0.05	2	(2.5)	
105	200.55 ± 0.07	0.50	0.25 ± 0.05	0.50	(1	0.5)	2
106	201.49 ± 0.02[b]	4.04	1.02 ± 0.05	0.58 ± 0.04	(1	1.5)	
107	202.520 ± 0.003	15.8 ± 0.9	0.40 ± 0.05	0.41 ± 0.05	1	(0.5)	
108	206.557 ± 0.008	7354. ± 15.	6.9 ± 1.0	6.9 ± 1.0	0	0.5	3
109	207.262 ± 0.002	161.8 ± 2.4	1.41 ± 0.08	0.71 ± 0.04	1	1.5	
110	209.31 ± 0.02	1.45	1.35 ± 0.06	1.26 ± 0.10	(2	1.5)	2
111	209.89 ± 0.04	0.80	0.65 ± 0.05	0.55 ± 0.08	(1	1.5)	2
112	211.045 ± 0.002	56.9 ± 1.6	0.75 ± 0.06	0.76 ± 0.06	0	0.5	

Table 2. (continued)

	E_0 (keV)	Γ_n (eV)	$g\Gamma_n\Gamma_\gamma/\Gamma$ (eV)	Γ_γ (eV)	ℓ^a	J^a	Notes
113	216.42	3.3	1.69 ± 0.10	1.14 ± 0.07	(1	1.5)	
114	216.55 ± 0.02[c]	9.8 ± 1.0[c]	2.42 ± 0.11	1.38 ± 0.07	2	(1.5)	
115	216.69 ± 0.01[c]	197.2 ± 3.5	0.50	0.50	1	0.5	
116	216.91	5.7 ± 0.6[c]	0.33	0.35	(1	0.5)	
117	217.92 ± 0.01[c]	5.2 ± 0.5	0.89 ± 0.15	0.49 ± 0.09	2	(1.5)	
118	218.124 ± 0.002	16.5 ± 0.8	1.88 ± 0.16	1.00 ± 0.09	1	1.5	
119	219.29 ± 0.06	1.17	0.46 ± 0.06	0.76 ± 0.20	(1	0.5)	2
120	220.34 ± 0.01[b]	3.9 ± 0.4[c]	3.87 ± 0.11	1.93 ± 0.08	2	(2.5)	
121	224.35 ± 0.01	1.9	1.48 ± 0.06	1.21 ± 0.07	(2	1.5)	2
122	229.40 ± 0.01[b]	1.45 ± 0.15[c]	2.84 ± 0.09	2.73 ± 0.22	(2	2.5)	
123	231.104 ± 0.001	44.2 ± 0.7	1.39 ± 0.08	0.71 ± 0.04	1	1.5	
124	232.54 ± 0.01[c]	6.4 ± 0.6[c]	0.93 ± 0.07	0.50 ± 0.04	2	(1.5)	
125	233.027 ± 0.006	5584. ± 13.	5.3 ± 0.7	5.3 ± 0.7	0	0.5	3
126	233.6 ± 0.2	0.70	0.29 ± 0.06	0.50	(1	0.5)	2
127	234.138 ± 0.003	21.5 ± 1.1	1.45 ± 0.09	0.75 ± 0.05	1	(1.5)	
128	235.38 ± 0.06	1.2	0.35 ± 0.06	0.50	(1	0.5)	2
129	236.82 ± 0.08	3.5	0.71 ± 0.15	0.89 ± 0.25	(1	0.5)	2
130	237.00 ± 0.05	2.3	0.64 ± 0.15	0.89 ± 0.28	(1	0.5)	2
131	241.10 ± 0.05	2.0	0.52 ± 0.06	0.70 ± 0.11	(1	0.5)	2
132	242.36 ± 0.07	3.0	0.61 ± 0.08	0.77 ± 0.12	(0	0.5)	2
133	242.772 ± 0.002	25.5 ± 1.0	1.31 ± 0.09	0.67 ± 0.05	1	1.5	
134	243.950 ± 0.006[c]	10.3 ± 0.5	3.27 ± 0.09	1.22 ± 0.04	2	2.5	
135	245.09	5.9	0.37	0.39	(1	0.5)	
136	245.25	16.3 ± 1.8[c]	0.70 ± 0.12	0.36 ± 0.06	(1	1.5)	
137	245.40	21.2 ± 2.5[c]	0.49	0.50	(1	0.5)	
138	245.551 ± 0.001	237.6 ± 2.7	0.55	0.55	0	0.5	
139	245.63 ± 0.01[c]	13.8 ± 1.5[c]	2.41 ± 0.14	1.32 ± 0.08	2	(1.5)	
140	245.88	3.0	0.71	0.40	2	(1.5)	
141	249.24 ± 0.15	0.65	0.28 ± 0.05	0.50	(1	0.5)	2
142	249.548 ± 0.001	165.8 ± 1.6	0.68 ± 0.09	0.34 ± 0.04	1	1.5	
143	250.794 ± 0.002	31.9 ± 1.0	1.55 ± 0.07	0.79 ± 0.04	2	(1.5)	
144	254.280 ± 0.006[c]	26.7 ± 1.4	0.97 ± 0.08	1.01 ± 0.09	1	(0.5)	
145	254.60	4.6 ± 0.6[c]	0.44	0.49	(1	0.5)	
146	255.09 ± 0.01[c]	7.2 ± 0.6[c]	2.24 ± 0.09	1.33 ± 0.07	1	(1.5)	
147	257.650 ± 0.006[c]	9.8 ± 0.5	1.84 ± 0.08	1.02 ± 0.05	2	(1.5)	
148	259.180 ± 0.005[c]	26.2 ± 1.2	0.57 ± 0.12	0.58 ± 0.12	1	0.5	
149	259.567 ± 0.002	23.6 ± 0.6	2.25 ± 0.15	0.78 ± 0.05	2	2.5	
150	260.28 ± 0.01[c]	2.9 ± 0.5[c]	2.69 ± 0.10	1.31 ± 0.08	2	(2.5)	
151	261.933 ± 0.005	14.2 ± 0.8	0.98 ± 0.08	1.05 ± 0.09	0	0.5	
152	263.32 ± 0.07	0.50	0.25 ± 0.05	0.50	(1	0.5)	2
153	265.590 ± 0.005[c]	9.1 ± 0.5	1.69 ± 0.09	0.93 ± 0.05	1	1.5	

Table 2. (continued)

	E_0 (keV)	Γ_n (eV)	$g\Gamma_n\Gamma_\gamma/\Gamma$ (eV)	Γ_γ (eV)	ℓ^a	J^a	Notes
154	267.910 ± 0.002	49.5 ± 1.2	0.40 ± 0.08	0.40 ± 0.08	1	0.5	
155	269.497 ± 0.001	30.6 ± 0.6	0.98 ± 0.07	0.50 ± 0.04	1	1.5	
156	272.488 ± 0.007	5390. ± 13.	5.4 ± 0.6	5.4 ± 0.6	0	0.5	3
157	273.66 ± 0.01[b]	24.2 ± 1.1	2.99 ± 0.10	1.59 ± 0.05	2	(1.5)	
158	275.71 ± 0.06	2.5	0.42 ± 0.06	0.50	(1	0.5)	2
159	277.50 ± 0.006[c]	34.7 ± 1.2	1.08 ± 0.07	0.55 ± 0.04	2	1.5	
160	278.641 ± 0.001	75.3 ± 1.3	1.49 ± 0.07	0.75 ± 0.04	1	1.5	
161	281.27 ± 0.04	1.7	1.05 ± 0.11	0.76 ± 0.11	(1	1.5)	2
162	281.599 ± 0.004	1947. ± 8.	1.75 ± 0.40	1.75 ± 0.40	0	0.5	3
163	284.70 ± 0.03[b]	2.3	1.31 ± 0.08	0.92 ± 0.08	(1	1.5)	
164	285.38 ± 0.15	4.0	0.78 ± 0.10	0.96 ± 0.15	(0	0.5)	2
165	286.01 ± 0.02[b]	1.05	1.94 ± 0.10	1.68 ± 0.20	(2	2.5)	
166	289.493 ± 0.002	104.7 ± 1.5	1.23 ± 0.15	0.62 ± 0.08	1	1.5	
167	289.95 ± 0.01[c]	6.3 ± 0.5[c]	4.33 ± 0.17	1.87 ± 0.09	2	(2.5)	
168	291.37 ± 0.02[c]	11.5 ± 1.0[c]	0.48 ± 0.10	0.50	1	(0.5)	
169	292.93 ± 0.03[b]	5.6 ± 0.6[c]	2.09 ± 0.09	1.28 ± 0.06	2	(1.5)	
170	295.39 ± 0.03[b]	3.0	1.50 ± 0.08	1.00 ± 0.07	(1	1.5)	
171	297.640 ± 0.006[c]	15.1 ± 0.8	2.45 ± 0.13	1.33 ± 0.08	2	(1.5)	
172	298.09 ± 0.08	4.0	0.49 ± 0.11	0.56 ± 0.15	(0	0.5)	2
173	299.44 ± 0.12	2.0	0.53 ± 0.09	0.72 ± 0.17	(1	0.5)	2
174	300.210 ± 0.003	16.9 ± 0.7	4.23 ± 0.15	1.54 ± 0.06	2	2.5	
175	301.330 ± 0.007[c]	24.0 ± 0.9	0.79	0.40	1	1.5	
176	301.630 ± 0.004[c]	47.4 ± 1.1	2.45 ± 0.11	1.26 ± 0.06	2	1.5	
177	304.85	2.5	0.34	0.40	(1	0.5)	
178	305.210 ± 0.004[c]	100.4 ± 1.2	2.27 ± 0.34	1.15 ± 0.18	2	(1.5)	
179	305.405 ± 0.003	655.9 ± 4.5	2.8 ± 0.5	2.8 ± 0.5	0	0.5	3
180	307.33 ± 0.03[b]	25.3 ± 1.2[c]	1.43 ± 0.10	1.52 ± 0.12	1	(0.5)	
181	307.471 ± 0.002	163.0 ± 3.1	0.70	0.70	1	0.5	
182	311.99 ± 0.02[c]	5.8 ± 0.4[c]	1.95 ± 0.10	1.17 ± 0.07	2	(1.5)	
183	313.00	1.9	1.47 ± 0.23	1.20 ± 0.30	(2	1.5)	
184	313.32 ± 0.02[c]	4.6 ± 0.4[c]	1.34 ± 0.21	0.78 ± 0.15	(1	1.5)	
185	317.203 ± 0.002	36.8 ± 0.9	1.85 ± 0.11	0.95 ± 0.06	1	1.5	
186	321.310 ± 0.004[c]	19.4 ± 0.8	1.87 ± 0.25	0.98 ± 0.14	2	(1.5)	
187	321.59	2.0	1.03 ± 0.23	0.69 ± 0.19	(1	1.5)	

Table 2. (continued)

	E_0 (keV)	Γ_n (eV)	$g\Gamma_n\Gamma_\gamma/\Gamma$ (eV)	Γ_γ (eV)	ℓ^a	J^a	Notes
188	325.18 ± 0.01[c]	5.5 ± 0.3[c]	1.43 ± 0.12	0.82 ± 0.07	1	1.5	
189	325.71	20.5	0.49	0.50	1	0.5	
190	325.88 ± 0.01[c]	27.8 ± 1.5[c]	2.05 ± 0.22	1.06 ± 0.07	1	1.5	
191	326.025 ± 0.003	1582. ± 7.	0.4 ± 0.4	0.4 ± 0.4	0	0.5	3
192	329.650 ± 0.006[c]	18.4 ± 0.9	1.44 ± 0.11	0.75 ± 0.06	1	1.5	
193	332.91 ± 0.07	0.60	0.72 ± 0.09	0.89 ± 0.29	(1	1.5)	2
194	334.895 ± 0.001	322.5 ± 2.0	1.00	0.50	1	1.5	
195	335.190 ± 0.006[c]	141.5 ± 2.9	2.49 ± 0.13	2.54 ± 0.13	0	0.5	
196	336.00 ± 0.10	0.95	1.72 ± 0.11	1.45 ± 0.20	(2	2.5)	2
197	337.60 ± 0.02[c]	3.8 ± 0.7[c]	1.20 ± 0.10	0.67 ± 0.07	2	(1.5)	
198	338.02 ± 0.15	0.70	0.85 ± 0.09	1.08 ± 0.27	(2	1.5)	2
199	341.17 ± 0.01[c]	4.8 ± 0.3[c]	2.58 ± 0.14	1.77 ± 0.13	(2	1.5)	
200	342.67 ± 0.005[c]	7.6 ± 0.4[c]	4.48 ± 0.18	1.86 ± 0.09	2	(2.5)	
201	343.572 ± 0.002	99.5 ± 1.3	2.02 ± 0.24	1.02 ± 0.12	1	1.5	
202	344.332 ± 0.001	77.7 ± 0.9	4.00 ± 0.22	1.36 ± 0.08	2	2.5	
203	346.490 ± 0.007[c]	3.8 ± 0.2[c]	3.6 ± 0.8	1.8 ± 0.6	(2	2.5)	
204	346.60	2.5 ± 0.3[c]	2.8 ± 0.8	1.5 ± 0.6	(2	2.5)	
205	349.660 ± 0.004	1779. ± 7.	0.8 ± 0.5	0.8 ± 0.5	0	0.5	3
206	355.29 ± 0.05	1.3	2.15 ± 0.15	1.58 ± 0.23	(2	2.5)	2
207	357.44	3.4	0.76 ± 0.15	0.98 ± 0.26	(1	0.5)	2
208	357.786 ± 0.001	155.9 ± 1.6	1.20 ± 0.25	0.60 ± 0.13	1	1.5	
209	359.920 ± 0.004[c]	62.5 ± 1.1	1.58 ± 0.22	0.80 ± 0.11	2	(1.5)	
210	360.18 ± 0.01[c]	4.0 ± 0.4[c]	1.01	0.58	(1	1.5)	
211	360.630 ± 0.006[c]	27.7 ± 1.0	2.96 ± 0.21	1.56 ± 0.12	1	(1.5)	
212	363.460 ± 0.006[c]	11.2 ± 0.7	2.42 ± 0.14	1.36 ± 0.09	2	(1.5)	
213	364.380 ± 0.007[c]	7.2 ± 0.4[c]	2.37 ± 0.16	0.89 ± 0.06	2	(2.5)	
214	365.368 ± 0.003	33.4 ± 1.0	1.87 ± 0.15	0.96 ± 0.08	1	1.5	
215	367.740 ± 0.003[c]	125.9 ± 2.1	0.40	0.40	0	0.5	
216	368.05 ± 0.10	2.9	1.48 ± 0.13	1.00 ± 0.11	(2	1.5)	2
217	370.12 ± 0.01[c]	7.2 ± 0.5[c]	2.14 ± 0.15	1.26 ± 0.10	2	(1.5)	
218	371.217 ± 0.002	53.3 ± 1.1	1.93 ± 0.16	0.98 ± 0.08	1	1.5	
219	374.03 ± 0.05	2.0	1.02 ± 0.13	0.68 ± 0.12	(1	1.5)	2
220	376.34	8.6 ± 0.7[c]	1.19 ± 0.17	0.64 ± 0.09	2	(1.5)	
221	376.76	0.53	1.15 ± 0.17	1.40 ± 0.21	(2	2.5)	2
222	377.140 ± 0.004	36.1 ± 1.0	1.18 ± 0.18	0.60 ± 0.09	1	1.5	
223	379.002 ± 0.001	77.6 ± 0.9	5.29 ± 0.21	1.80 ± 0.07	2	2.5	
224	379.947 ± 0.003	226.6 ± 3.3	0.90 ± 0.19	0.91 ± 0.19	1	0.5	

Table 2. (continued)

	E_0 (keV)	Γ_n (eV)	$g\Gamma_n\Gamma_\gamma/\Gamma$ (eV)	Γ_γ (eV)	ℓ^a	J^a	Notes
225	384.56 ± 0.01[c]	5.0 ± 0.5[c]	3.83 ± 0.14	1.71 ± 0.08	2	(2.5)	
226	390.020 ± 0.008[c]	9.2 ± 1.0[c]	1.86 ± 0.14	1.04 ± 0.09	1	1.5	
227	391.57 ± 0.06	0.95	1.08 ± 0.13	1.25 ± 0.34	(2	1.5)	2
228	395.027 ± 0.003	694. ± 5.	0.50	0.50	0	0.5	
229	395.10	16.3	1.52 ± 0.09	0.80 ± 0.05	2	(1.5)	
230	395.34 ± 0.007[c]	26.5 ± 1.0	3.04 ± 0.16	1.05 ± 0.06	2	(2.5)	
231	395.66	13.7	0.48	0.50	(1	0.5)	
232	397.410 ± 0.004[c]	147.4 ± 1.8	1.94 ± 0.35	0.97 ± 0.18	1	1.5	
233	397.850 ± 0.005[c]	270.7 ± 4.4	1.02 ± 0.35	1.02 ± 0.35	1	0.5	
234	400.650 ± 0.008[c]	8.1 ± 0.6[c]	1.29 ± 0.14	0.70 ± 0.08	2	(1.5)	
235	401.11	1.0	2.06 ± 0.25	2.2 ± 0.5	(2	2.5)	2
236	405.950 ± 0.005[c]	16.9 ± 0.8	0.96 ± 0.17	0.49 ± 0.09	1	1.5	
237	407.017 ± 0.003	48.1 ± 1.1	0.99	0.50	2	(1.5)	
238	408.23	3.2	0.36	0.40	(1	0.5)	
239	408.49 ± 0.01[c]	8.7 ± 0.6[c]	2.05 ± 0.18	1.16 ± 0.12	2	(1.5)	
240	409.550 ± 0.004[c]	76.1 ± 1.9	0.50	0.50	1	0.5	
241	410.020 ± 0.005[c]	20.3 ± 0.7	3.22 ± 0.19	1.13 ± 0.07	2	(2.5)	
242	411.31	2.3	0.43	0.53	(1	0.5)	
243	413.551 ± 0.002	100.8 ± 1.2	1.61 ± 0.20	0.81 ± 0.10	1	1.5	
244	414.74	3.2	2.38 ± 0.17	1.05 ± 0.11	(2	2.5)	
245	416.318 ± 0.002	266.8 ± 2.3	4.70 ± 0.24	2.37 ± 0.12	1	1.5	
246	417.492 ± 0.013	9359. ± 34.	2.6 ± 1.4	2.6 ± 1.4	0	0.5	3
247	420.650 ± 0.008[c]	35.6 ± 1.4	1.52 ± 0.19	0.77 ± 0.10	1	1.5	
248	424.619 ± 0.011	7714. ± 29.	3.3 ± 1.8	3.3 ± 1.8	0	0.5	3
249	425.40 ± 0.01[c]	12.0 ± 1.0[c]	2.43 ± 0.22	1.35 ± 0.14	2	(1.5)	
250	425.96 ± 0.01[c]	30.0 ± 2.0[c]	0.87	0.90	(1	0.5)	
251	426.780 ± 0.006[c]	165.9 ± 2.2	1.79 ± 0.24	0.90 ± 0.12	2	(1.5)	
252	428.049 ± 0.004	1084. ± 15.	0.9 ± 0.6	0.9 ± 0.6	0	0.5	3
253	428.70	7.2	1.43 ± 0.24	0.79 ± 0.15	2	(1.5)	
254	429.860 ± 0.008[c]	52.0 ± 1.2	6.0 ± 0.3	2.07 ± 0.11	2	2.5	
255	431.78	4.5	1.06	0.60	(1	1.5)	
256	433.097 ± 0.003	112.7 ± 2.1	1.34 ± 0.16	0.67 ± 0.08	1	1.5	
257	434.82	7.6	2.36 ± 0.24	1.40 ± 0.16	(2	1.5)	
258	435.020 ± 0.008[c]	388. ± 6.	1.00	1.00	1	0.5	
259	435.910 ± 0.007[c]	57.3 ± 1.4	5.3 ± 0.3	1.83 ± 0.11	2	(2.5)	
260	436.603 ± 0.003	113.0 ± 2.0	3.00	1.50	1	1.5	
261	439.220 ± 0.006[c]	71.4 ± 1.6	2.00	1.00	2	1.5	
262	439.52	2.9	2.91 ± 0.20	1.46 ± 0.15	(2	2.5)	
263	441.80 ± 0.15	6.0	0.38 ± 0.10	0.40	(1	0.5)	2
264	443.55 ± 0.15	3.0	1.20 ± 0.17	0.75 ± 0.13	(1	1.5)	2
265	444.95 ± 0.02[b]	2.9 ± 0.4[c]	2.71 ± 0.20	1.31 ± 0.13	(2	2.5)	
266	446.971 ± 0.002	112.7 ± 1.4	3.16 ± 0.21	1.06 ± 0.07	2	2.5	

Table 2. (continued)

	E_0 (keV)	Γ_n (eV)	$g\Gamma_n\Gamma_\gamma/\Gamma$ (eV)	Γ_γ (eV)	ℓ^a	J^a	Notes
267	452.188 ± 0.002	182.8 ± 2.1			1	1.5	
268	455.09	10.5			(1	0.5)	
269	455.495 ± 0.007	1787. ± 11.			0	0.5	
270	455.54	40.5 ± 1.9			1	1.5	
271	457.536 ± 0.004	43.4 ± 1.2			2	(2.5)	
272	459.666 ± 0.002	288.1 ± 2.9			1	1.5	
273	462.253 ± 0.003	437. ± 5.			0	0.5	
274	463.311 ± 0.002	153.5 ± 2.1			2	1.5	
275	466.167 ± 0.009	18.2 ± 1.2			1	(1.5)	
276	469.259 ± 0.002	172.5 ± 2.3			1	1.5	
277	470.409 ± 0.003	469. ± 6.			0	0.5	
278	476.074 ± 0.003	51.2 ± 1.2			2	2.5	
279	477.281 ± 0.004	164.8 ± 3.6			1	0.5	
280	479.902 ± 0.004	38.8 ± 1.1			2	2.5	
281	482.729 ± 0.012	12.0 ± 1.1			2	(1.5)	
282	485.78	9.7			(1	1.5)	
283	487.140 ± 0.012[c]	16.5 ± 1.1			2	(1.5)	
284	487.62	15.9			(1	0.5)	
285	491.470 ± 0.004[c]	91.6 ± 1.7			1	1.5	
286	491.810 ± 0.006[c]	178.2 ± 4.4			0	0.5	
287	493.176 ± 0.004	390. ± 7.			1	0.5	
288	493.750 ± 0.005[c]	87.6 ± 1.7			2	(2.5)	
289	495.32	9.4			(2	1.5)	
290	496.03	14.8			(1	0.5)	
291	496.317 ± 0.005	1384. ± 10.			0	0.5	
292	496.38	30.7			(1	0.5)	
293	496.846 ± 0.005	244. ± 5.			1	0.5	
294	498.928 ± 0.009	22.7 ± 1.4			1	(1.5)	
295	503.852 ± 0.004	32.6 ± 1.0			2	(2.5)	
296	506.860 ± 0.007[c]	35.4 ± 1.2			2	(1.5)	
297	507.64	26.2			(1	0.5)	
298	507.780 ± 0.006	1496. ± 10.			0	0.5	
299	508.24	76.2 ± 2.4			2	(1.5)	
300	508.61	55.5 ± 2.6[c]			2	(1.5)	
301	508.860 ± 0.008[c]	61.0 ± 3.1[c]			1	1.5	
302	509.50	10.5			2	(1.5)	
303	511.205 ± 0.003	145.2 ± 2.0			1	1.5	
304	513.359 ± 0.002	177.7 ± 2.1			1	1.5	
305	513.97	15.3			2	(2.5)	
306	514.38	10.5			2	(2.5)	
307	515.89	5.7			(2	1.5)	
308	518.471 ± 0.003	48.9 ± 1.1			2	2.5	
309	520.80	12.5			(1	0.5)	
310	521.700 ± 0.004[c]	119.0 ± 3.1			1	0.5	

Table 2. (continued)

	E_0 (keV)	Γ_n (eV)	$g\Gamma_n\Gamma_\gamma/\Gamma$ (eV)	Γ_γ (eV)	ℓ^a	J^a	Notes
311	523.25	9.1			(1	0.5)	
312	523.516 ± 0.004	1276. ± 9.			0	0.5	
313	524.080 ± 0.005[c]	68.0 ± 1.5			2	2.5	
314	527.830 ± 0.004	46.4 ± 1.2			2	2.5	
315	529.250 ± 0.004	195.7 ± 3.7			0	0.5	
316	529.420 ± 0.005[c]	81.8 ± 2.4			1	1.5	
317	530.678 ± 0.006	24.3 ± 1.0			2	(2.5)	
318	539.860 ± 0.003	84.5 ± 1.7			2	(1.5)	
319	540.53	10.2			(1	0.5)	
320	541.206 ± 0.003	506. ± 7.			0	0.5	
321	541.890 ± 0.007[c]	47.6 ± 2.0			1	1.5	
322	543.733 ± 0.009	16.5 ± 1.1			2	(2.5)	
323	544.819 ± 0.005	36.6 ± 1.1			2	(2.5)	
324	545.81 ± 0.01[c]	30.1 ± 2.2			(1	0.5)	
325	547.878 ± 0.005	47.0 ± 1.4			1	1.5	
326	550.170 ± 0.005	54.1 ± 1.5			2	(1.5)	
327	552.12	15.9			(1	0.5)	
328	552.534 ± 0.004	78.8 ± 1.5			1	1.5	
329	553.713 ± 0.006	2390. ± 16.			0	0.5	
330	553.89	29.7			2	(1.5)	
331	555.570 ± 0.008[c]	64.2 ± 2.0			1	1.5	
332	558.30	8.9			(2	1.5)	
333	559.725 ± 0.004	847. ± 13.			0	0.5	
334	560.425 ± 0.004	368. ± 9.			1	0.5	
335	566.36 ± 0.01[c]	23.5 ± 2.0			2	(1.5)	
336	567.72	7.9			(1	0.5)	
337	567.740 ± 0.014	9092. ± 33.			0	0.5	
338	569.550 ± 0.008[c]	52.2 ± 1.8			2	(1.5)	
339	574.193 ± 0.006	41.4 ± 1.3			2	(2.5)	
340	575.891 ± 0.003	410.0 ± 3.4			1	1.5	
341	582.537 ± 0.008	30.0 ± 1.2			2	2.5	
342	585.549 ± 0.005	178.4 ± 4.2			1	0.5	
343	587.695 ± 0.003	101.1 ± 1.3			2	2.5	
344	588.830 ± 0.006	2284. ± 15.			0	0.5	
345	591.848 ± 0.008	38.2 ± 1.9			1	1.5	
346	595.597 ± 0.003	127.1 ± 2.0			1	1.5	
347	598.52	6.8			(1	0.5)	
348	599.460 ± 0.007[c]	45.4 ± 1.5			2	(1.5)	
349	600.15	11.3			(1	0.5)	
350	600.622 ± 0.016	7845. ± 30.			0	0.5	
351	601.520 ± 0.004[c]	222.0 ± 3.1			2	1.5	
352	604.400 ± 0.002	313.4 ± 2.4			2	2.5	
353	609.440 ± 0.003	210.1 ± 2.7			2	1.5	
354	610.978 ± 0.002	271.1 ± 2.2			2	2.5	
355	612.47	22.7			(1	0.5)	

Table 2. (continued)

	E_0 (keV)	Γ_n (eV)	$g\Gamma_n\Gamma_\gamma/\Gamma$ (eV)	Γ_γ (eV)	ℓ^a	J^a	Notes
356	613.25 ± 0.02[c]	45.3 ± 5.0[c]			(1	0.5)	
357	613.60	22.7			(1	0.5)	
358	614.25	29.5			(1	0.5)	
359	616.51 ± 0.01	37.6 ± 1.8			2	(1.5)	
360	617.19	19.3			(1	0.5)	
361	618.202 ± 0.005	399. ± 6.			0	0.5	
362	618.31 ± 0.01	30.7			2	(1.5)	
363	622.168 ± 0.005	57.6 ± 1.5			2	(2.5)	
364	625.080 ± 0.005	109.0 ± 2.3			1	1.5	
365	627.100 ± 0.006[c]	997. ± 7.			2	1.5	
366	628.390 ± 0.008[c]	464. ± 8.			1	0.5	
367	629.590 ± 0.007[c]	97.6 ± 2.1			1	1.5	
368	630.970 ± 0.007[c]	155. ± 7.			0	0.5	
369	631.750 ± 0.006[c]	382. ± 9.			1	0.5	
370	631.97 ± 0.02[c]	79. ± 10.[c]			1	(1.5)	
371	633.040 ± 0.002	344.4 ± 2.3			2	2.5	
372	635.73 ± 0.01[c]	80.1 ± 2.1			(1	1.5)	
373	636.37 ± 0.02	9189. ± 45.			0	0.5	
374	636.51 ± 0.01[c]	72.0 ± 2.2			2	(1.5)	
375	637.06 ± 0.01[c]	131.0 ± 2.8			2	(1.5)	
376	640.454 ± 0.005	85.8 ± 1.8			2	(2.5)	
377	644.050 ± 0.008[c]	43.1 ± 1.5			2	(2.5)	
378	644.35	14.7			(1	1.5)	
379	646.041 ± 0.007	170.9 ± 4.7			1	0.5	
380	649.760 ± 0.006[c]	168.3 ± 2.5			2	(2.5)	
381	650.561 ± 0.003	521. ± 5.			1	1.5	
382	654.964 ± 0.003	342.6 ± 3.6			2	1.5	
383	656.84 ± 0.01[c]	16.9			(2	1.5)	
384	660.272 ± 0.006	1200. ± 12.			0	0.5	
385	661.115 ± 0.007	545. ± 9.			1	0.5	
386	664.94	11.5			(2	1.5)	
387	665.520 ± 0.004[c]	230.6 ± 3.0			1	1.5	
388	667.843 ± 0.004	155.7 ± 2.3			2	(1.5)	
389	668.60	9.0			(1	1.5)	
390	670.120 ± 0.017	5310. ± 29.			0	0.5	
391	670.650 ± 0.004[c]	201.1 ± 2.7			2	2.5	
392	672.820 ± 0.008[c]	237.4 ± 3.3			1	1.5	
393	673.620 ± 0.008[c]	87.3 ± 1.8			2	(2.5)	
394	674.993 ± 0.004	237.5 ± 3.2			2	1.5	
395	677.491 ± 0.006	99.1 ± 2.4			2	1.5	
396	678.570 ± 0.008[c]	40.2 ± 2.0			2	(1.5)	
397	680.610 ± 0.008[c]	64.1 ± 2.1			2	(1.5)	
398	681.650 ± 0.008[c]	49.6 ± 2.0			1	1.5	
399	686.739 ± 0.006	225. ± 6.			1	0.5	
400	690.319 ± 0.008	71.4 ± 2.5			1	1.5	

Table 2. (continued)

	E_0 (keV)	Γ_n (eV)	$g\Gamma_n\Gamma_\gamma/\Gamma$ (eV)	Γ_γ (eV)	ℓ^a	J^a	Notes
401	691.254 ± 0.003	528. ± 5.			2	1.5	
402	692.55	54.2			(1	0.5)	
403	693.00 ± 0.01[c]	104. ± 15.[c]			2	(1.5)	
404	693.565 ± 0.002	303.5 ± 2.8			2	2.5	
405	695.556 ± 0.007	825. ± 17.			0	0.5	
406	696.162 ± 0.005	398. ± 5.			1	1.5	
407	698.03	28.2			2	(1.5)	
408	699.085 ± 0.006	1199. ± 15.			0	0.5	
409	700.77	24.8			1	(0.5)	
410	703.119 ± 0.006	1169. ± 16.			1	0.5	
411	705.480 ± 0.006[c]	418. ± 9.			1	0.5	
412	707.092 ± 0.003	361.4 ± 4.0			1	1.5	
413	708.417 ± 0.003	253.4 ± 2.5			2	2.5	
414	711.010 ± 0.004	214.0 ± 3.0			2	1.5	
415	712.38 ± 0.01[c]	131.0 ± 4.7			1	0.5	
416	712.80	9.7			(1	1.5)	
417	713.10	33.9			1	(0.5)	
418	714.690 ± 0.004	111.5 ± 1.8			2	(2.5)	
419	715.715 ± 0.005	141.9 ± 2.5			1	(1.5)	
420	718.62 ± 0.01[c]	18.2 ± 1.4			2	(1.5)	
421	719.702 ± 0.006	60.8 ± 1.7			2	(2.5)	
422	720.291 ± 0.018	5303. ± 40.			0	0.5	
423	720.94 ± 0.01[c]	92.1 ± 3.4			(1	1.5)	
424	723.05	8.5			(2	1.5)	
425	728.15	20.7			2	(1.5)	
426	731.70	24.8			(0	0.5)	
427	732.142 ± 0.004	243.9 ± 3.1			2	1.5	
428	732.75	28.2			(1	0.5)	
429	734.00	47.			2	(2.5)	
430	734.142 ± 0.003	513.1 ± 4.2			2	1.5	
431	735.50	16.9			(1	0.5)	
432	737.247 ± 0.007	87.2 ± 2.3			2	(1.5)	
433	738.194 ± 0.011	3885. ± 42.			0	0.5	
434	740.10	31.6			(1	0.5)	
435	740.908 ± 0.006	320. ± 7.			1	0.5	
436	744.44	18.0			(1	1.5)	
437	745.198 ± 0.003	439.6 ± 4.1			2	1.5	
438	746.260 ± 0.004[c]	243.9 ± 3.9			2	1.5	
439	746.36	50.			2	(2.5)	
440	746.87	29.8			(2	1.5)	
441	747.729 ± 0.037	21499. ± 99.			0	0.5	
442	747.97 ± 0.01[c]	31.7 ± 2.8			(2	2.5)	
443	749.50	24.8			(1	0.5)	
444	749.955 ± 0.005	161.6 ± 3.0			1	1.5	
445	750.40	15.4			(2	1.5)	
446	751.80 ± 0.015	206.1 ± 4.8			2	(1.5)	
447	752.15 ± 0.02	101.4 ± 2.9			2	(2.5)	
448	753.702 ± 0.008	1185. ± 25.			0	0.5	

Table 2. (continued)

	E_0 (keV)	Γ_n (eV)	$g\Gamma_n\Gamma_\gamma/\Gamma$ (eV)	Γ_γ (eV)	ℓ^a	J^a	Notes
449	759.01 ± 0.01[c]	123. ± 5.			1	0.5	
450	759.98	52.			(1	0.5)	
451	761.05 ± 0.01[c]	60.4 ± 2.5			2	(1.5)	
452	762.29 ± 0.008[c]	245. ± 7.			1	0.5	
453	764.12	27.			(2	1.5)	
454	765.05 ± 0.01[c]	64.0 ± 2.7			1	(1.5)	
455	768.713 ± 0.011	4121. ± 28.			0	0.5	
456	775.156 ± 0.007	432. ± 9.			0	0.5	
457	776.059 ± 0.005	476. ± 5.			2	1.5	
458	778.270 ± 0.008[c]	93.4 ± 2.2			2	(2.5)	
459	780.02 ± 0.006[c]	124.6 ± 2.6			2	(2.5)	
460	781.42	20.3			(1	1.5)	
461	782.140 ± 0.005[c]	208.3 ± 3.2			2	1.5	
462	783.996 ± 0.005	214.5 ± 3.4			1	1.5	
463	784.663 ± 0.019	7361. ± 47.			0	0.5	
464	789.31	20.3			(1	0.5)	
465	790.40	22.5			(1	0.5)	
466	791.155 ± 0.005	171.0 ± 2.4			2	(2.5)	
467	792.600 ± 0.006[c]	269.3 ± 4.0			2	1.5	
468	793.40 ± 0.01[c]	73.4 ± 2.9			1	(1.5)	
469	795.80	44.			(1	0.5)	
470	796.42 ± 0.01[c]	73.8 ± 2.8			1	1.5	
471	797.45	36.0			(1	0.5)	
472	798.535 ± 0.016	5018. ± 44.			0	0.5	
473	800.661 ± 0.004	262.4 ± 3.3			2	2.5	
474	801.45 ± 0.01[c]	104.6 ± 3.5			2	1.5	
475	802.70	36.6			(0	0.5)	
476	804.82 ± 0.01[c]	34.5 ± 2.3			1	(1.5)	
477	806.96 ± 0.01[c]	46.2 ± 2.9			1	1.5	
478	809.290 ± 0.006	133.9 ± 2.6			2	2.5	
479	811.05	39.4			(1	0.5)	
480	821.5 ± 0.5	1.12E+4 ± 8.E+2			0	0.5	1
481	868.	8.0E+3 ± 2.5E+3			0	0.5	1
482	1000.	2.00E+5 ± 4.E+3			0	0.5	1

[a]parentheses are used to indicate that the assignment is uncertain.

[b]This resonance is seen in both data sets, but its energy is better defined in the capture data; therefore, the uncertainty obtained from the fit to the capture data is given.

[c]This parameter was not adjusted in the final transmission fit with SAMMY. This uncertainty was obtained from earlier fits to the data.

Note 1. Fictitious *s*-wave resonance outside the range of the analysis.

Note 2. Resonance seen in capture data only. The value of the neutron width, Γ_n, was chosen to be consistent with the transmission data. When possible, the radiation width, Γ_γ, was arbitrarily set at 0.50 eV. The uncertainty given for the energy of the resonance was obtained from the fit to the capture data.

Note 3. The capture kernel and the radiation width were corrected for the neutron sensitivity of the detector. The uncertainties given for these parameters include the large uncertainties due to this correction which are combined with the statistical uncertainties.

together and treated as a single Gaussian resolution function whose full width at half maximum (FWHM) is shown as a function of the neutron incident energy in Fig. 1. The code includes an approximate correction for attenuation in the sample but no correction for multiple scattering.

The comparison of the experimental data for four elastic-scattering angles with the theoretical calculations for the resonance at 82.88 keV (Fig. 2) illustrates how the spin and parity of a well separated resonance, clearly seen in the transmission and differential elastic scattering data, can be assigned without any ambiguity. The two full lines, for each of the four angles shown, are the theoretical curves obtained with an angular orbital momentum, ℓ, equal to 1 and a spin of 1/2 (thin line) or 3/2 (thick line). The dashed line is obtained with $\ell = 2$ and a spin of 3/2. The three theoretical curves for the 39° angle do not display any striking differences: the shapes are similar, only the positions and the amplitudes are slightly different whereas at 90° the shapes for the $\ell = 1$ and the $\ell = 2$ resonances are very different. From this observation on the 90° data we can conclude that this resonance is a p-wave resonance and, most likely, has a spin of 3/2 since the agreement between the data and the thick line curve is much better than with the thin one (note that both curves display the proper symmetrical shape.) At 90° an important feature of the data is that the $\ell = 1$ resonances have a symmetrical shape about the resonance energy whereas the $\ell = 2$ resonances have an asymmetrical shape. As was the case at 39°, the curves at 120° are not very different but seem to confirm the $p_{3/2}$ assignment for this resonance. The theoretical calculations at 160° show (as was the case at 90°) a striking difference in the shape of the curves corresponding to a $\ell = 1$ and a $\ell = 2$ resonance. The data at 160° are also in better agreement with the thick line curve than with the thin one. Therefore a $p_{3/2}$ assignment is adopted with a good degree of confidence.

Unfortunately few cases are as clear as this one because the resonances are either too weak or show interference with large s-wave resonances. Above 200 keV many of the resonances are multiplets, and this makes assignment of spin and parity difficult but still possible for some resonances.

The difference in the amplitudes at 39°, 90°, and 160° for a $p_{1/2}$ and a $p_{3/2}$ resonance is often large enough to distinguish between the two possible spins of a p-wave resonance. This is usually not true in the case of a d-wave resonance. For clarity the theoretical curve calculated for a $d_{5/2}$ resonance was not shown on Fig. 2. At 39° the curves for $d_{3/2}$ and $d_{5/2}$ resonances are almost indistinguishable. At 90° and 160° the amplitudes are slightly larger for a $d_{5/2}$ than for a $d_{3/2}$ resonance; therefore, very few spin assignments are possible for d-wave resonances.

In a few cases when good agreement between the theoretical calculations and the data could not be obtained with a combination of p- and d-wave resonances, f-wave resonances ($\ell = 3$) were tried but without any noticeable improvement; therefore, no resonance in Table 2 has an ℓ assignment larger than 2.

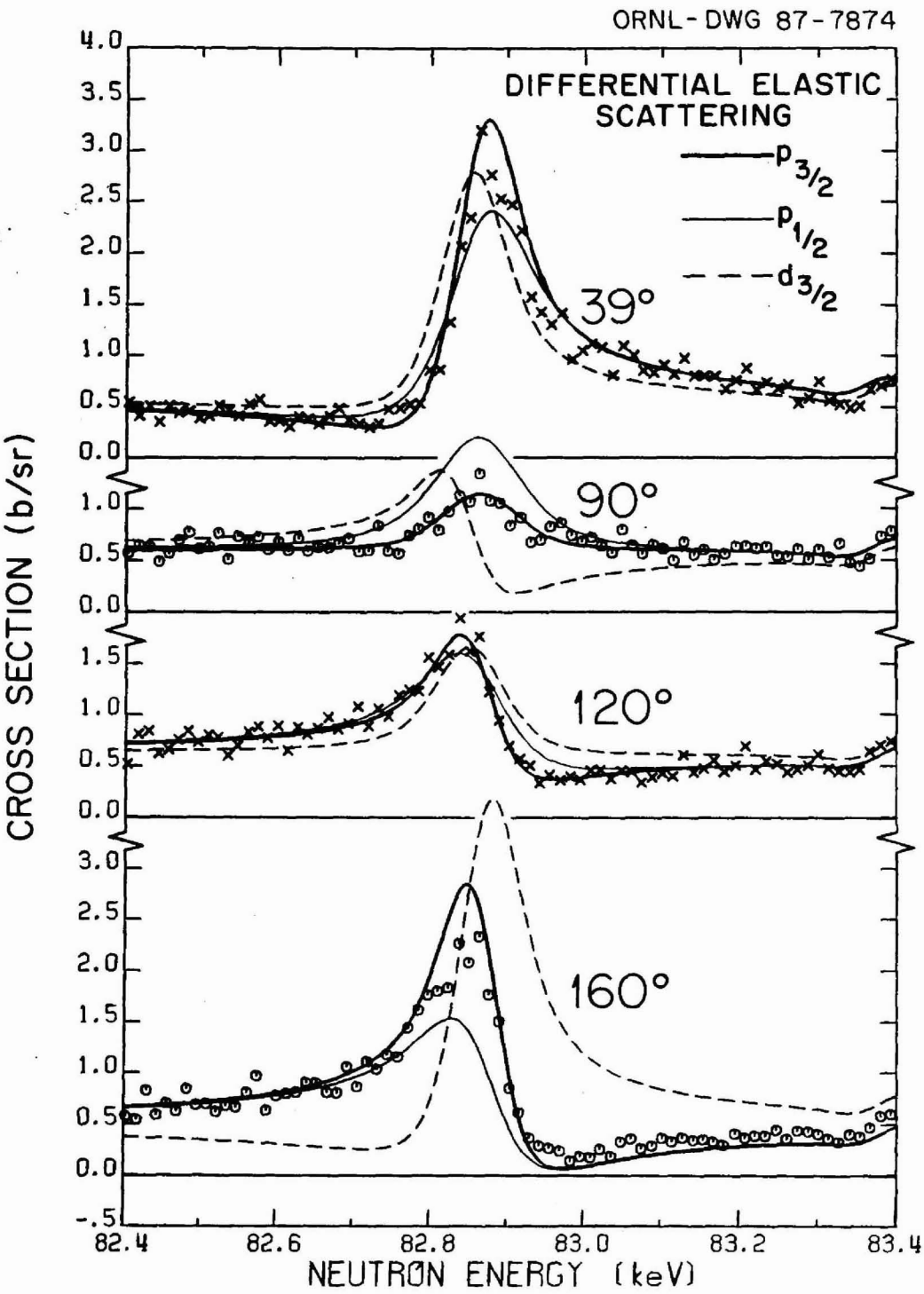

Fig. 2. The theoretical calculations with three different spin and parity assignments are compared with the data for four of the six elastic scattering angles to illustrate that the $p_{3/2}$ assignment for this resonance is unequivocal.

3.4 CAPTURE DATA ANALYSIS

The corrected data were converted to effective cross section vs neutron energy and fitted to resonance parameters by least-squares adjustment using the Breit-Wigner formula through the computer code LSFIT (MAC76). The program iterates upon trial parameters applying corrections for energy resolution, Doppler width, self-shielding, and multiple scattering.

Although the manner in which corrections for self-shielding and multiple scattering are done in LSFIT has been described before (MAC76, GAR78), since these corrections are only approximate for some of the resonances analyzed in this paper, we will briefly review how LSFIT performs these corrections. When performing corrections for self-shielding and multiple scattering, LSFIT makes the assumption that every resonance is isolated, even though in a given energy region analyzed there may be several resonances close to each other and even some narrow resonances within the width of a broad s-wave resonance. In LSFIT the self-shielding and multiple-scattering corrections are performed differently depending upon whether a resonance is considered "broad" or "narrow". The criterion used to classify a resonance as broad or narrow is the energy loss that a neutron suffers in being scattered through 90 degrees in the sample. In the vicinity of a resonance at energy E_r, neutrons scattered through 90 degrees lose an energy approximately equal to $2E_r/(A+1)$, where A is the target nuclide atomic number. If the total width of a resonance is less than 15% of the energy loss suffered by a neutron in a 90-degree collision, the resonance is treated as narrow; if it is larger than this value it is assumed broad.

For a narrow resonance the total cross section used for performing the self-shielding is calculated as the sum of the resonance total cross section and a non-interfering constant potential scattering, provided as an input number to the code for the complete energy region for which the data are being analyzed simultaneously, an energy region which may contain as many as 16 resonances. For narrow resonances, the multiple-scattering contribution to the capture yield (MAC76) is based upon the product of the capture area of a resonance and the average potential scattering in the energy region being analyzed. This procedure was tested by comparison with more exact calculations in the case of isolated narrow resonances and works well for extracting both s-wave and p-wave resonance capture parameters.

A different method is used in LSFIT to calculate in greater detail the multiple-scattering contribution due to broad resonances. This feature was also tested with Monte Carlo calculations (GAR78). All broad resonances are treated as s-waves and the total cross section, calculated with the single-level Breit-Wigner formula, includes an interference term between the resonance amplitude and the potential scattering specified at the resonance energy. Although in ^{58}Ni there are frequently narrow resonances in the vicinity of large s-waves and both the scattering and

capture from these narrow resonances are ignored, it is not thought that this seriously affects the multiple-scattering contribution calculated by LSFIT for broad resonances.

In ^{58}Ni above 150 keV and in particular in the vicinity of the large s-wave resonances, the assumptions concerning the total cross sections in LSFIT for performing the self-shielding and multiple-scattering calculations may lead to severe under- or over-estimation of the corrections applied to the narrow resonances. In order to calculate the multiple-scattering contribution to the observed capture yields one needs the values of the scattering and capture cross sections in the vicinity of each resonance, in particular above the resonance energies.

In order to test the validity of the self-shielding and multiple-scattering corrections performed by LSFIT, exact calculations were made for the self-shielding of some ^{58}Ni resonances, using total cross sections based upon the analysis of the transmission data. Exact calculations were also made for the contributions due to capture following one elastic scattering, including angular distribution effects based upon the scattering data; but an approximation was used in treating capture following two elastic scatterings. The corrections calculated by LSFIT were found to be very good for isolated narrow resonances. However, in the vicinity of large s-waves the capture areas determined by LSFIT were found to be over or underpredicted by as much as 10%.

The thin sample capture data were analyzed up to 22 keV and the thick sample data were used above 22 keV and up to 450 keV. At still higher energies average corrections for sample thickness were applied to the thick sample data to derive average neutron capture cross sections as detailed in Section 6.7

For the resonances seen clearly in both data sets energies and neutron widths were taken from the transmission data analysis. Between 5 and 450 keV about 30% more resonances were seen in the capture data than in the transmission data. For these 61 resonances only the resonance energies and the capture kernels, $g\Gamma_n\Gamma_\gamma/(\Gamma_n+\Gamma_\gamma)$, are defined. The neutron widths were set to be consistent with the lack of observation in the transmission data and, when possible, their radiation widths were set equal to 0.5 eV with spin and parity of a p resonance. However, as explained in Section 3.2, four of these resonances were assigned as s-wave.

The effective Gaussian resolution, FWHM, of the analyzed capture data is shown as a function of the neutron incident energy in Fig. 1. Since these data showed a small low-energy (i.e., time-delayed) tail on the usual Gaussian resolution function, a resolution shape modification was included in the code. The fraction of the neutrons which showed an asymmetric resolution function was 15% at 6 keV increasing up to 50% for 200-keV neutrons. The asymmetric part is convoluted with an exponential whose time constant is given as a fraction of the Gaussian resolution. Here the decay constant is 69% of the resolution.

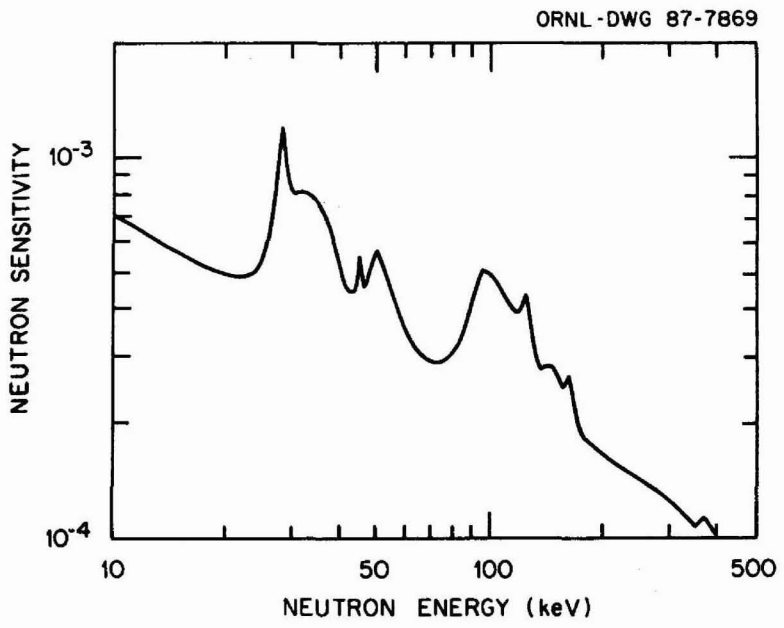

Fig. 3. Detector neutron sensitivity as a function of the incident neutron energy for the ^{58}Ni targets. Note 3 in Table 2 indicates the resonances for which this correction applies. See Section 3.4 for details.

A correction for the capture in the detector environment of neutrons scattered from discrete resonances in the sample is required (ALL77). This prompt neutron sensitivity can be formulated as a correction to the radiation width such that $\Gamma_\gamma(\text{corr.}) = \Gamma_\gamma - C\Gamma_n$, where C is dependent on the amount and distribution of absorber in the vicinity of the detector. This correction factor is energy dependent and varies from 10^{-4} to 10^{-3} over the energy range of this analysis, as shown in Fig. 3, with an uncertainty of ~40%. Note 3 in Table 2 indicates the 19 s-wave resonances below 450 keV for which the radiation widths and capture kernels were corrected for this effect.

As discussed in Section 2.3.3, because of the incorrect weighting function used in acquiring the capture data some of the radiation widths given in Table 2 may be too large by as much as 16%.

4. RESULTS AND DISCUSSION OF THE UNCERTAINTIES

4.1 RESONANCE PARAMETERS AND THEIR UNCERTAINTIES

The resonance parameters obtained from the simultaneous analyses of the ^{58}Ni transmission, capture and differential elastic-scattering data as described in Section 3 are given in Table 2. The fits to the transmission and capture data obtained with this set of resonance parameters and the comparison of the theoretical calculations with the differential elastic scattering data are shown in Fig. 4 to 44.

In Table 2 the groups of resonances corresponding to each figure are separated by a blank line. The first column gives the resonance numbers. The next four columns show the energies of the resonances, the neutron widths, the capture kernels, and the radiation widths with their uncertainties given either by the fit to the transmission data through the code SAMMY or by the fit to the capture data through the code LSFIT. The orbital angular momentum ℓ and the spin J for each level are given in columns 6 and 7. Parentheses indicate that assignments are uncertain. The numbers in the last column correspond to notes found at the end of the table. Brackets are used to indicate unresolved resonances either in the transmission data (brackets in the third column) or in the capture data (brackets in the fourth column.) Above 200 keV more resonances are unresolved in the capture data than in the transmission data since, in this region, the 200-m transmission data are used which have much better energy resolution than the capture data ($\sim$110 eV, FWHM, compared to $\sim$400 eV at 200 keV.) See Fig 1.

The uncertainties given by the code SAMMY on the 459 parameters adjusted in the last fit to the transmission data are given in Table 2. The covariance matrix associated with these 459 adjusted parameters is available. A representative sample of this covariance matrix for the uncertainties of 17 of the 459 adjusted parameters is given in Table 3.

In Table 2 the footnote "c" associated with some of the resonance energies and neutron widths indicates that these parameters were not adjusted in the last fit to the transmission data but were adjusted in earlier fits; therefore the correlation coefficients associated with the uncertainties of these parameters are not included in the final covariance matrix.

Between 5 and 450 keV, where the capture data were also analyzed, 61 resonances seen clearly in capture were too weak to be detected in the transmission data (Note 2 in Table 2); also 43 resonances analyzed in both data sets were seen more clearly in the capture data than in the transmission data (footnote "b" in the first column of Table 2.) In the case of these 104 resonances the energy of the resonances and their uncertainties were obtained from the fit to the capture data.

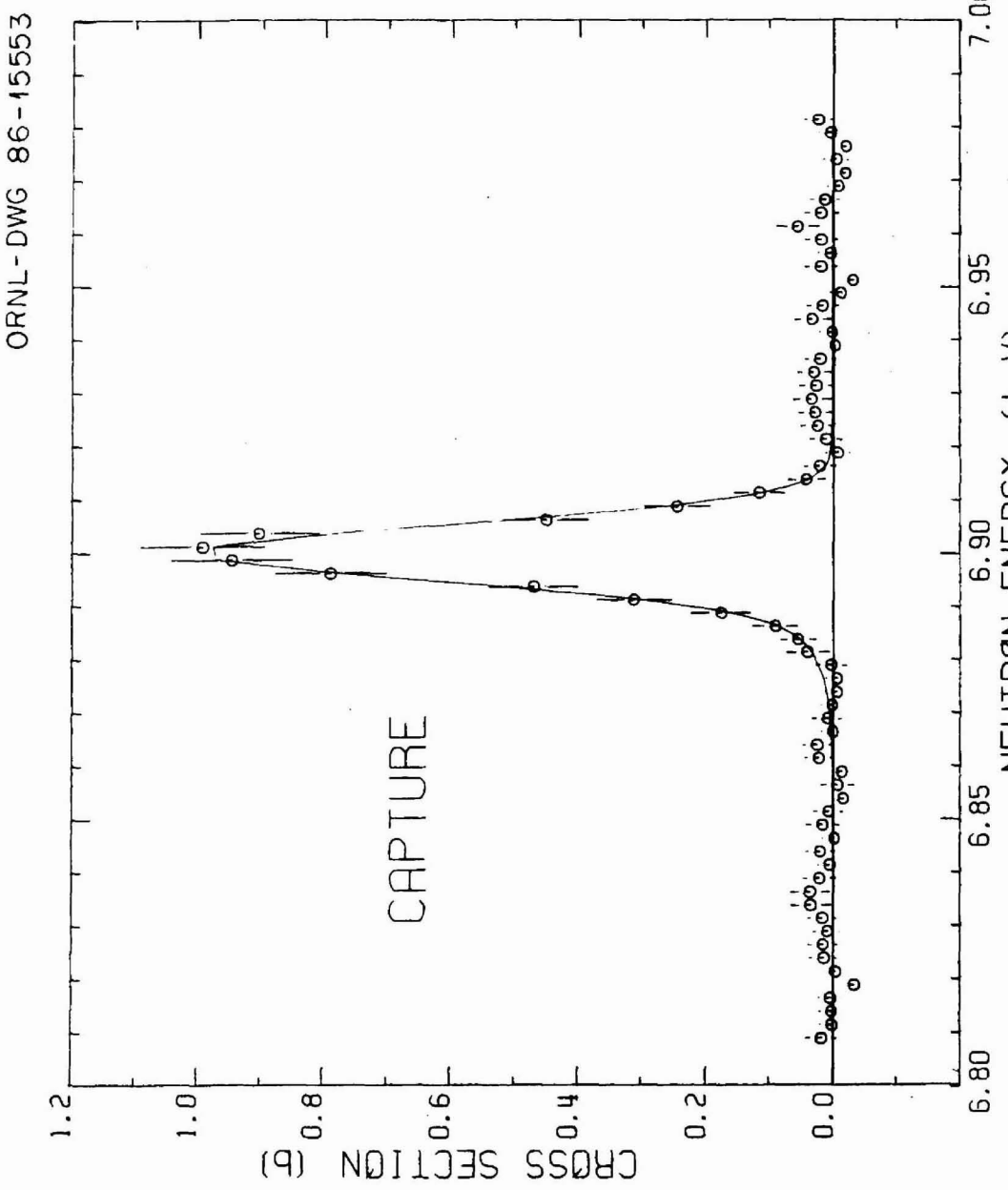

Fig. 4. Fit to the capture data for the resonance at 6.906 keV. The thin ^{58}Ni sample (0.0038 atoms/b) was used.

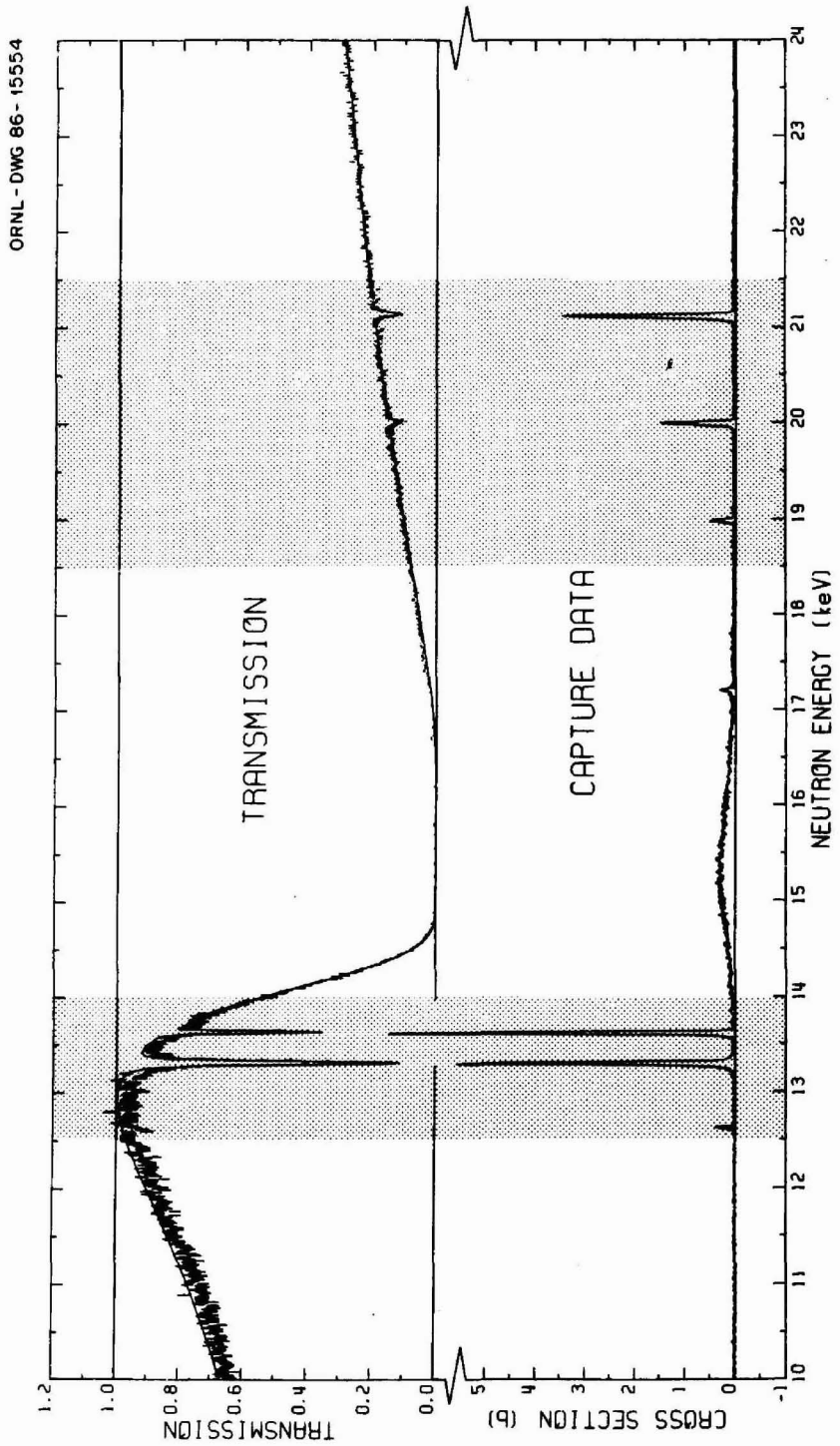

Fig. 5. The fit to the 78-m transmission data taken with the ^{6}Li-glass detector is shown from 10 to 24 keV, along with the capture data obtained with the thin ^{58}Ni sample (0.0038 atoms/b).

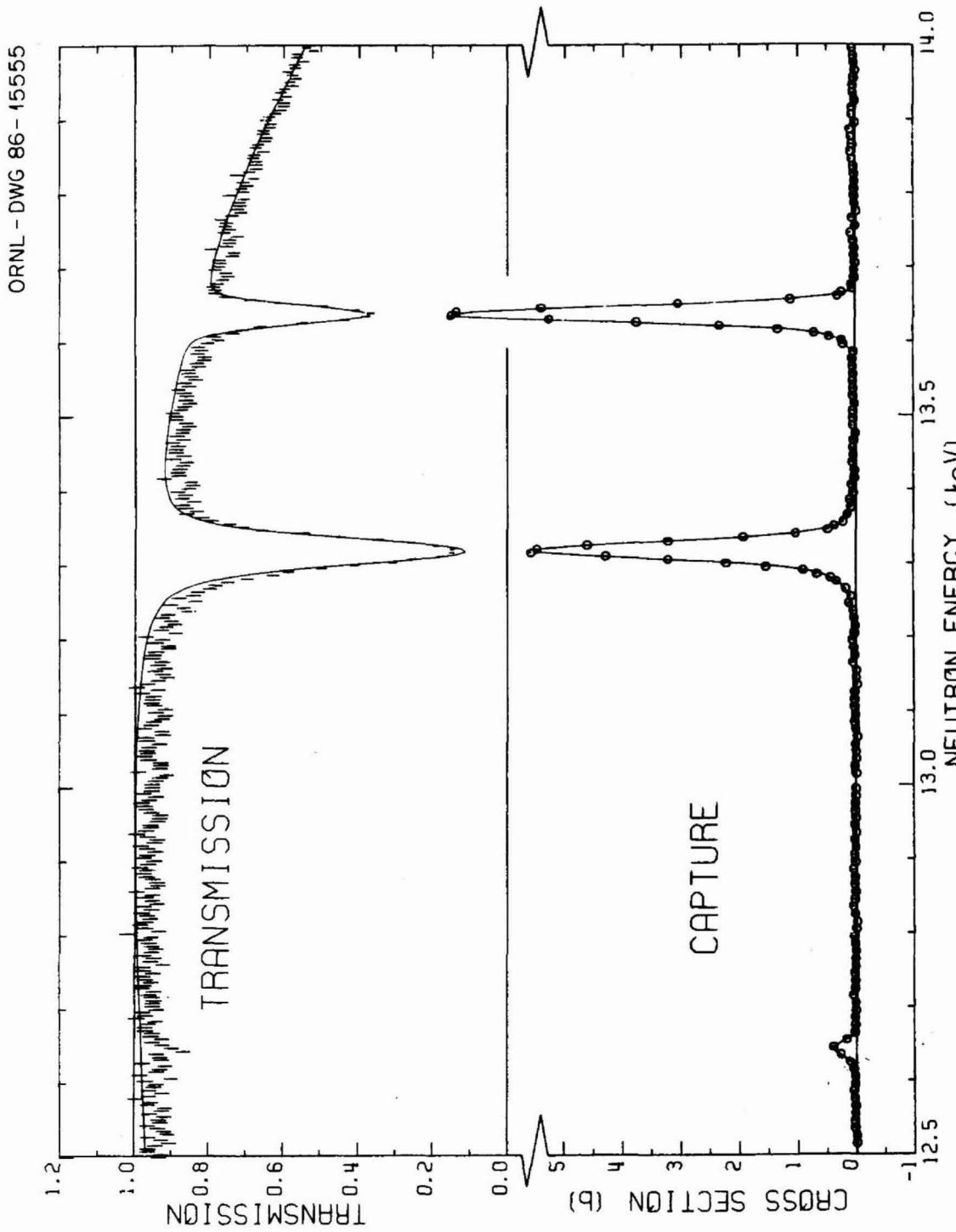

Fig. 6. The first shaded area of Fig. 5 was enlarged to show in detail the simultaneous fits to the transmission and capture data between 12.5 and 14 keV obtained with the parameters of Table 2.

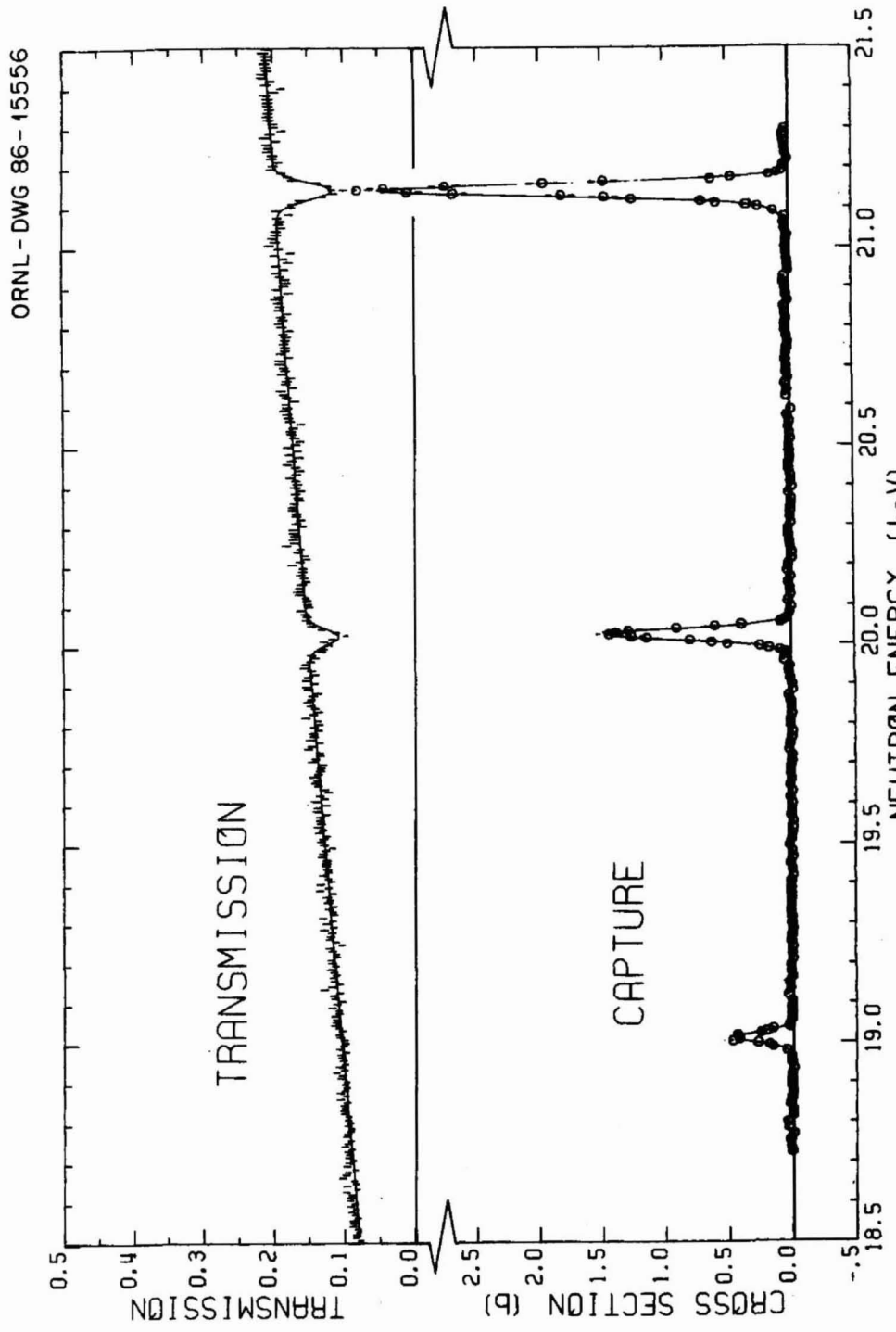

Fig. 7. The second shaded area of Fig. 5 was enlarged to show in detail the simultaneous fits to the transmission and capture data between 18.5 and 21.5 keV obtained with the parameters of Table 2.

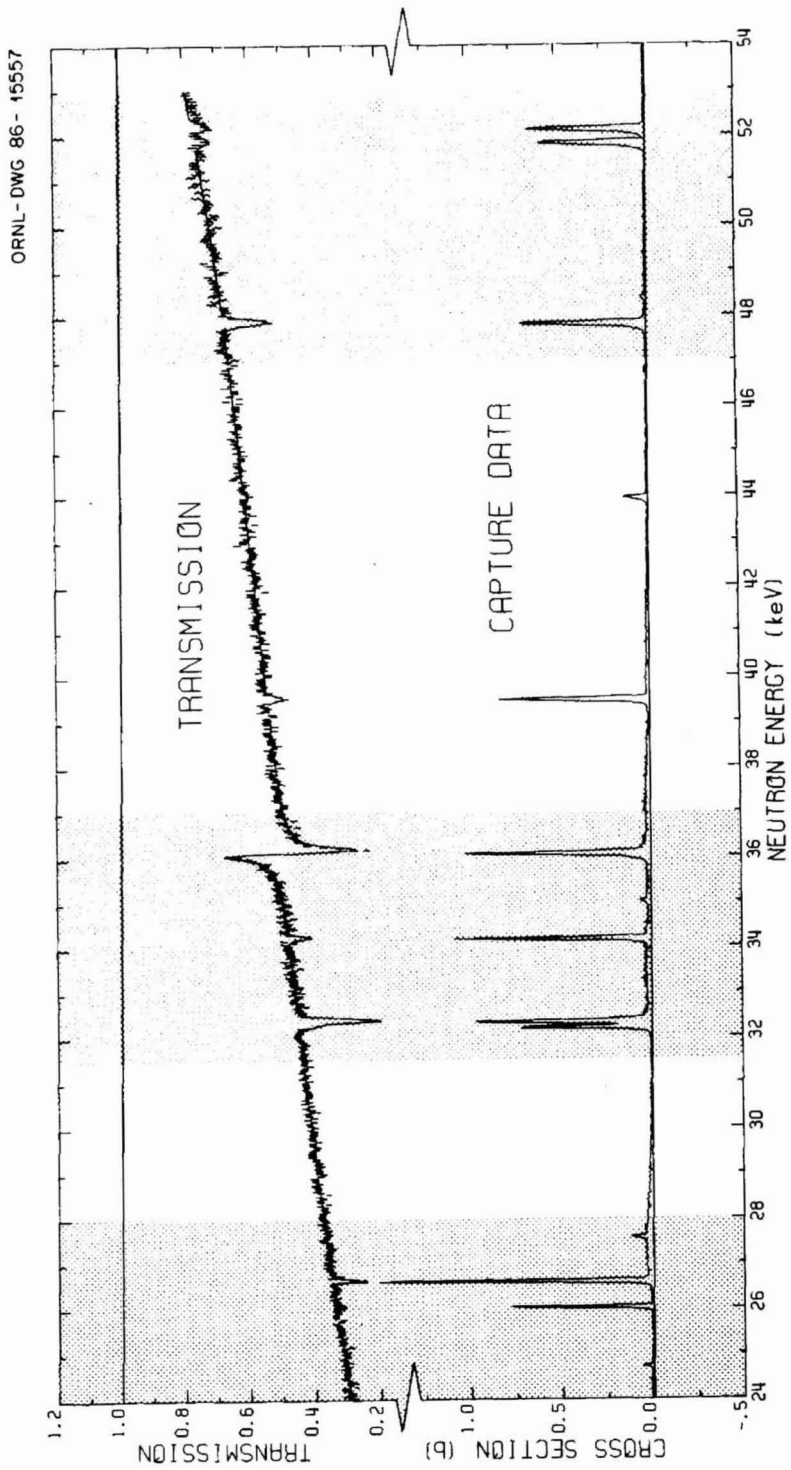

Fig. 8. The fit to the 78-m transmission data taken with the ^{6}Li-glass detector is shown from 24 to 53 keV, along with the capture data obtained with the thick ^{58}Ni sample (0.0382 atoms/b).

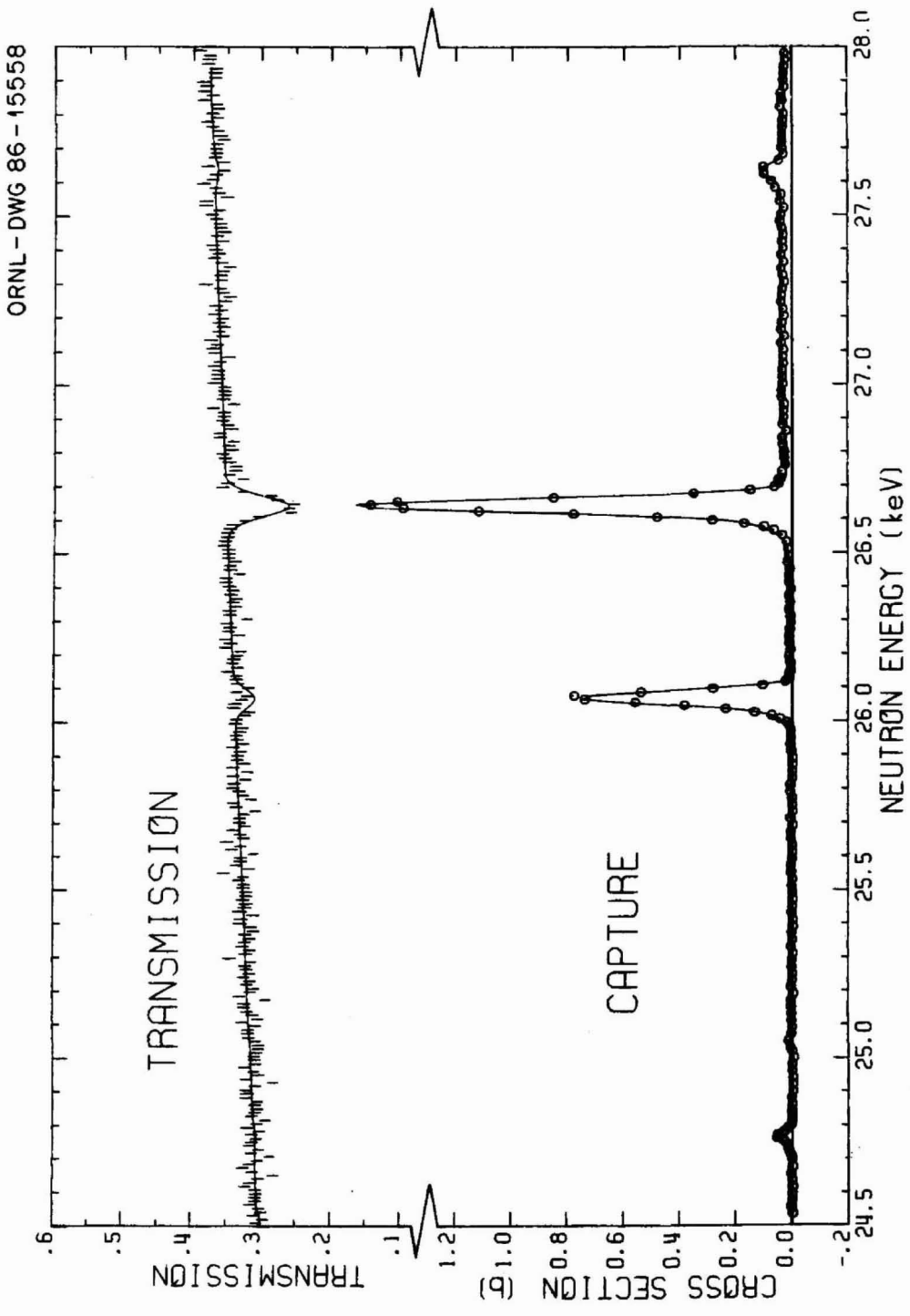

Fig. 9. The first shaded area of Fig. 8 was enlarged to show in detail the simultaneous fits to the transmission and capture data between 24.5 and 28 keV obtained with the parameters of Table 2.

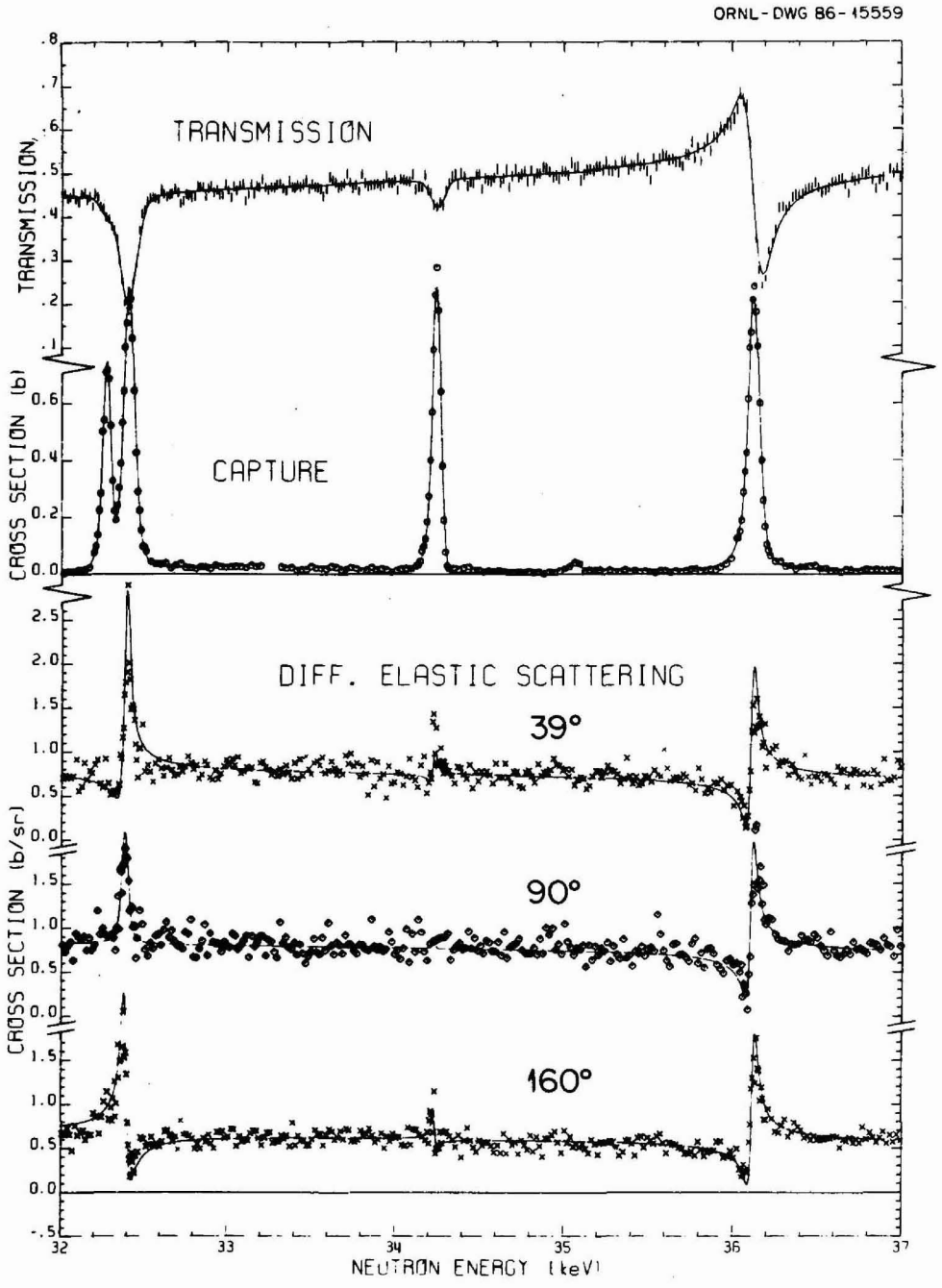

Fig. 10. TOP: The second shaded area of Fig. 8 was enlarged to show in detail the simultaneous fits to the transmission and capture data between 32 and 37 keV obtained with the parameters of Table 2. BOTTOM: The data for three of the six differential elastic-scattering angles are compared with the theoretical cross sections calculated with the same parameters as above. The combination of spins and parities adopted is the one which yields the best agreement with the elastic-scattering data.

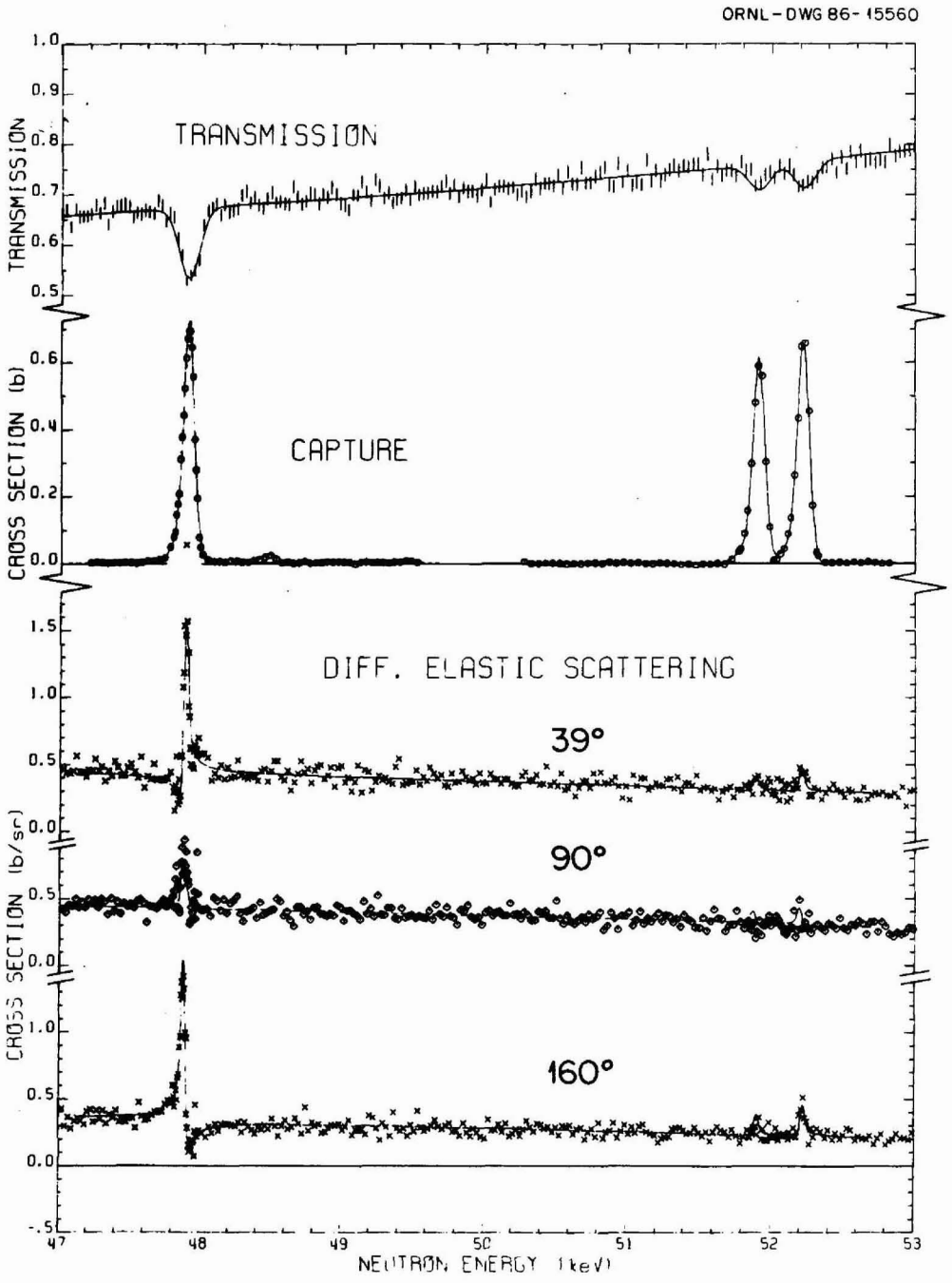

Fig. 11. TOP: The last shaded area of Fig. 8 was enlarged to show in detail the simultaneous fits to the transmission and capture data between 47 and 53 keV obtained with the parameters of Table 2. BOTTOM: The data for three of the six differential elastic-scattering angles are compared with the theoretical cross sections calculated with the same parameters as above. The combination of spins and parities adopted is the one which yields the best agreement with the elastic-scattering data.

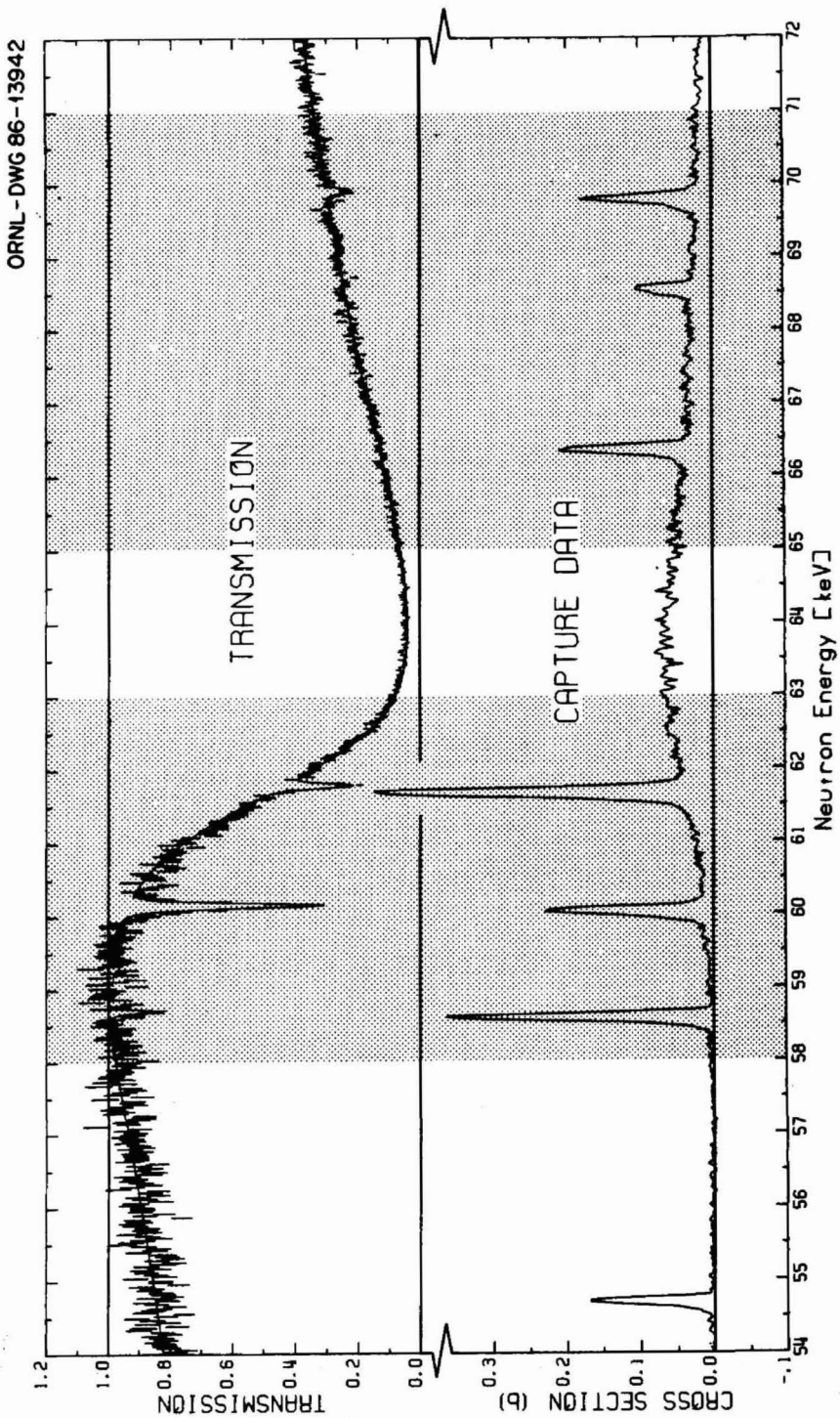

Fig. 12. The fit to the 78-m transmission data taken with the NE-110 detector is shown from 54 to 72 keV, along with the capture data obtained with the thick ^{58}Ni sample (0.0382 atoms/b).

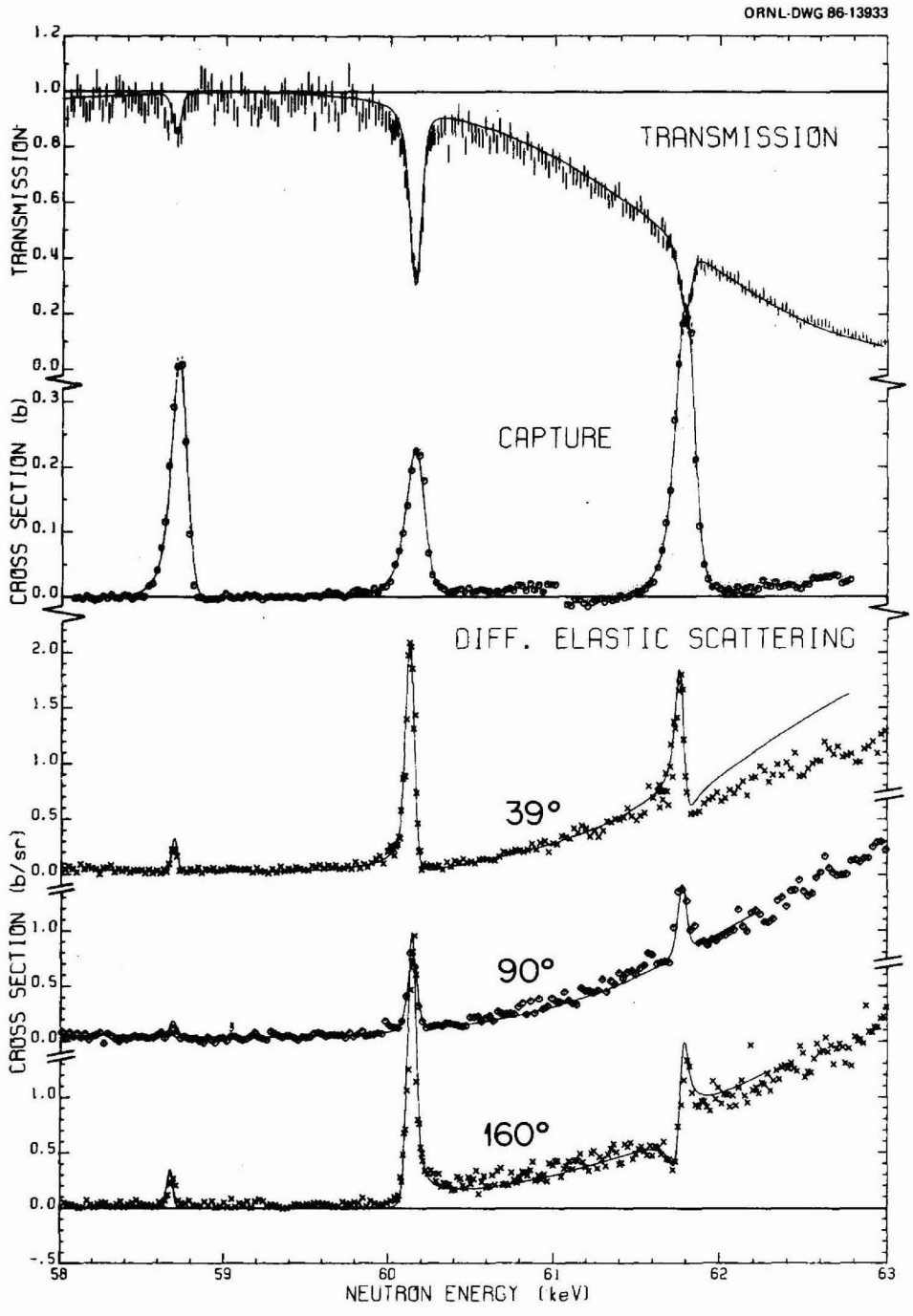

Fig. 13. TOP: The first shaded area of Fig. 12 was enlarged to show in detail the simultaneous fits to the transmission and capture data between 58 and 63 keV obtained with the parameters of Table 2. BOTTOM: The data for three of the six differential elastic-scattering angles are compared with the theoretical cross sections calculated with the same parameters as above. The combination of spins and parities adopted is the one which yields the best agreement with the elastic-scattering data.

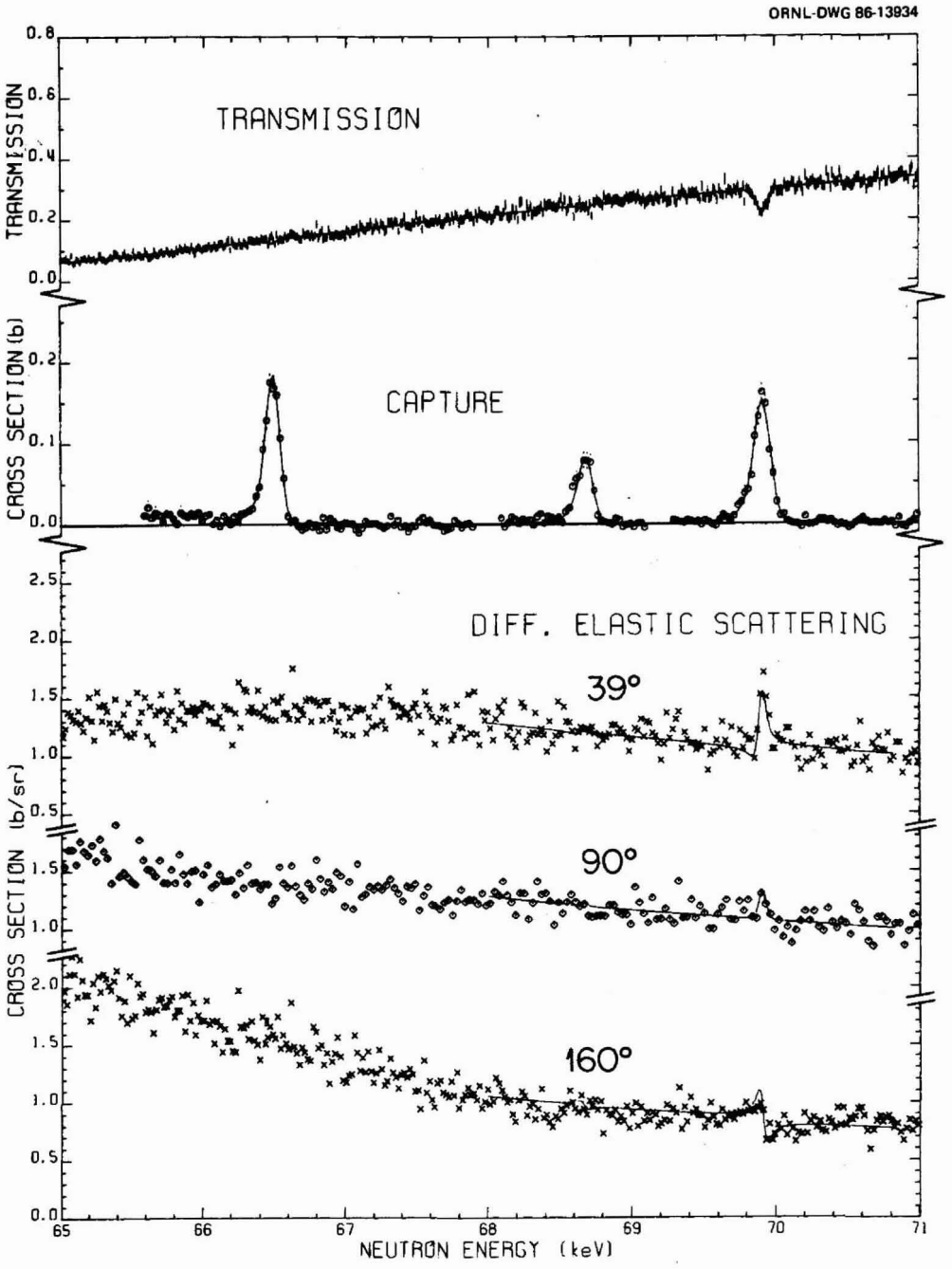

Fig. 14. TOP: The second shaded area of Fig. 12 was enlarged to show in detail the simultaneous fits to the transmission and capture data between 65 and 71 keV obtained with the parameters of Table 2. BOTTOM: The data for three of the six differential elastic-scattering angles are compared with the theoretical cross sections calculated with the same parameters as above. The combination of spins and parities adopted is the one which yields the best agreement with the elastic-scattering data.

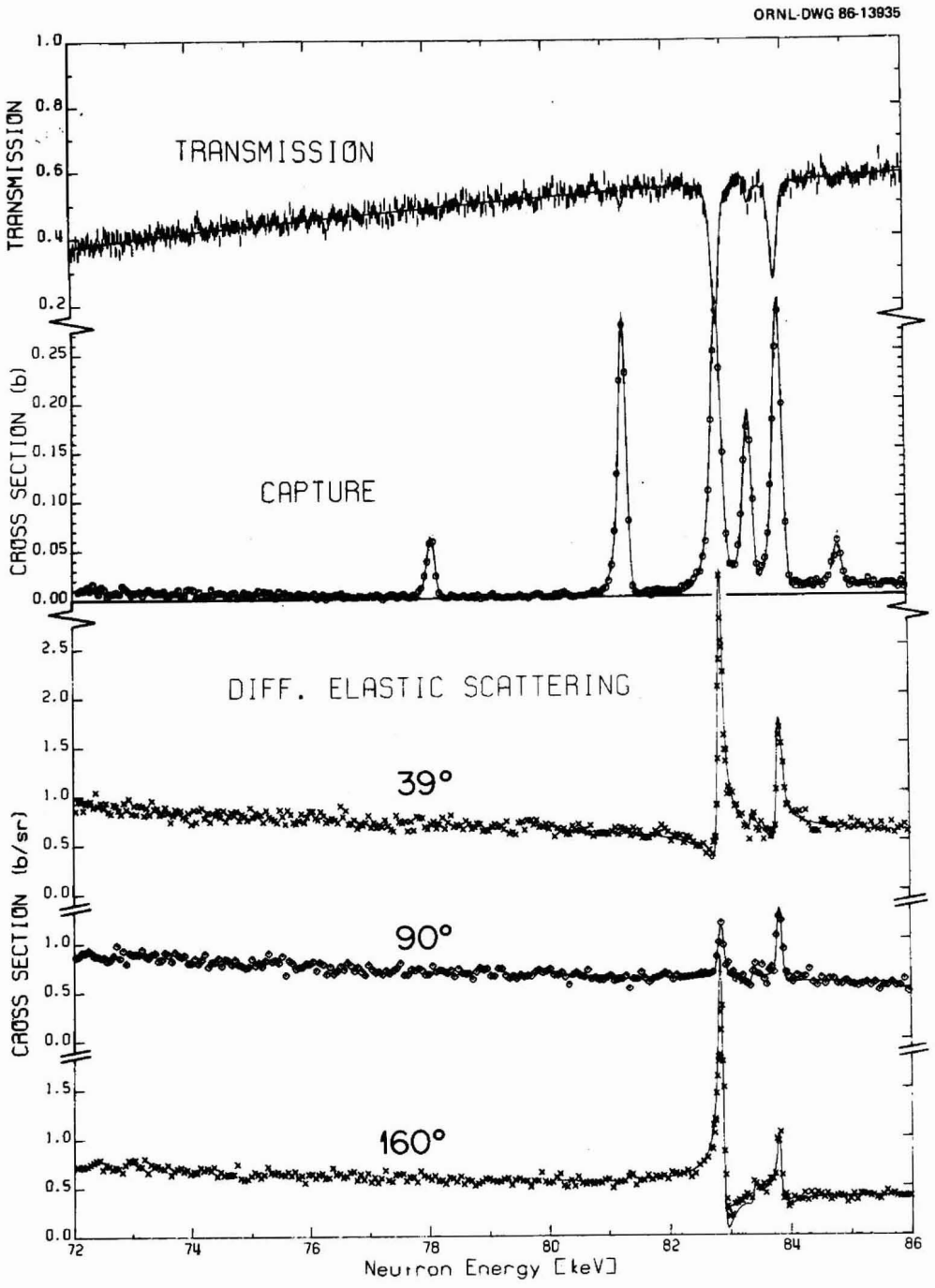

Fig. 15. TOP: Simultaneous fits, from 72 to 86 keV, to the 78-m transmission data taken with the NE-110 detector and to the capture data obtained with the thick ^{58}Ni sample (0.0382 atoms/b). The theoretical curves were calculated with the parameters of Table 2. BOTTOM: The data for three of the six differential elastic-scattering angles are compared with the theoretical cross sections calculated with the same parameters as above. The combination of spins and parities adopted is the one which yields the best agreement with the elastic-scattering data.

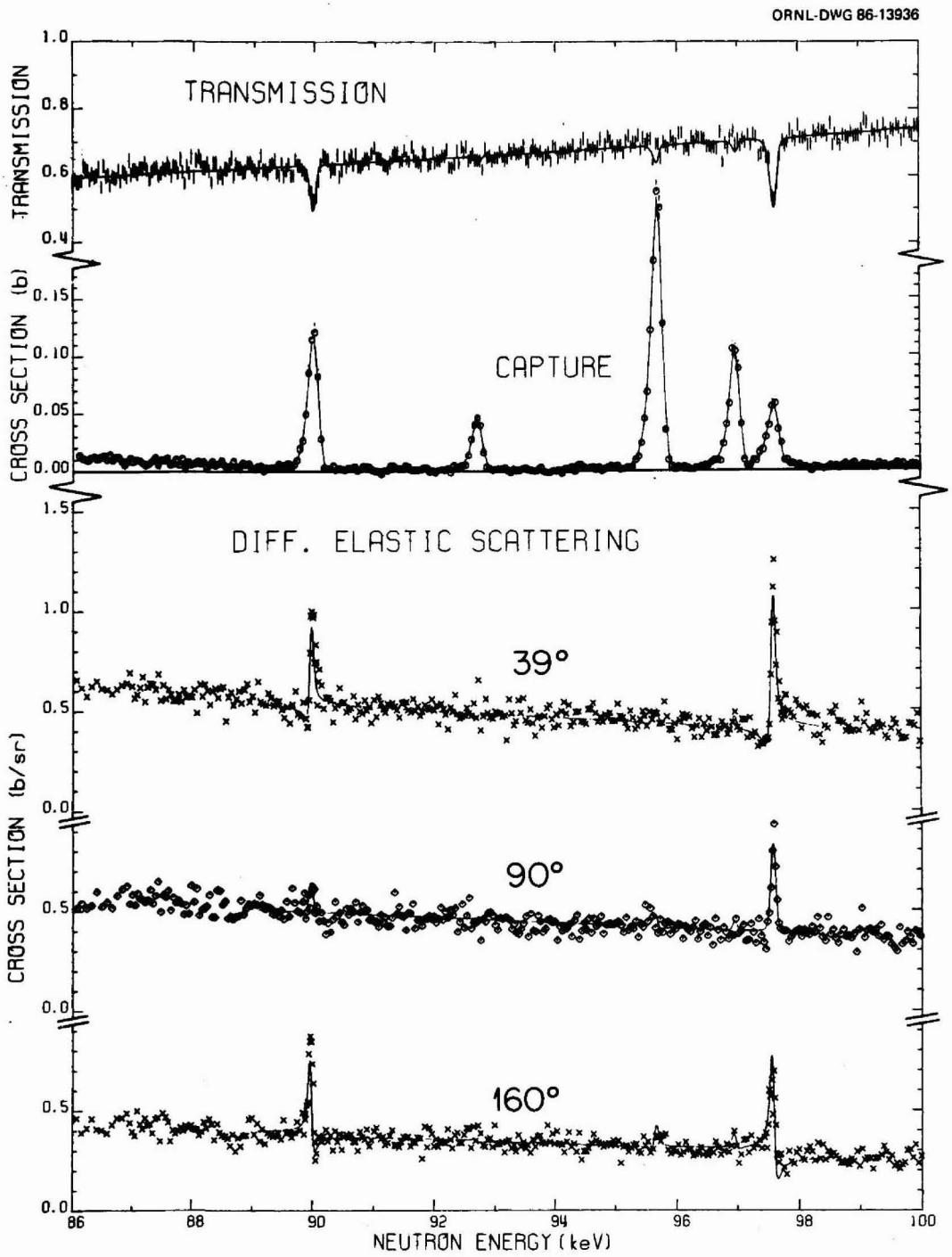

Fig. 16. Same as Fig. 15 except for 86 to 100 keV.

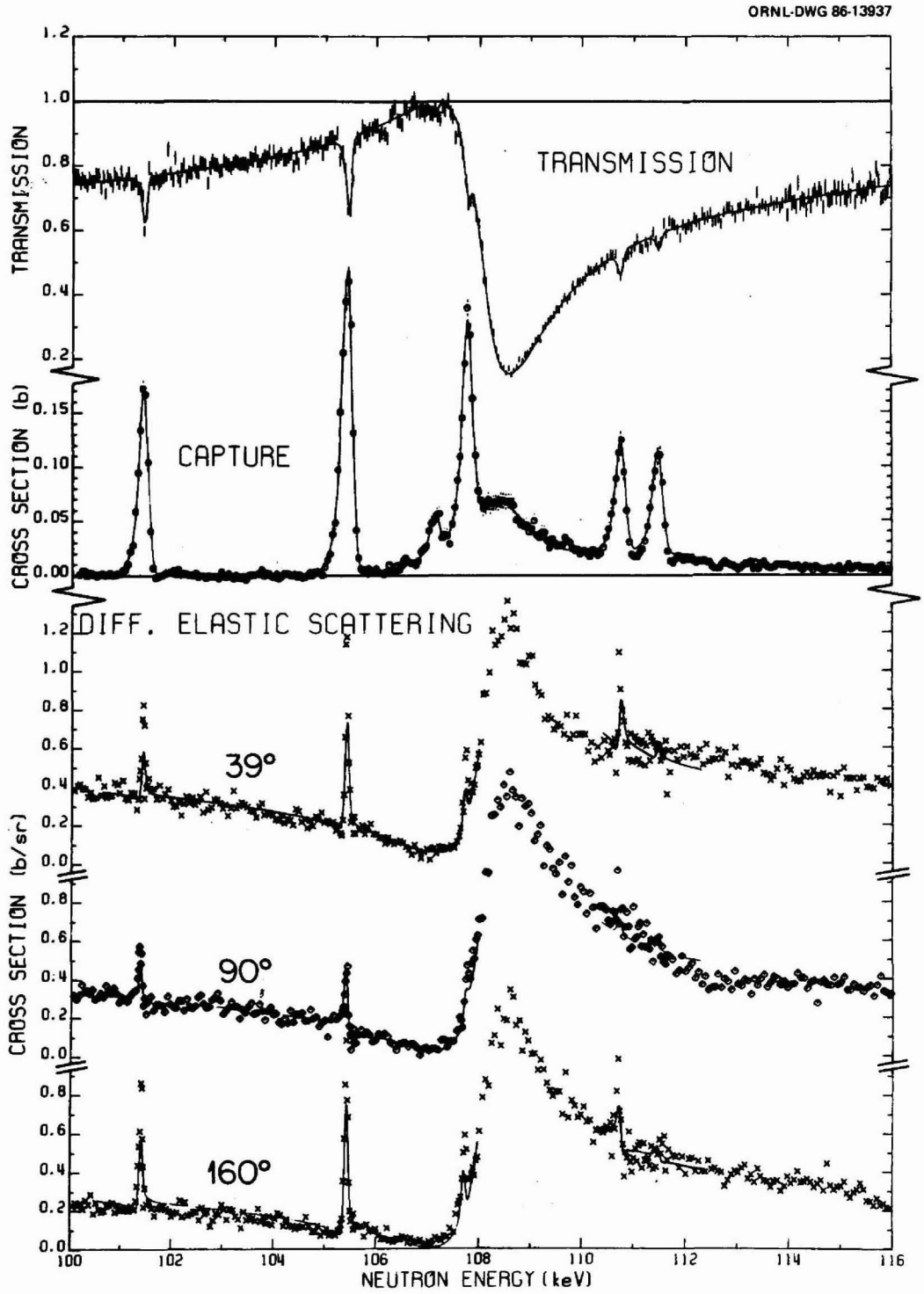

Fig. 17. Same as Fig. 15 except for 100 to 116 keV.

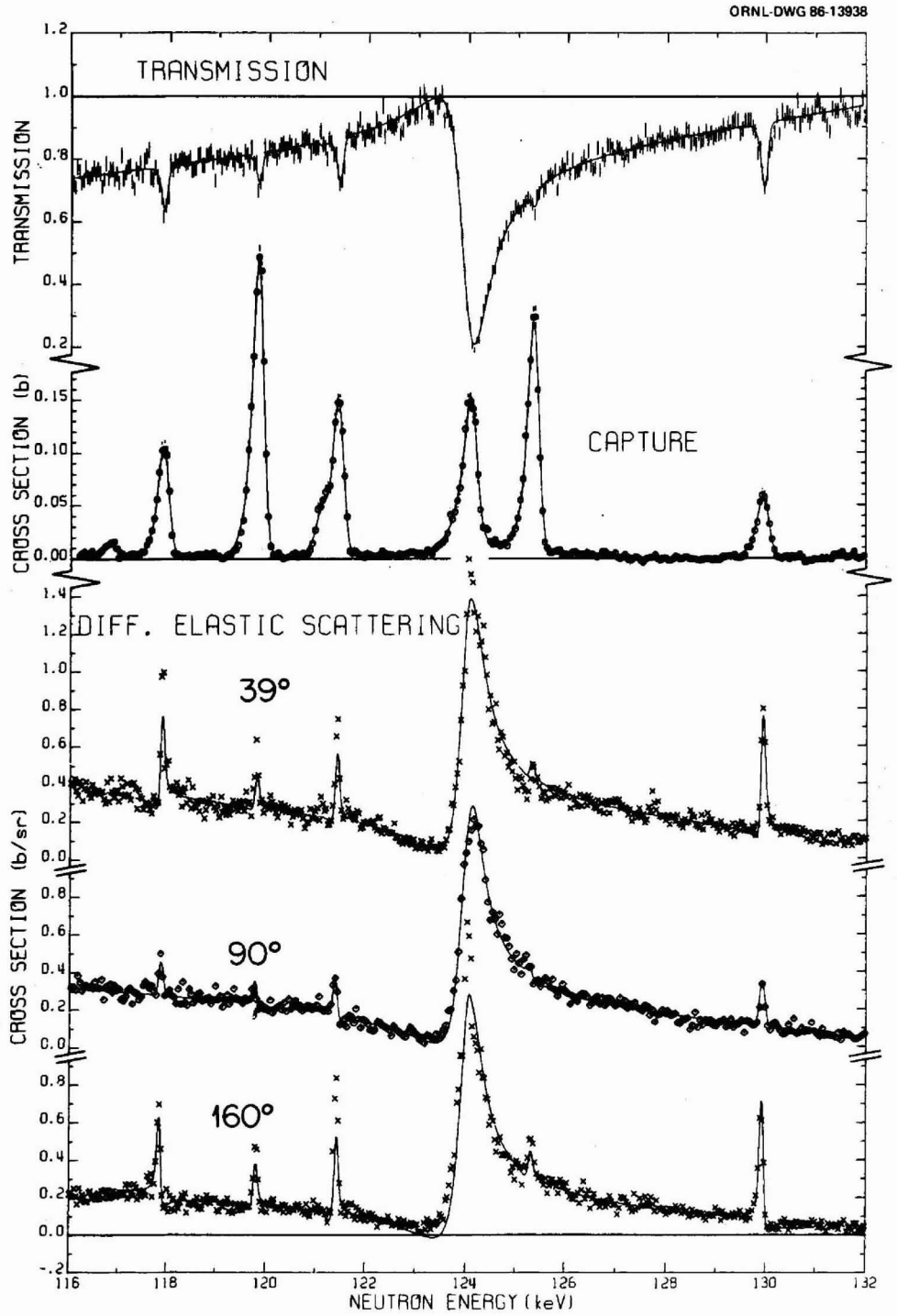

Fig. 18. Same as Fig. 15 except for 116 to 132 keV.

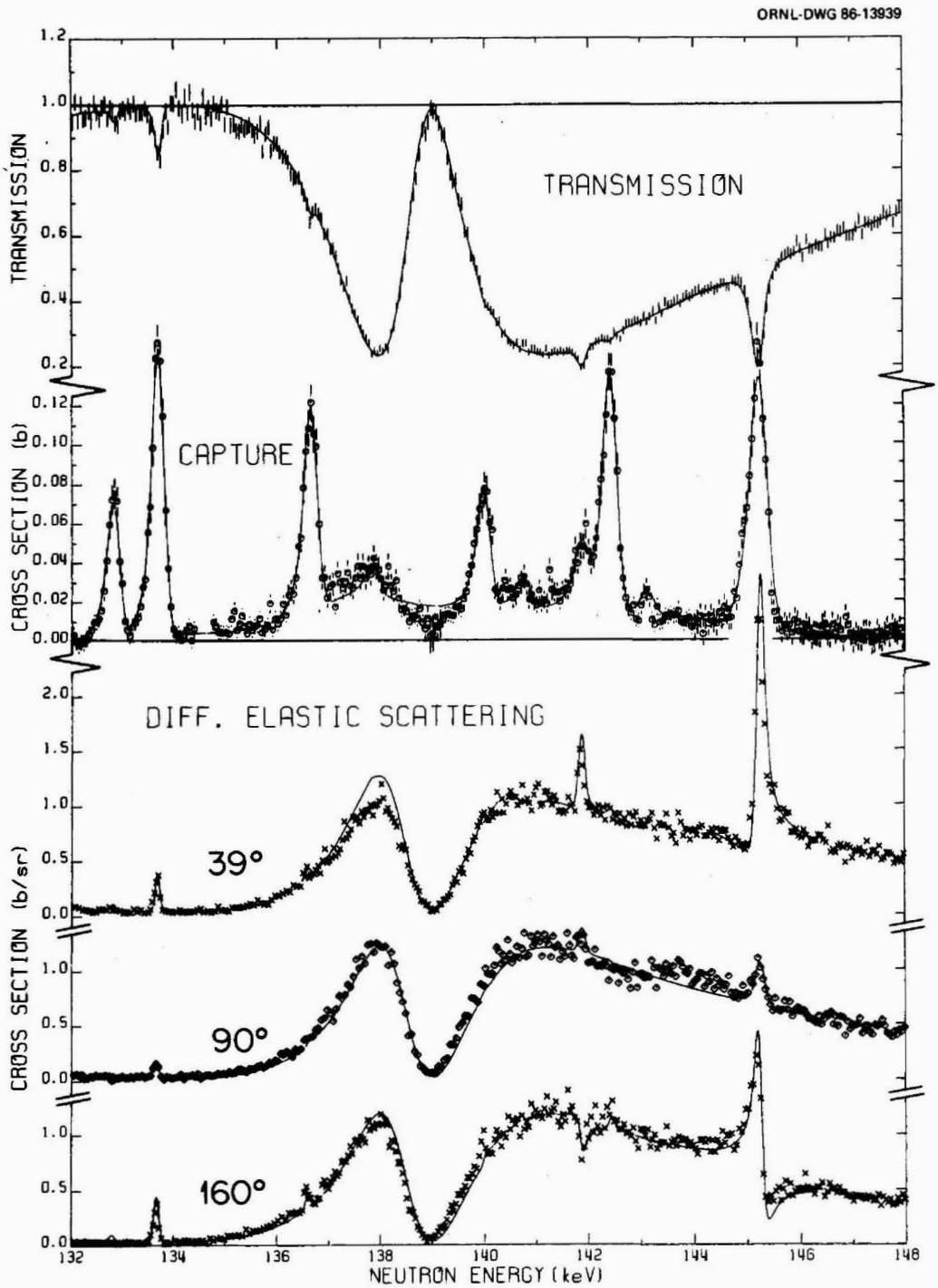

Fig. 19. Same as Fig. 15 except for 132 to 148 keV.

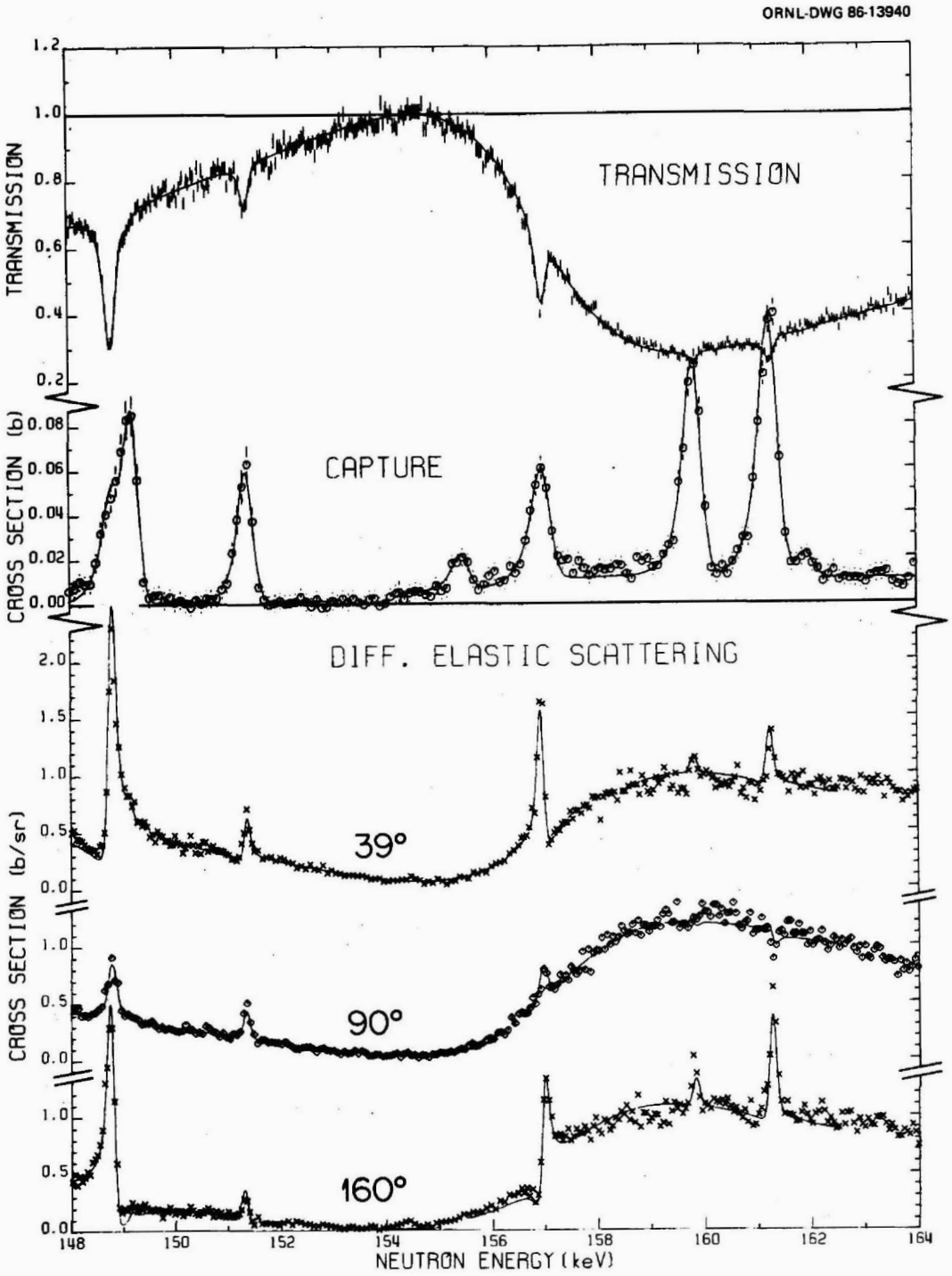

Fig. 20. Same as Fig. 15 except for 148 to 164 keV.

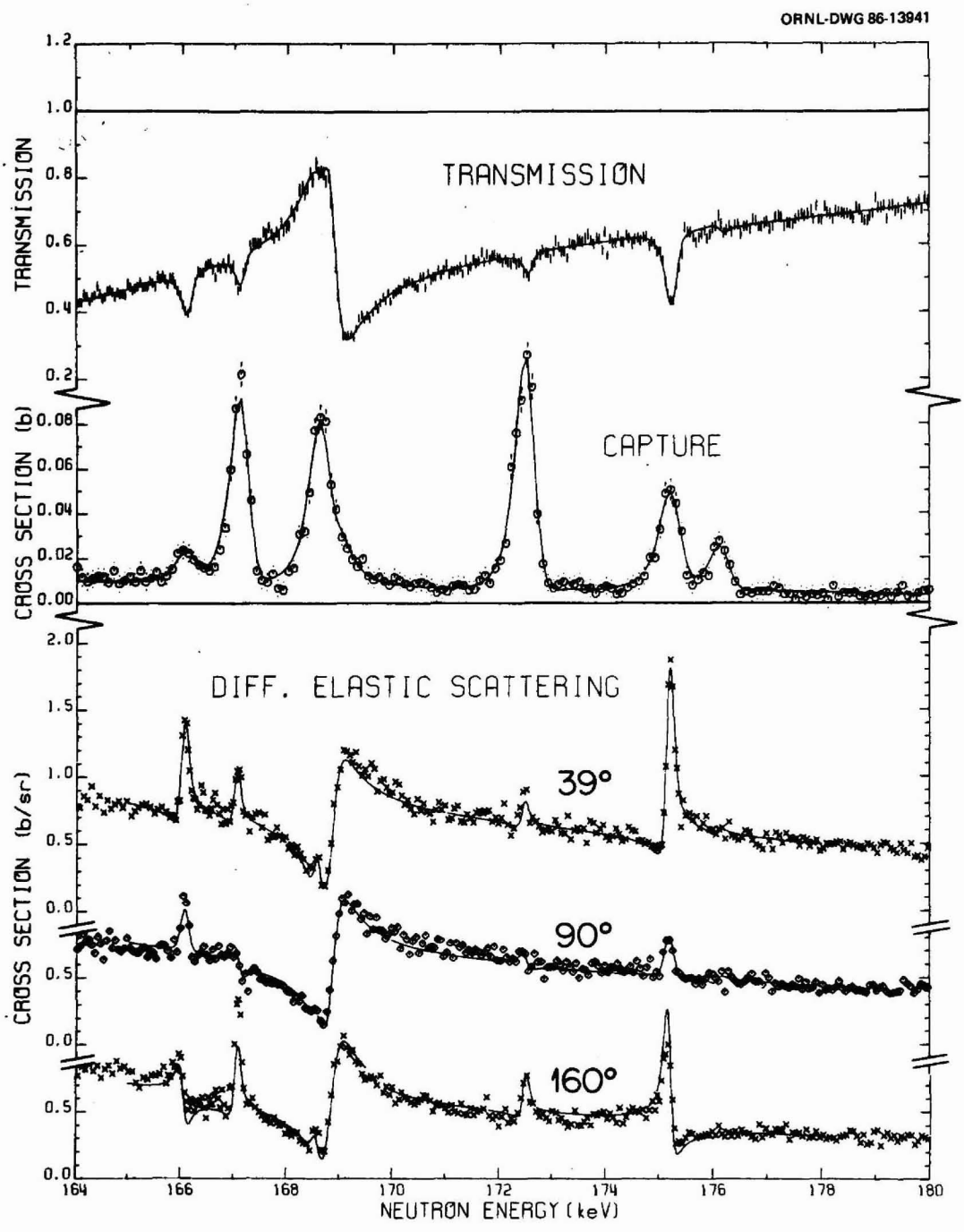

Fig. 21. Same as Fig. 15 except for 164 to 180 keV.

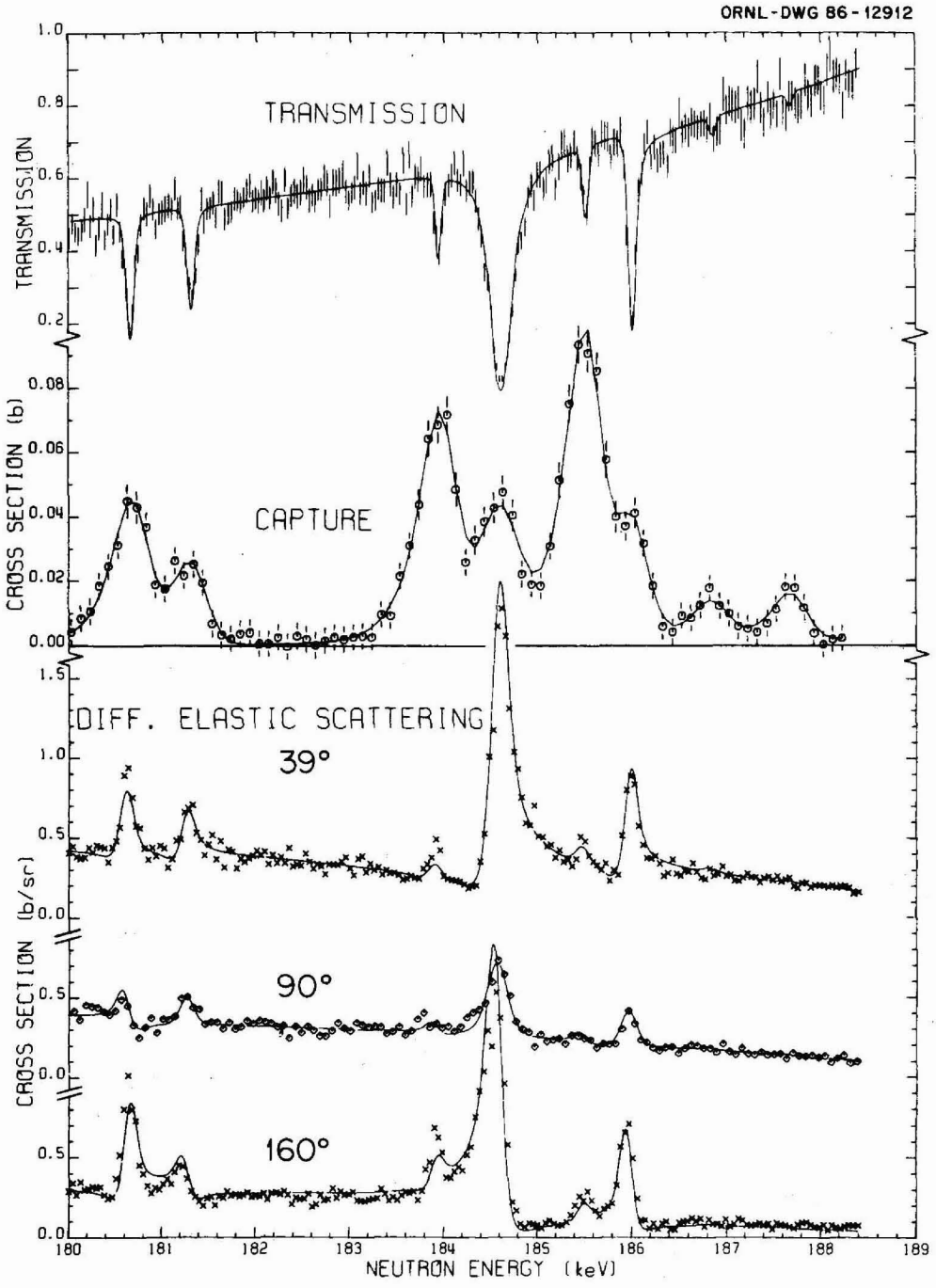

Fig. 22. TOP: Simultaneous fits, from 180 to 188.5 keV, to the 200-m transmission data taken with the NE-110 detector and to the capture data obtained with the thick ^{58}Ni sample (0.0382 atoms/b). The theoretical curves were calculated with the parameters of Table 2. BOTTOM: The data for three of the six differential elastic-scattering angles are compared with the theoretical cross sections calculated with the same parameters as above. The combination of spins and parities adopted is the one which yields the best agreement with the elastic-scattering data.

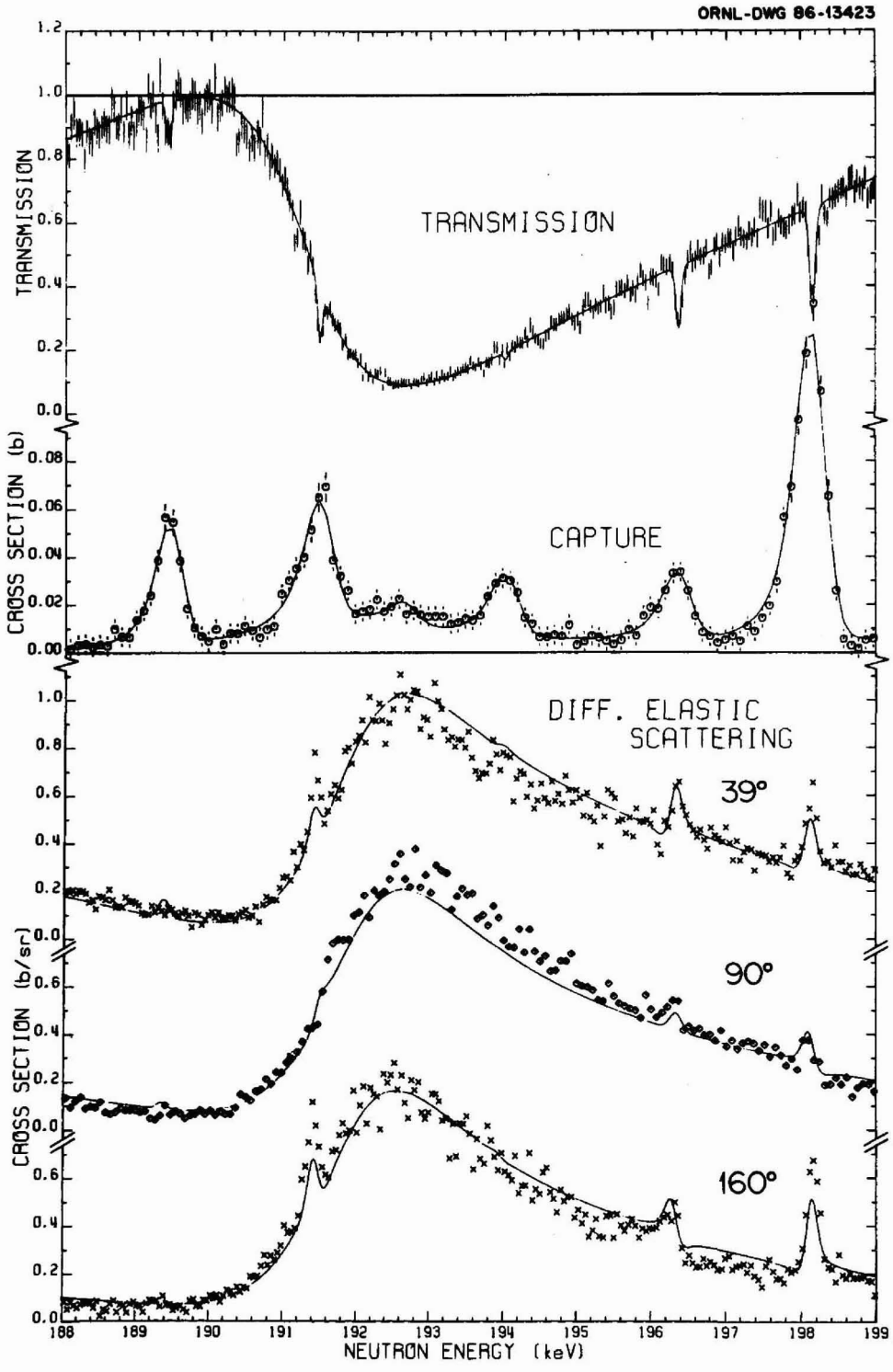

Fig. 23. Same as Fig. 22 except for 188 to 199 keV.

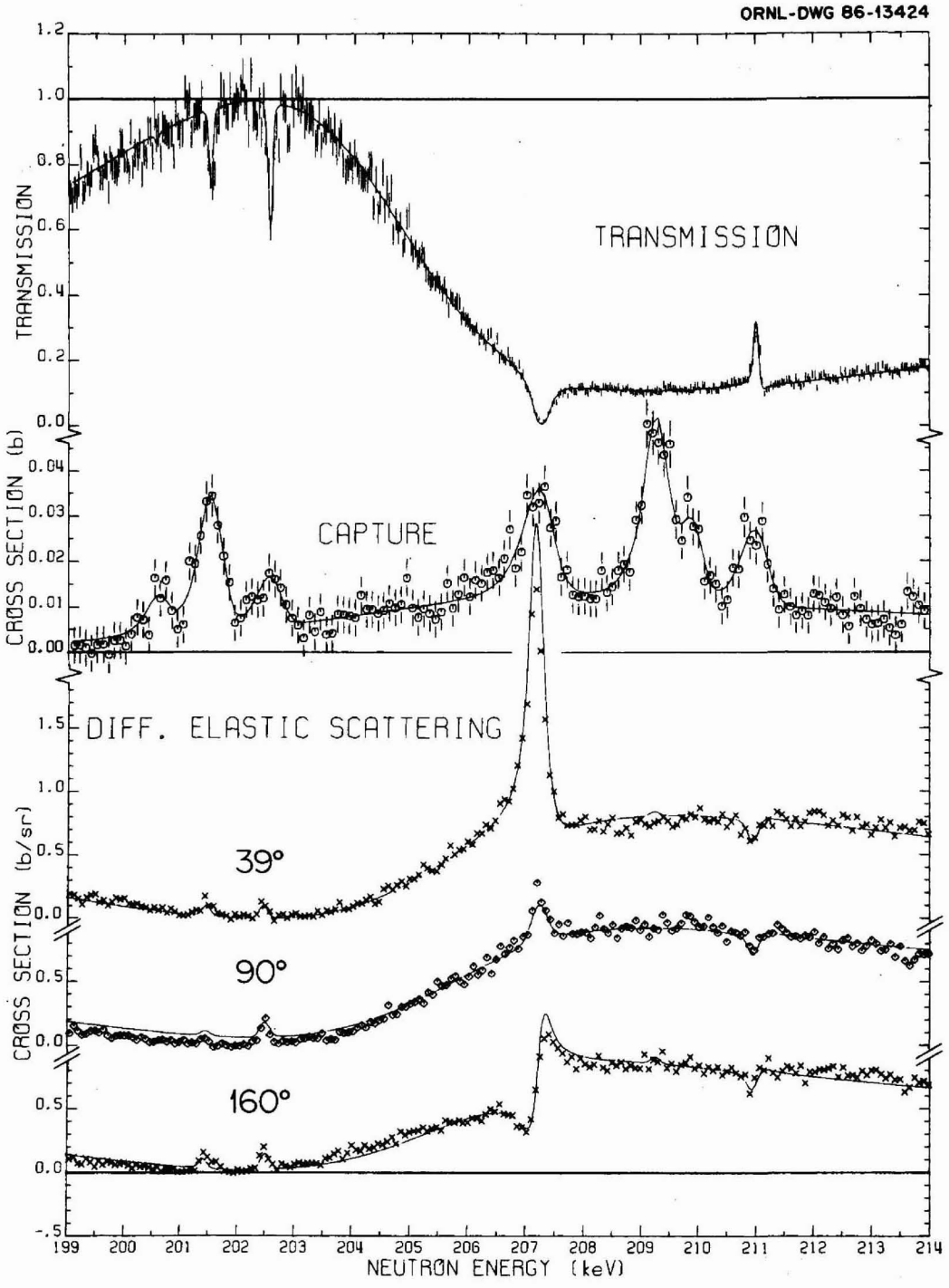

Fig. 24. Same as Fig. 22 except for 199 to 214 keV.

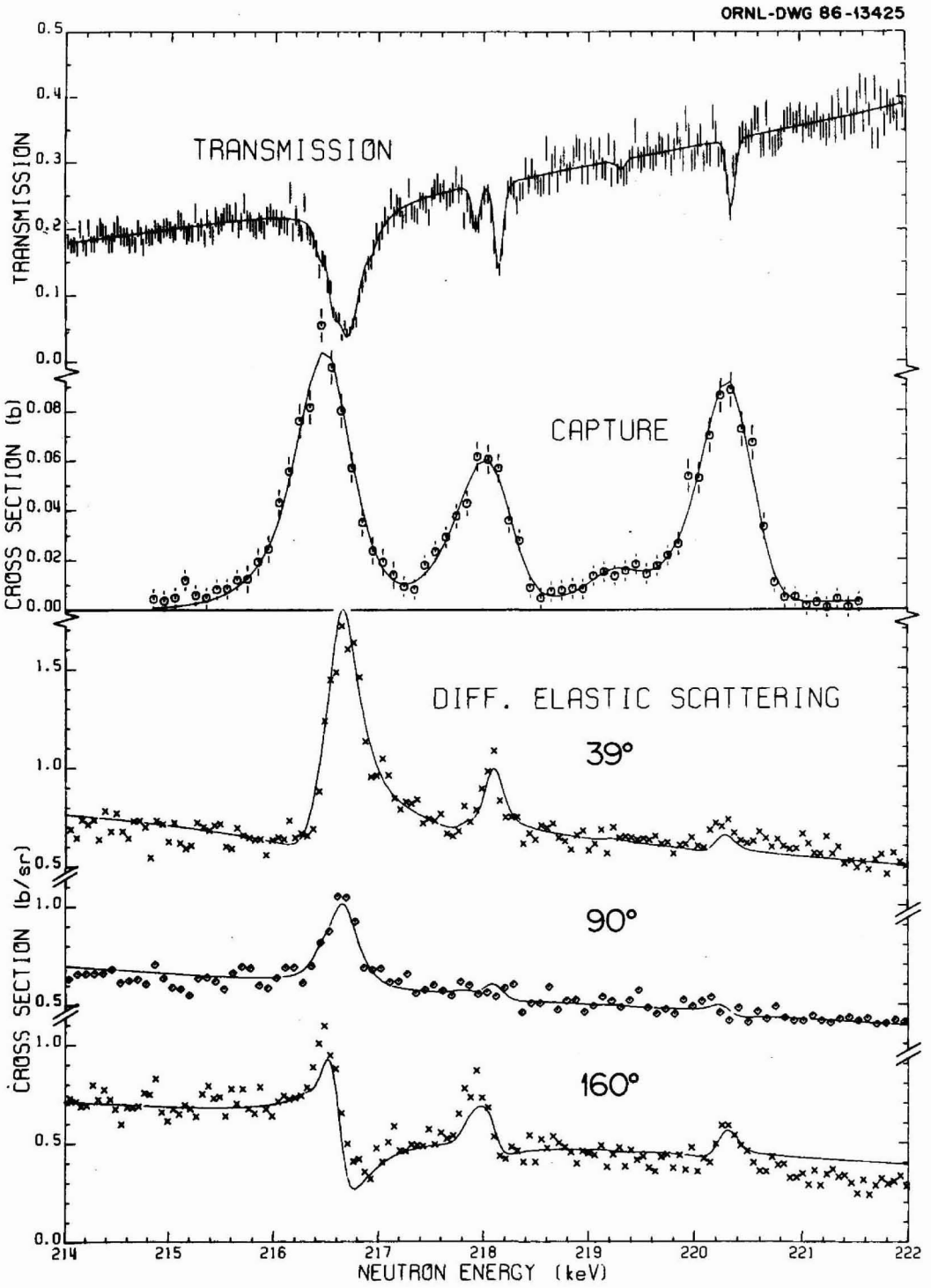

Fig. 25. Same as Fig. 22 except for 214 to 222 keV.

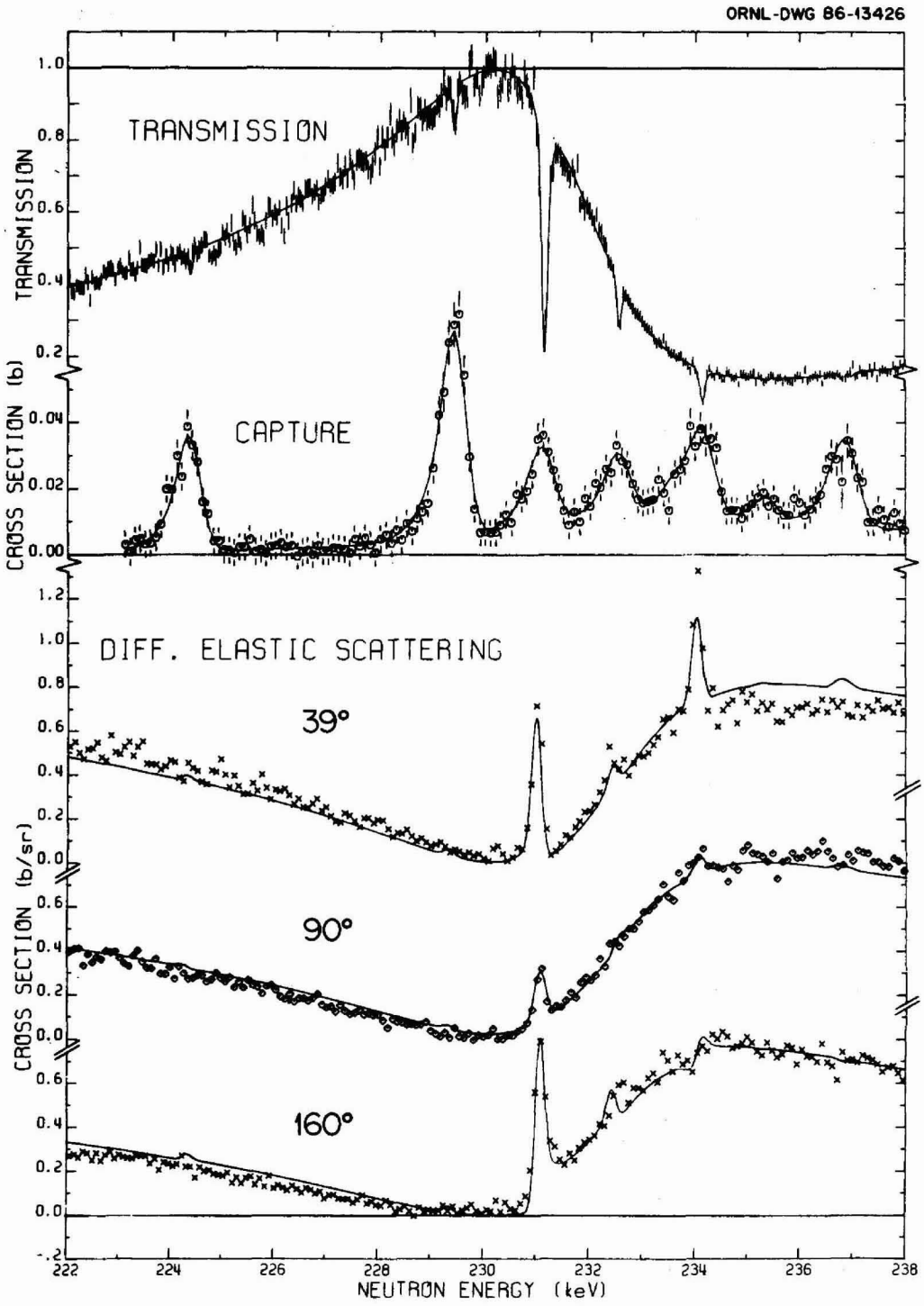

Fig. 26. Same as Fig. 22 except for 222 to 238 keV.

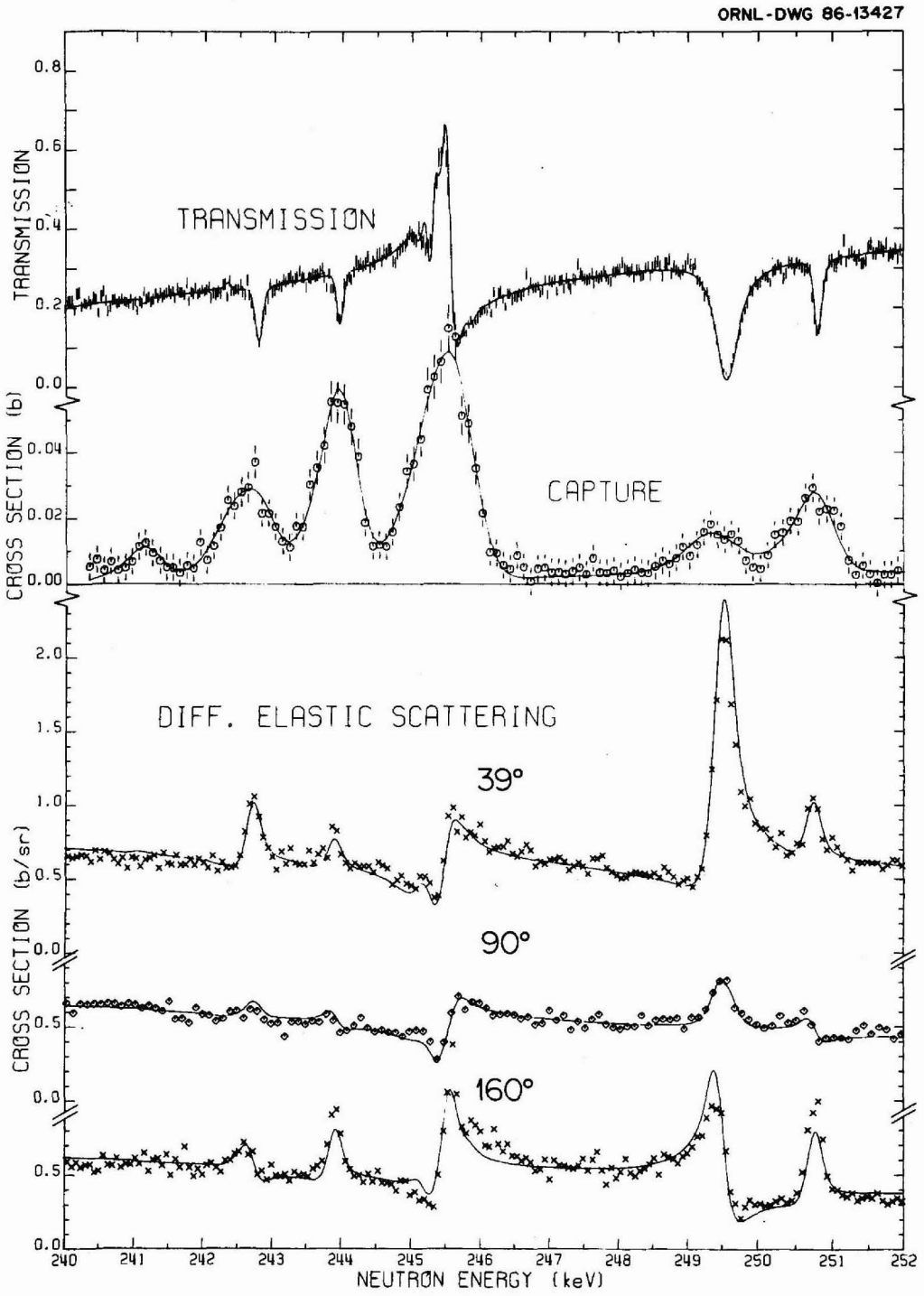

Fig. 27. Same as Fig. 22 except for 238 to 252 keV.

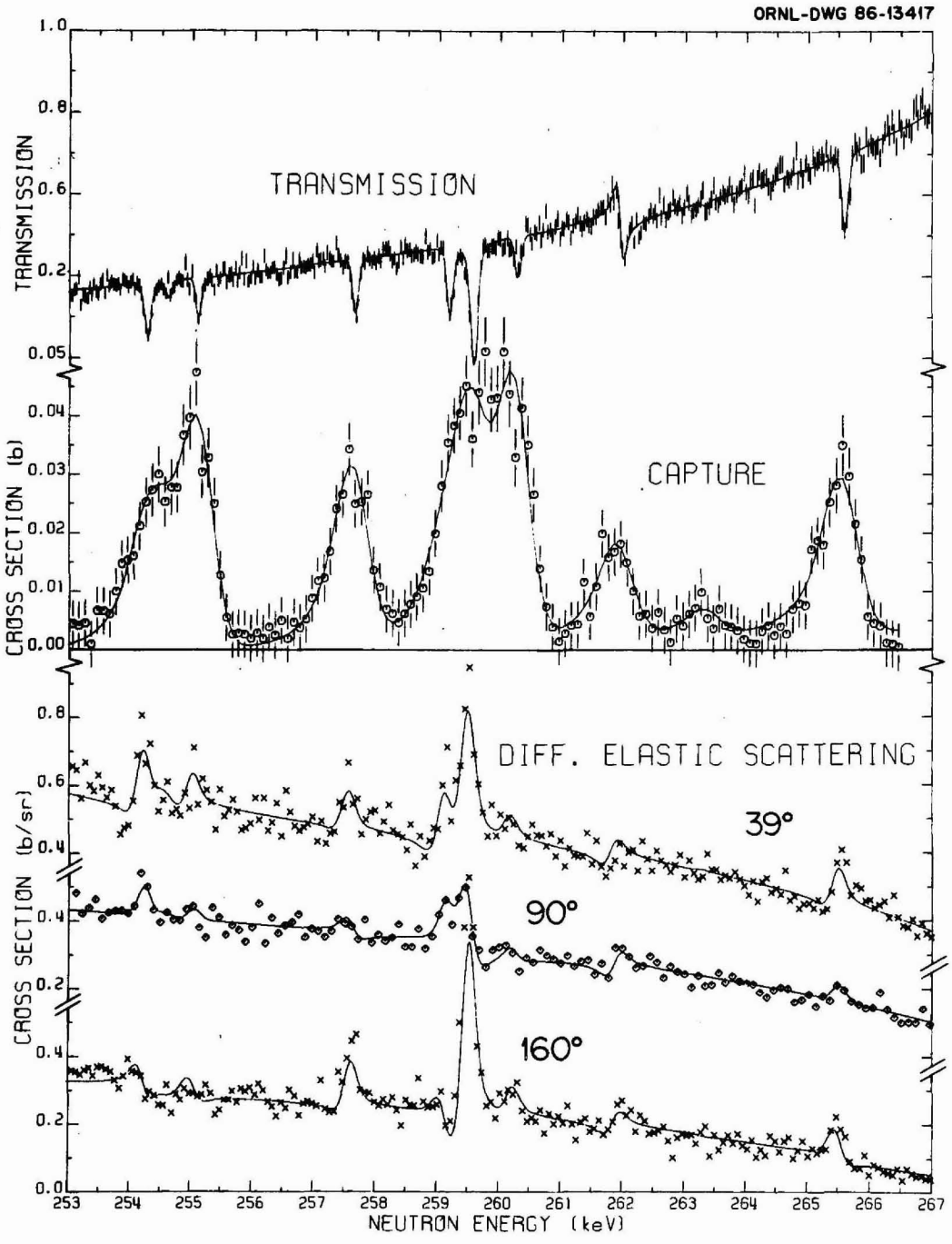

Fig. 28. Same as Fig. 22 except for 252 to 267 keV.

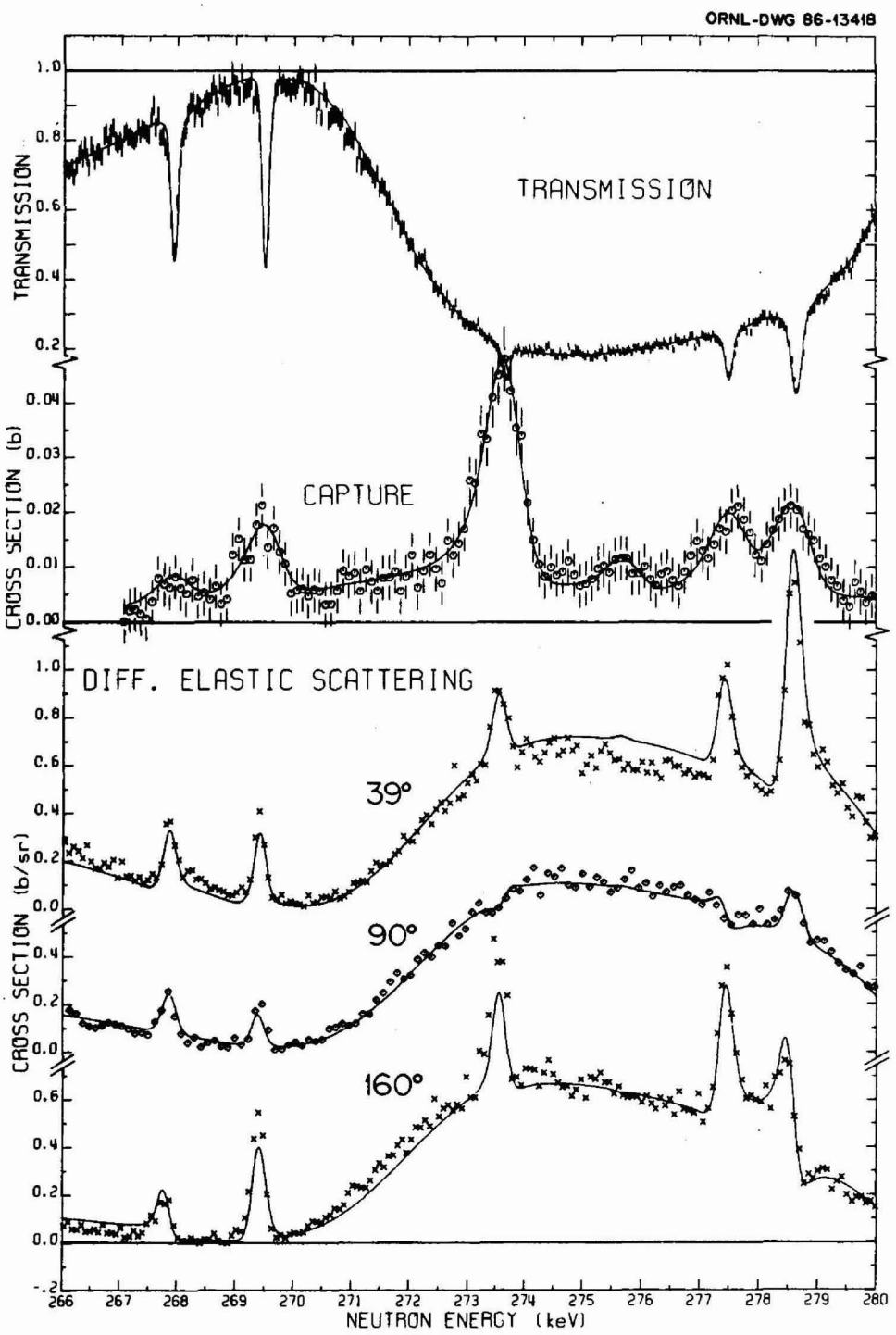

Fig. 29. Same as Fig. 22 except for 267 to 280 keV.

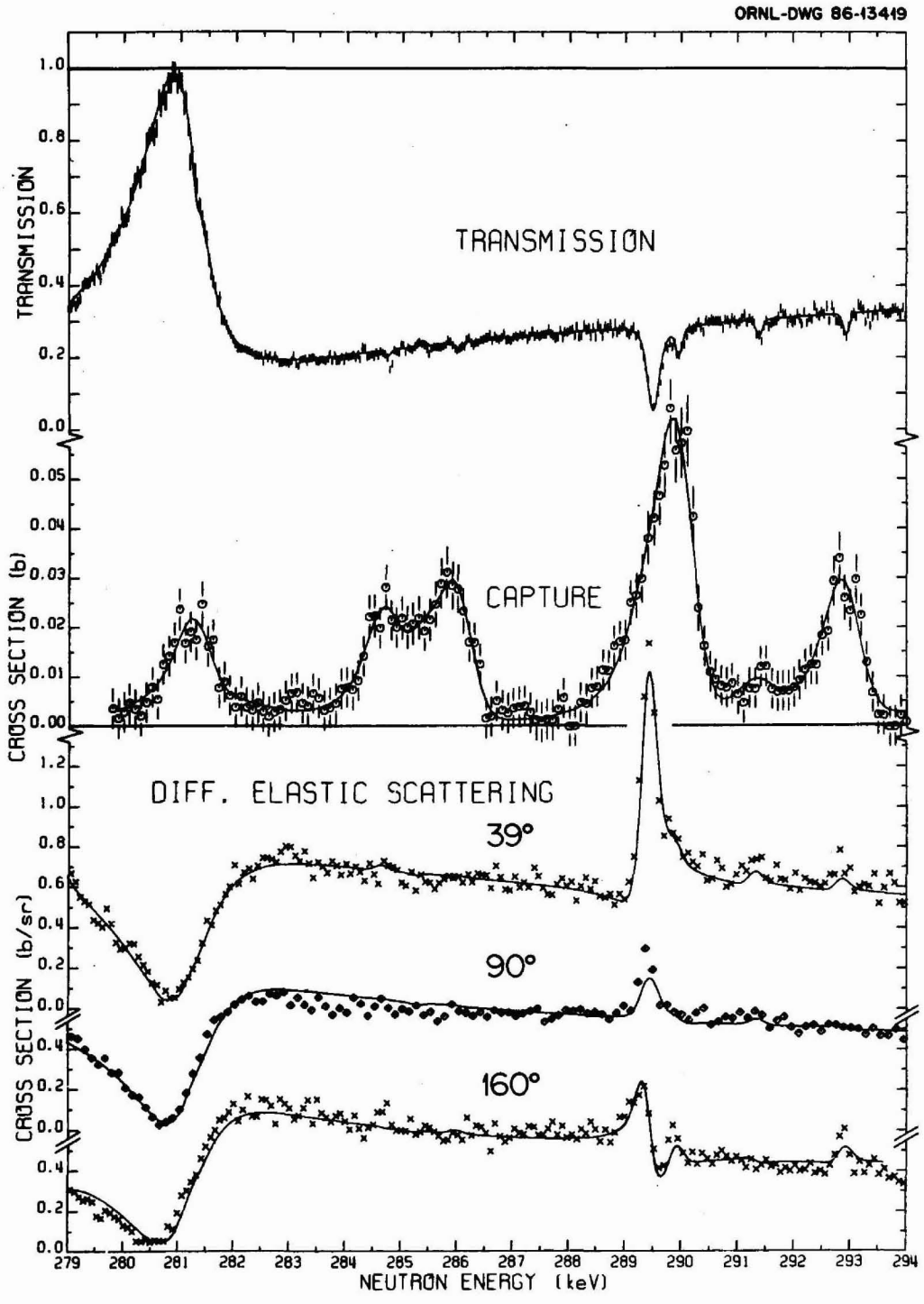

Fig. 30. Same as Fig. 22 except for 279 to 294 keV.

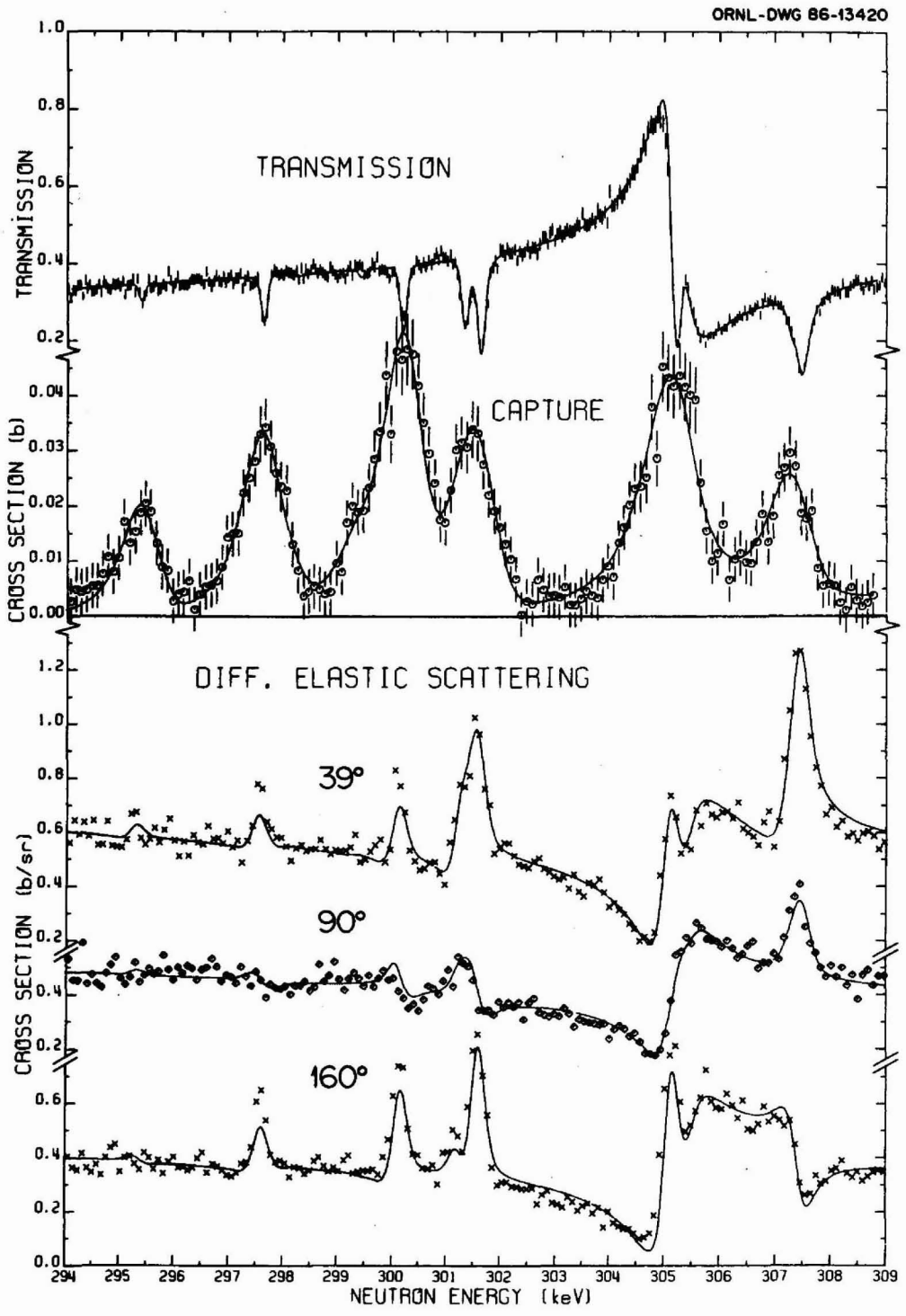

Fig. 31. Same as Fig. 22 except for 294 to 309 keV.

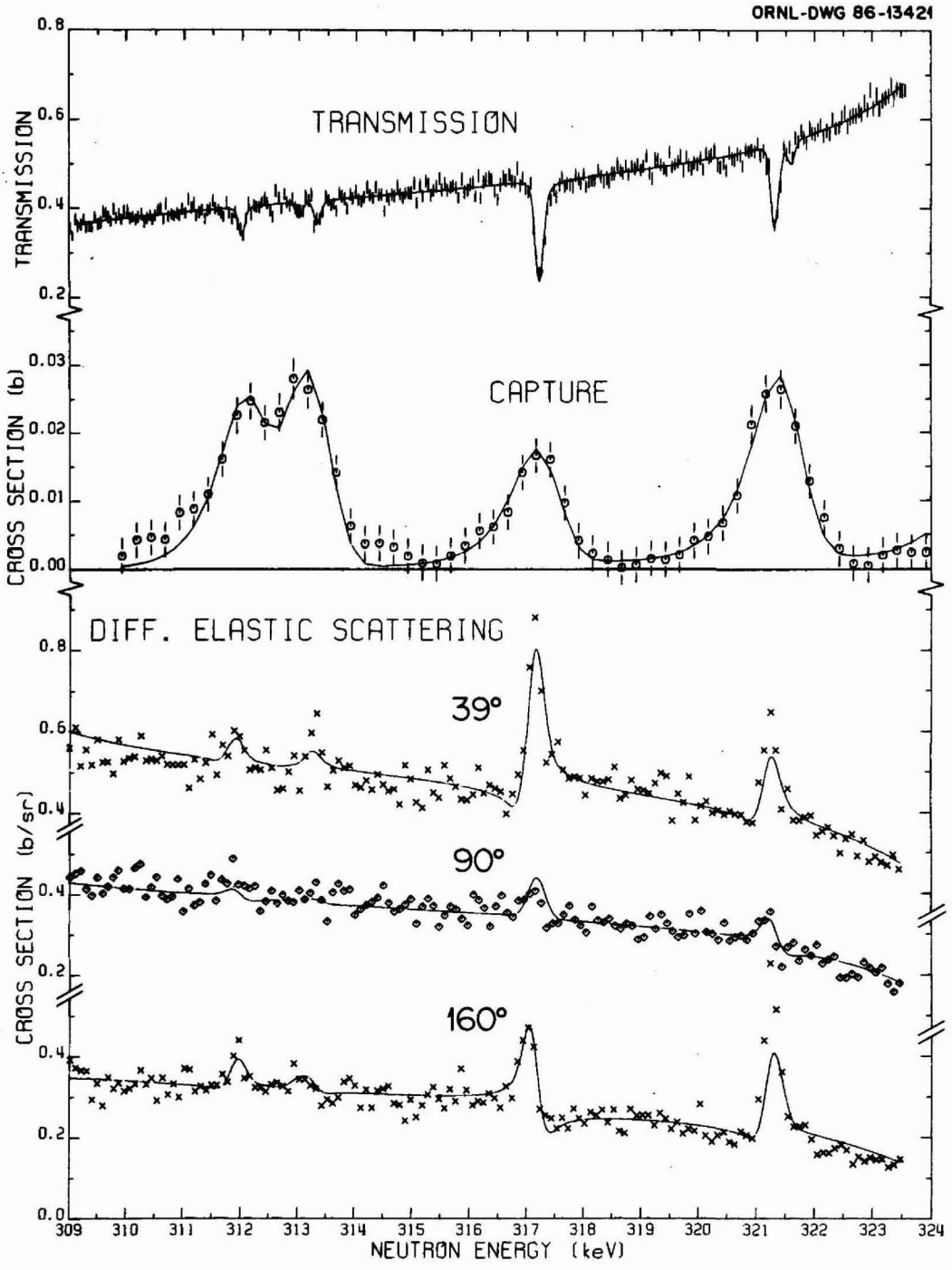

Fig. 32. Same as Fig. 22 except for 309 to 323 keV.

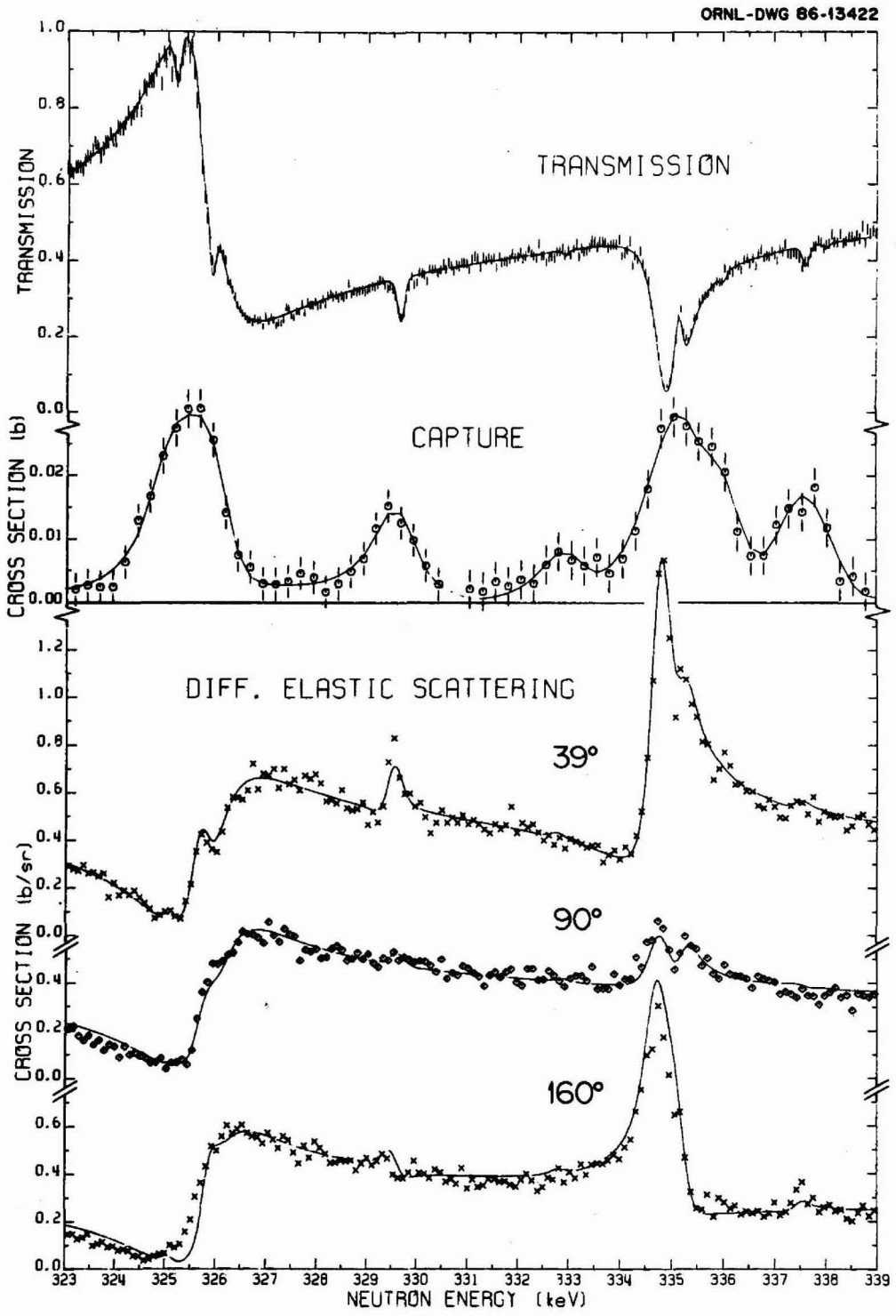

Fig. 33. Same as Fig. 22 except for 323 to 339 keV.

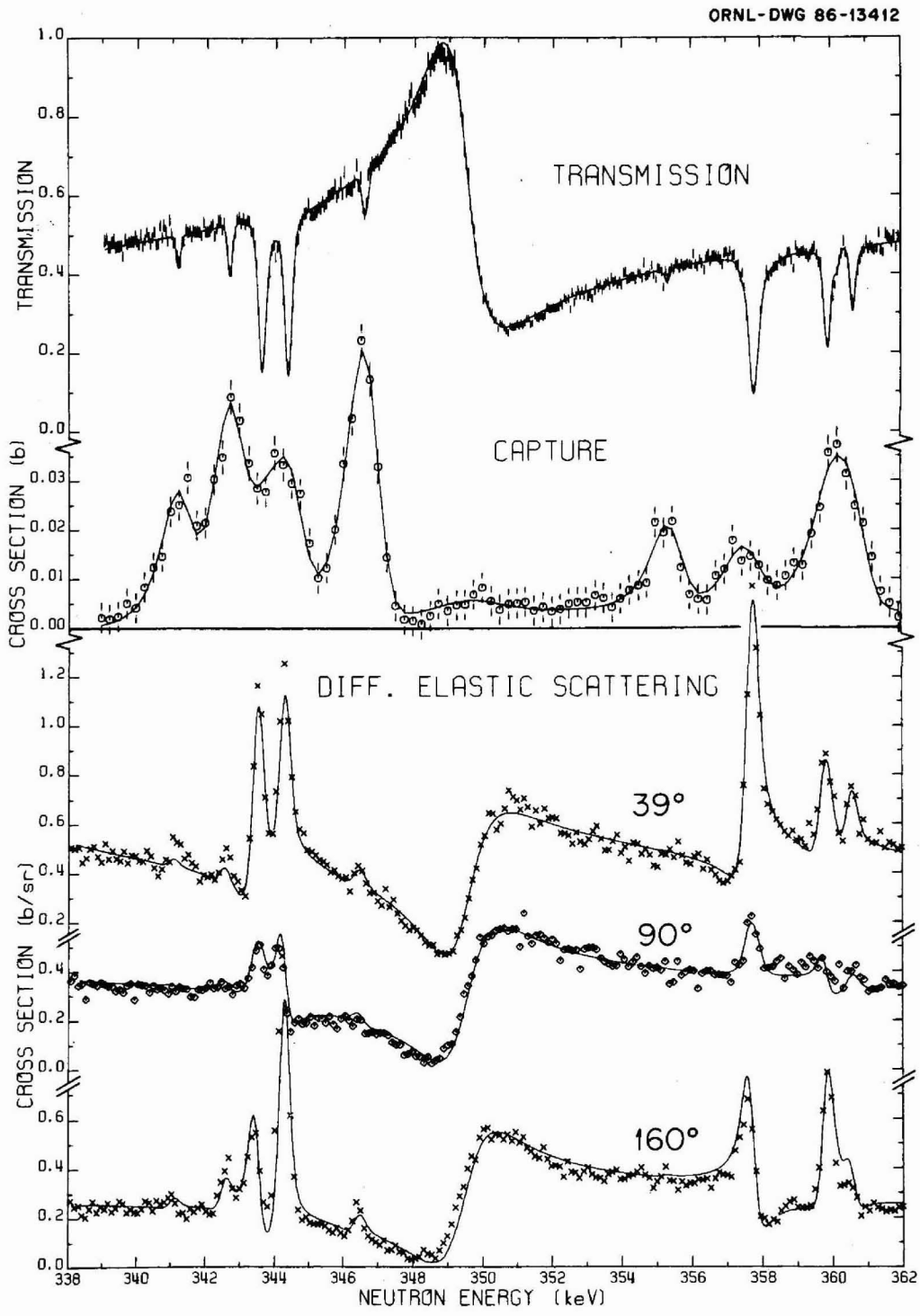

Fig. 34. Same as Fig. 22 except for 339 to 362 keV.

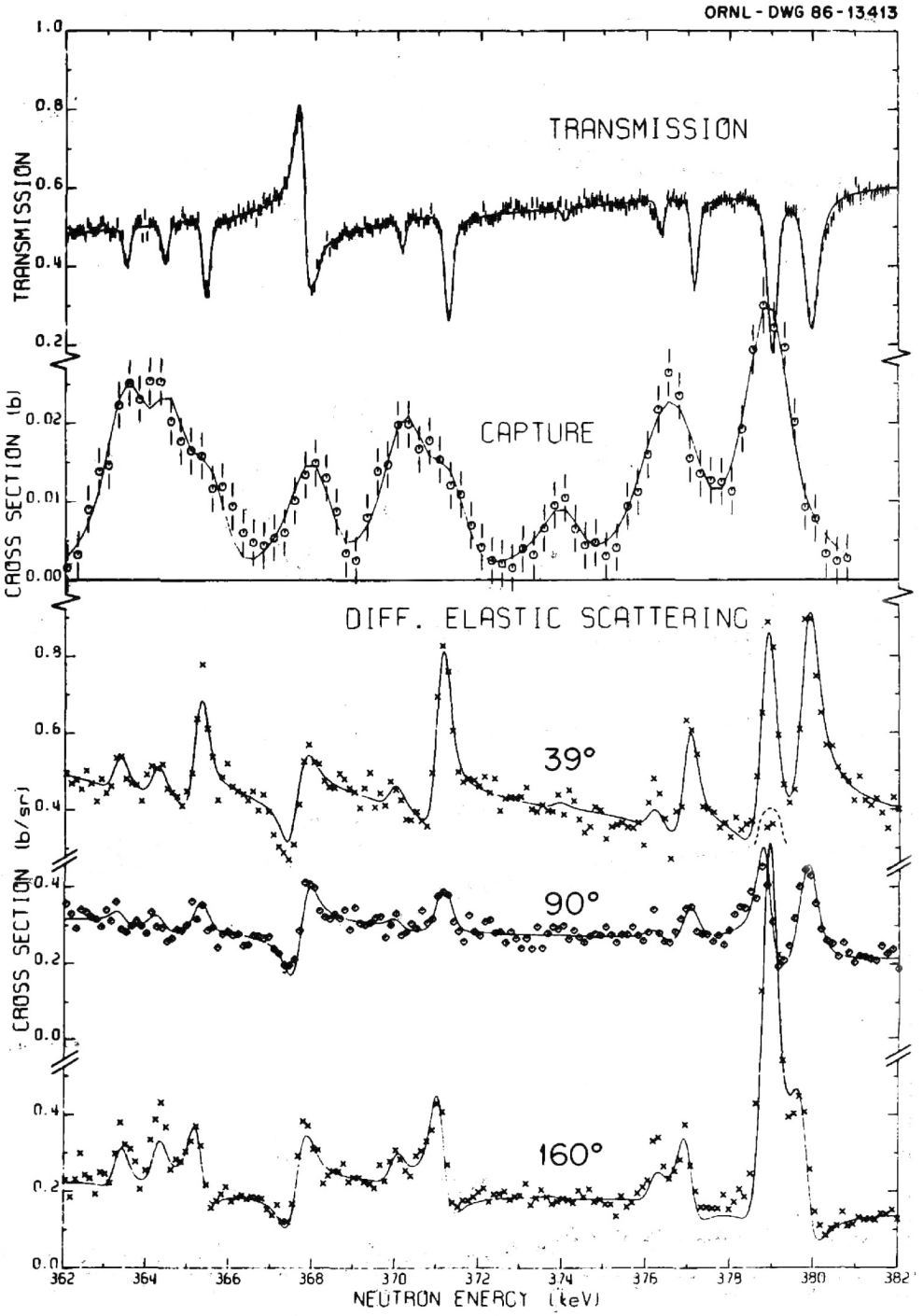

Fig. 35. Same as Fig. 22 except for 362 to 382 keV.

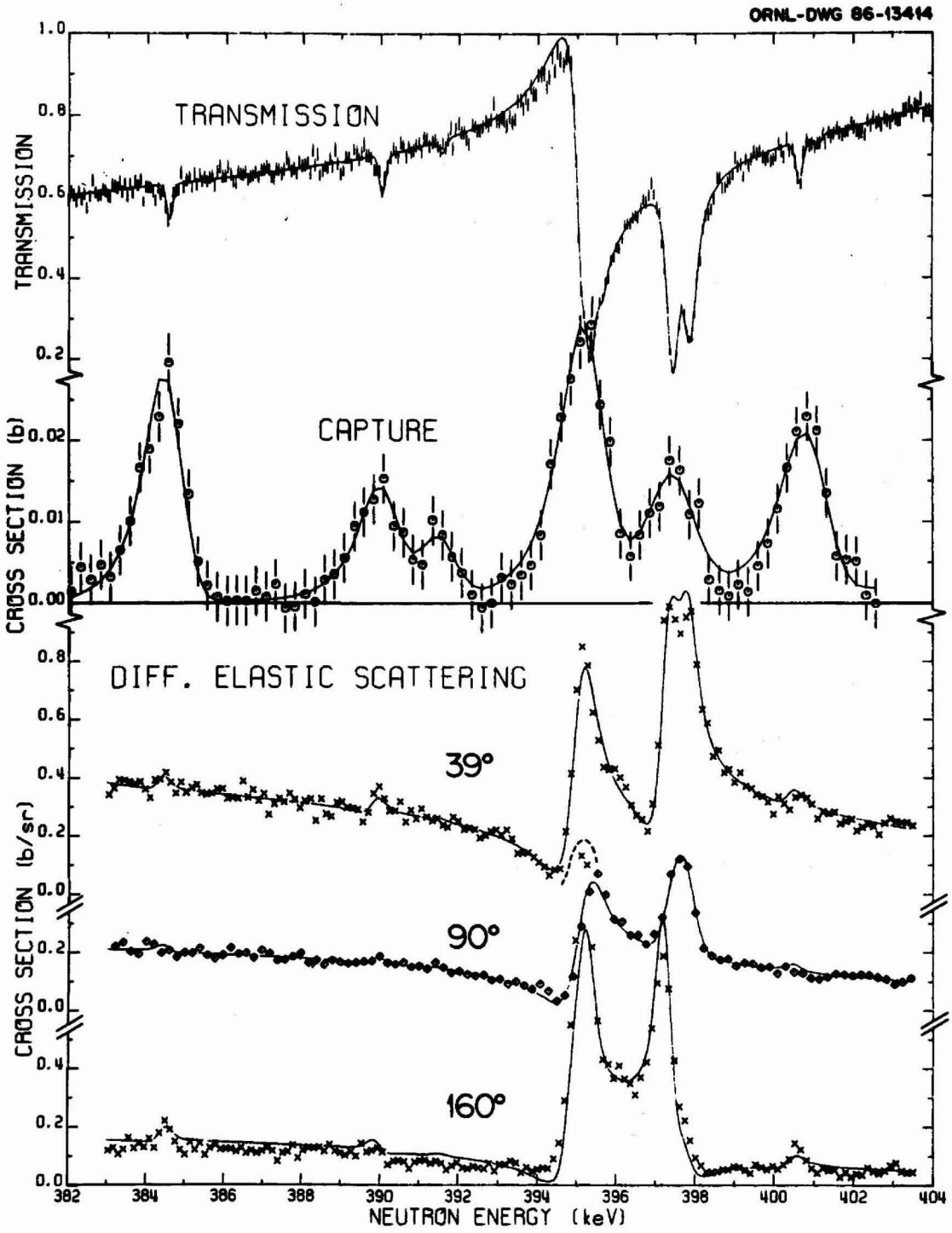

Fig. 36. Same as Fig. 22 except for 382 to 404 keV.

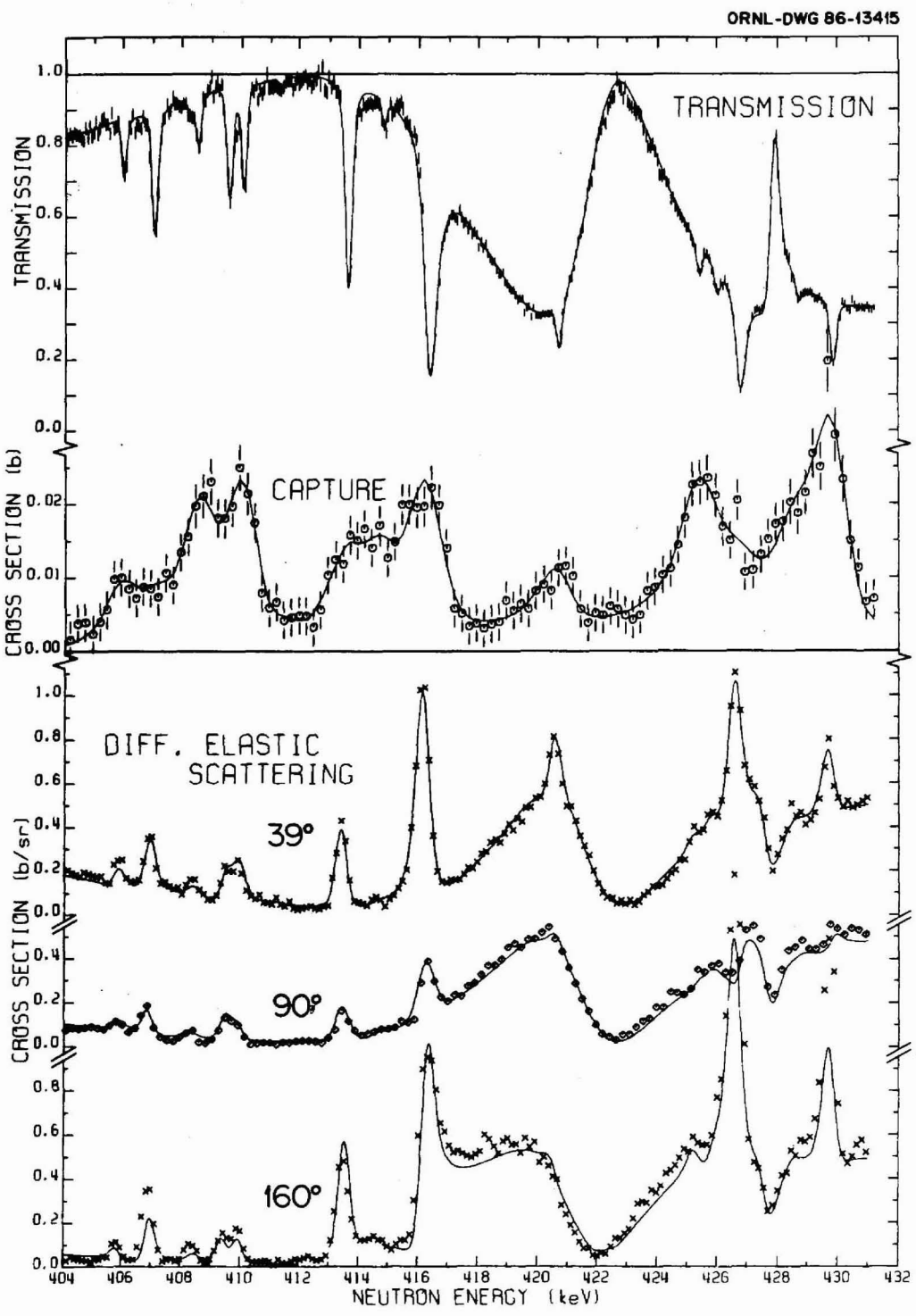

Fig. 37. Same as Fig. 22 except for 404 to 431 keV.

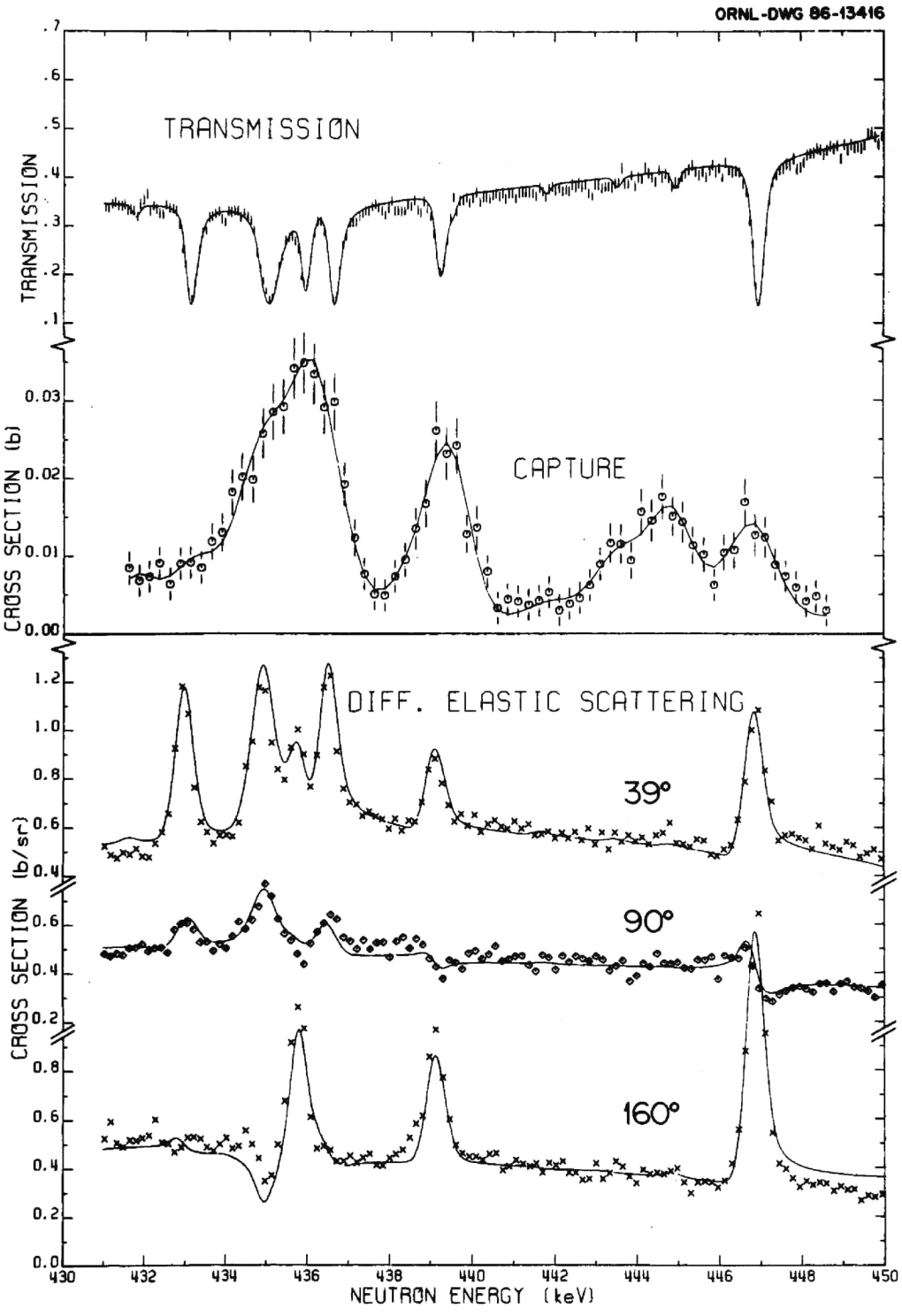

Fig. 38. Same as Fig. 22 except for 431 to 450 keV.

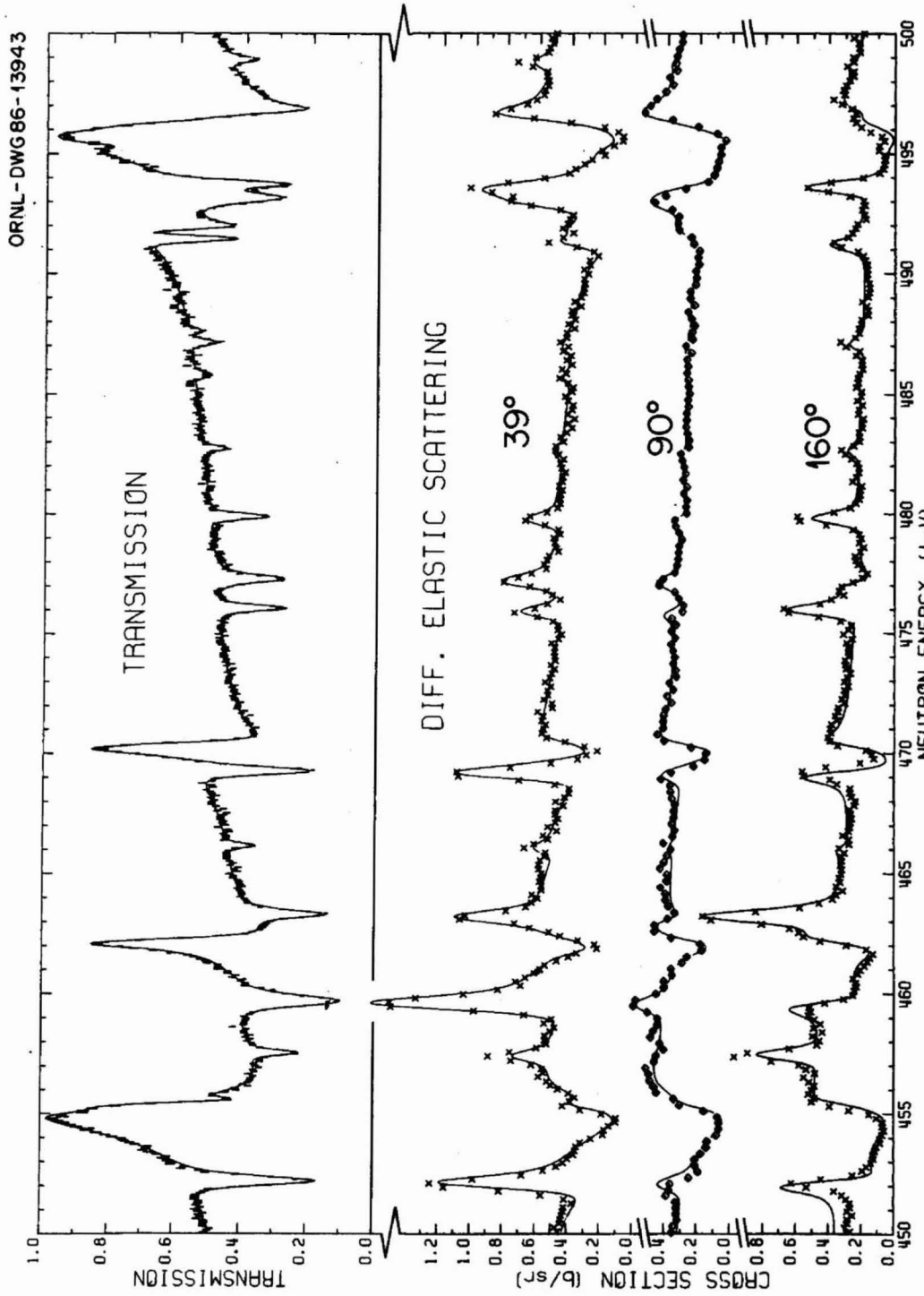

Fig. 39. TOP: Fit to the 200-m transmission data taken with the NE-110 detector, from 450 to 500 keV, obtained with the parameters of Table 2. BOTTOM: The data for three of the six differential elastic-scattering angles are compared with the theoretical cross sections calculated with the same parameters as above. The combination of spins and parities adopted is the one which yields the best agreement with the elastic-scattering data.

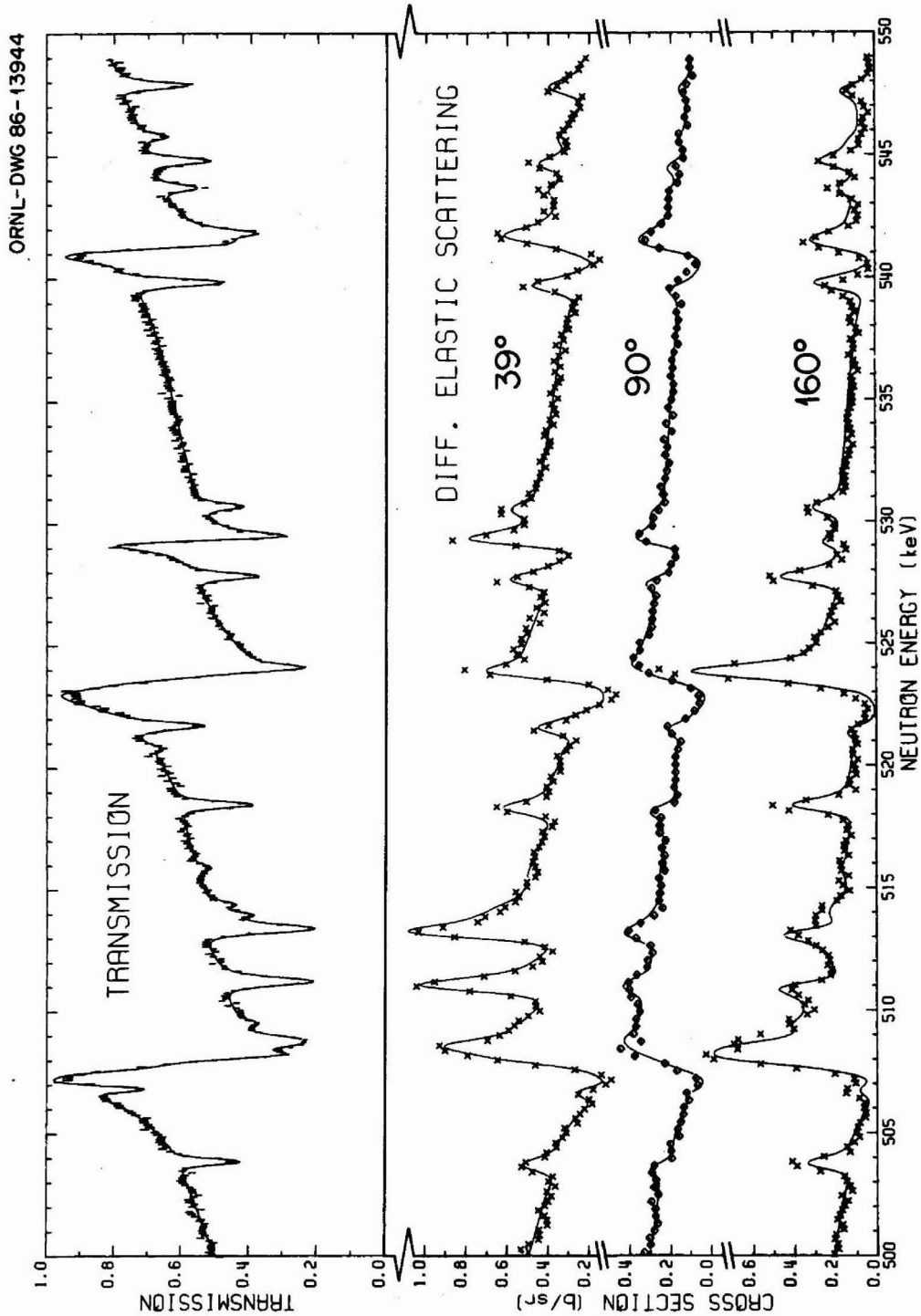

Fig. 40. Same as Fig. 39 except for 500 to 549 keV.

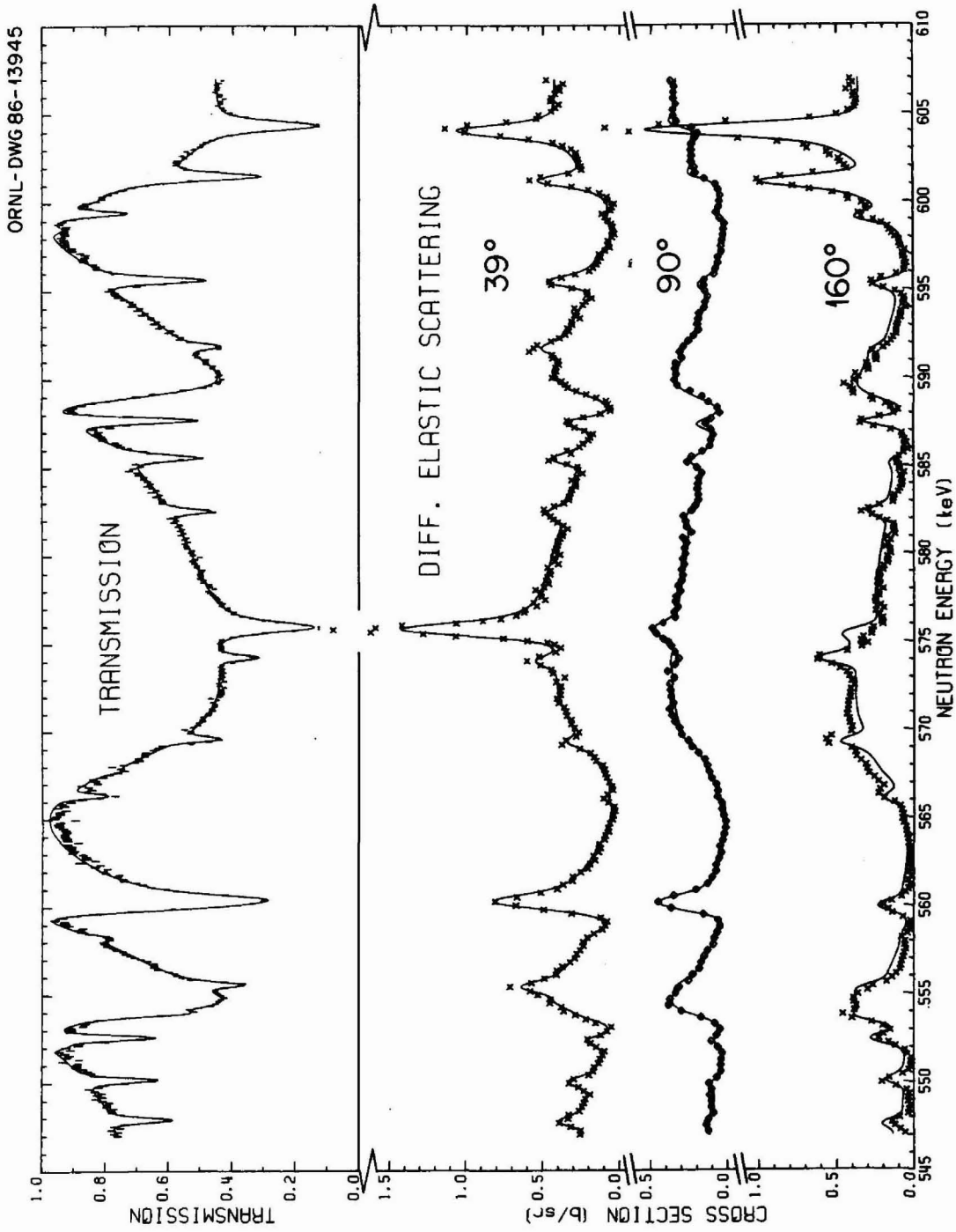

Fig. 41. Same as Fig. 39 except for 547 to 607 keV.

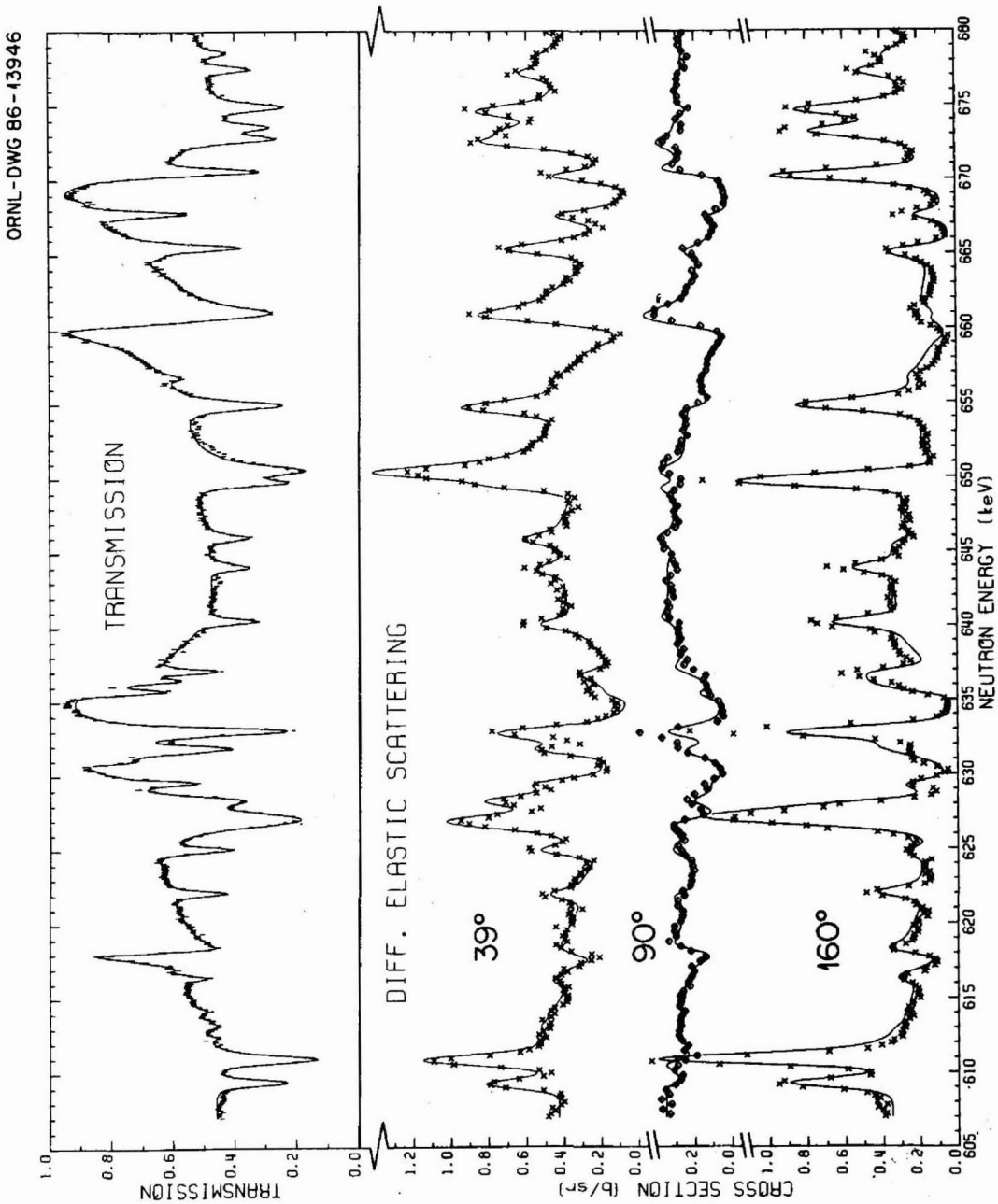

Fig. 42. Same as Fig. 39 except for 607 to 680 keV.

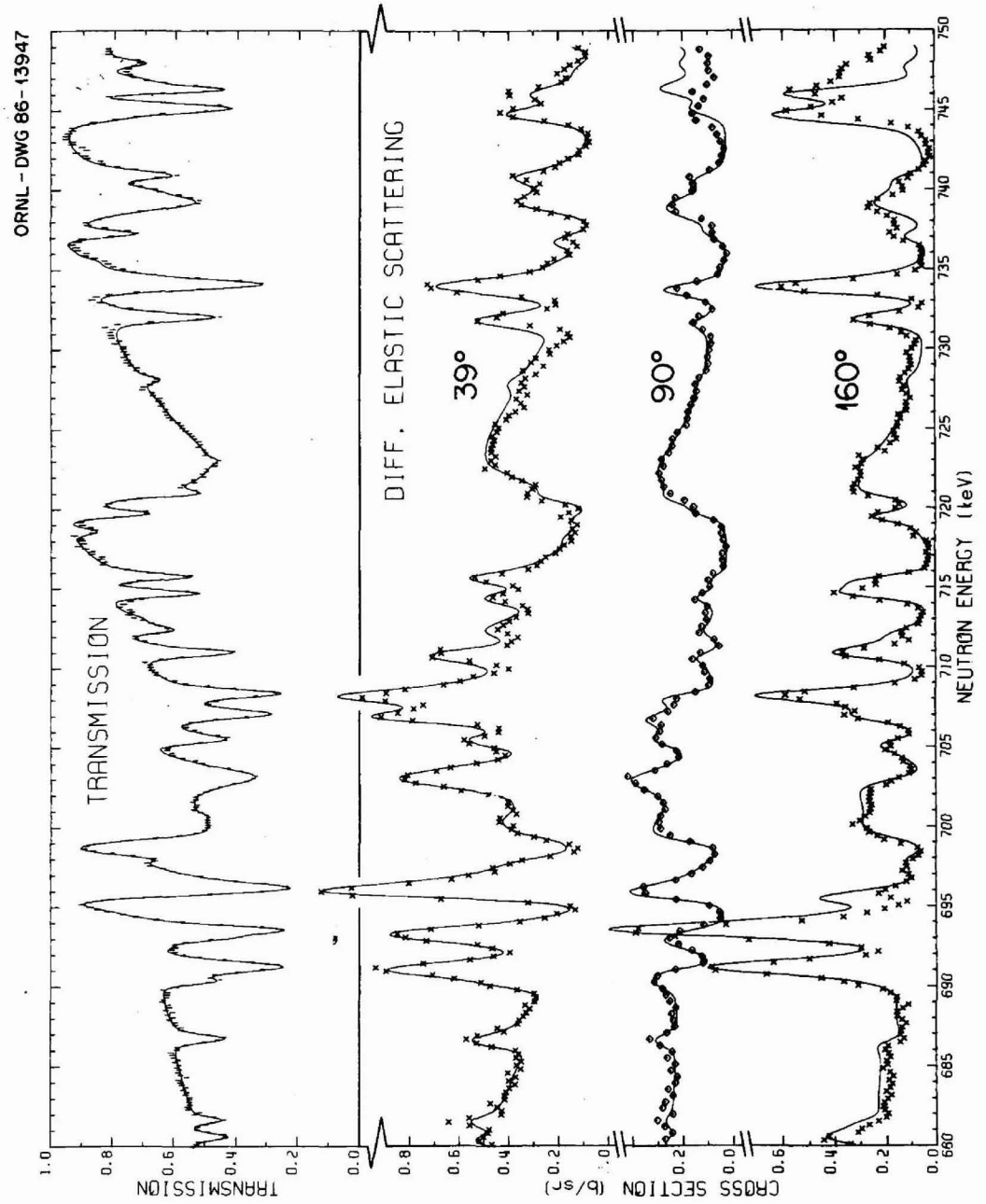

Fig. 43. Same as Fig. 39 except for 680 to 749 keV.

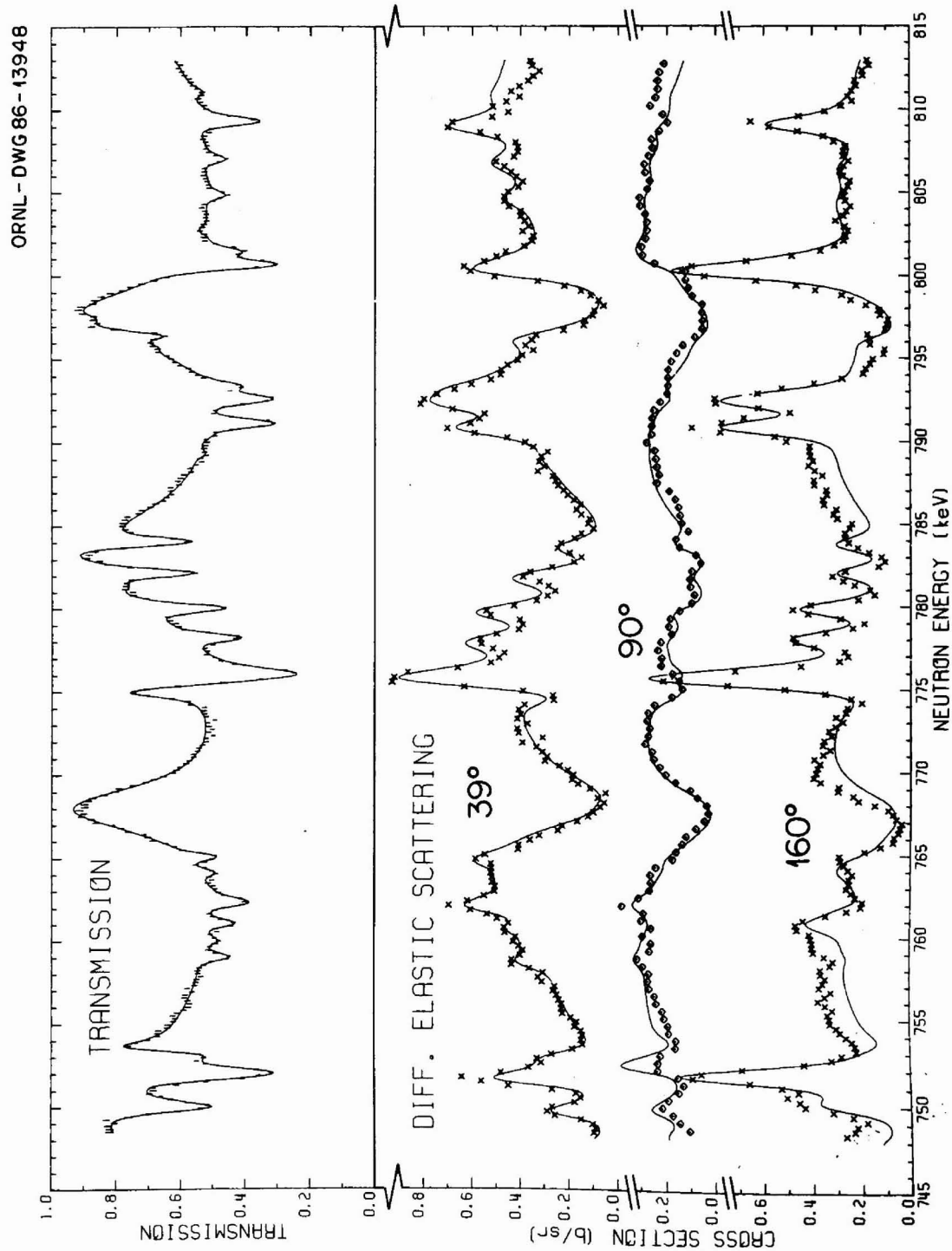

Fig. 44. Same as Fig. 39 except for 748 to 813 keV.

The energy of these resonances were then translated to the energy scale of the 200-m transmission data as reported earlier in Section 3.1. The uncertainty associated with the translation of the energy scale is not included in the standard deviation reported in the first column of Table 2 and is of the order of 0.01% of the resonance energy.

Table 3. Correlations between the uncertainties of some of the parameters of Table 2[a]

	R1	R2	E1	G1	E5	G5	E7	G7	E30	G30	E333	G333	E334	G334	E463	G463	G482
R1	100																
R2	-16	100															
E1	34	-8	100														
G1	-64	19	-68	100													
E5	0	0	0	0	100												
G5	13	0	-3	-3	-1	100											
E7	0	-10	5	27	0	-1	100										
G7	0	-7	-10	25	-12	-12	91	100									
E30	1	-22	-1	1	0	0	-2	0	100								
G30	1	-3	23	-20	1	1	-10	-9	35	100							
E333	-18	5	-8	14	0	0	2	2	4	0	100						
G333	16	-2	7	-13	0	0	-2	-1	-3	-1	-47	100					
E334	0	-3	-1	1	0	0	0	0	0	0	-4	-30	100				
G334	2	0	-3	4	0	0	0	1	0	0	40	74	22	100			
E463	-30	14	-12	22	0	0	3	2	6	0	6	-6	0	1	100		
G463	-6	36	3	-2	0	0	0	-1	3	2	1	0	-1	-1	-15	100	
G482	41	-5	-28	19	0	0	0	4	-13	-7	-5	0	1	3	-21	-4	100

[a] R1 and R2 are the channel radii as given in Table 2. E and G stand for E_o and Γ_n of Table 2. The numbers associated with E and G indicate the resonance (column 1 of Table 2) to which these correlation coefficients apply.

All resonances reported below 450 keV were seen in the capture data. For the resonances also seen in the transmission data the neutron widths were determined through the fit to the transmission data. The capture kernels, the radiation widths, and their uncertainties were obtained by fitting the capture data with the code LSFIT. As discussed in Section 3.4, the approximations used in this code for the calculations of self-shielding and multiple-scattering corrections for narrow resonances in the vicinity of large s-wave resonances could lead to an under or overestimation of the capture area by as much as 10%. This uncertainty is not included in the uncertainties given for the capture kernels and radiation widths in columns 4 and 5 of

Table 2. For resonances too weak to be seen in the transmission data (Note 2) only the capture kernels and their uncertainties were determined. The radiation widths were arbitrarily set equal to 0.5 eV with a $p_{1/2}$ assignment for these resonances. If the corresponding value of the neutron width gave a theoretical transmission consistent with the data this value of 0.5 eV was adopted, otherwise the neutron width was set to a small value consistent with the transmission data and the radiation width was adjusted to obtain the best fit to the capture data. If in this process the radiation width became larger than 1 eV a $p_{3/2}$ or a d-assignment was given to the resonance but the assignment is uncertain as indicated by the parentheses. Uncertainties on the neutron widths are given only when the resonances were analyzed in the transmission data.

No uncertainties are reported on the parameters of the weak resonances seen in the transmission data above 450 keV. Most of these resonances were adjusted by trial and error. The estimated uncertainties are 20 eV on the resonance energy and 10 to 20% on the neutron widths.

4.2 SPIN AND PARITY ASSIGNMENTS

The differential elastic scattering data are compared with the theoretical calculations for three elastic scattering angles from 30 to 813 keV in Figs. 10 to 44. The manner in which the spin and parity of some of the resonances can be determined through this comparison was reported in Section 3.3.

From 30 to 813 keV 311 $\ell > 0$ resonances could be identified in the differential scattering data but a definite spin and parity assignment could not be made for all of them (in the same energy region 353 resonances could be seen in the transmission data.) Of these 311 resonances 46 were too weak to provide any information on the spin and parity of the resonance. Definite ℓ-assignments can be made for 265 resonances, i.e., for 75% of the $\ell > 0$ resonances seen in the transmission data above 30 keV. The spin of 84% of the 126 p-wave resonances can be assigned with some degree of confidence (34 have a spin of 1/2 and 72 a spin of 3/2) but only 29% of the 139 d-wave resonances could be given a definite spin assignment (19 have a spin of 3/2 and 22 a spin of 5/2.) It is interesting to note that among the p-wave resonances where a definite J assignment can be made there are twice as many resonances with a J value of 3/2 than with a J value of 1/2. This ratio is in agreement with the $(2J + 1)$ weighting factor. Too few definite J assignments can be made in the case of d waves to draw conclusions regarding the ratio of the number of $d_{3/2}$ and $d_{5/2}$ resonances.

5. COMPARISON WITH OTHER WORKS

None of the previously reported ^{58}Ni resonance parameters were obtained through simultaneous analyses of two or three different nuclear reactions as done here. Among the transmission data analyses reported earlier, the most recent and extensive one is the Harwell data analysis (SYM77 and SYM78) between 10 and 650 keV which we will compare with our results along with the parameters given in an evaluation by Fröhner (FRO77) based on an analysis of capture yield measurements made at Karlsruhe (ERN70). These two sets of resonance parameters were extensively used by Mughabghab et al. (MUG81) in the most recent ^{58}Ni BNL resonance parameter evaluation. The recent capture measurements of Wisshak et al. (WIS84) below 30 keV will also be discussed.

5.1 COMPARISON WITH HARWELL RESONANCE PARAMETERS

The Harwell transmission data (SYM77) taken between 10 keV and a few MeV has an experimental resolution (0.075 ns/m)) comparable to the resolution of our 80-m data (0.050 ns/m), but above 180 keV our parameters were obtained from the data taken at the 200-m flight path station which has a much better resolution (0.025 ns/m). For example at 500 keV our resolution (FWHM) is 260 eV compared to ~700 eV for the Harwell data.

The parameters for the s-wave resonances were taken from a subsequent report (SYM78) where the data were analyzed with a single channel multilevel R-Matrix code in which an energy dependent effective scattering radius was used. At 400 keV this radius was equal to about 6 f.

In Table 4 the energies and the neutron widths for the s-wave resonances reported in Table 2 are compared with the parameters of Syme et al. (SYM78) up to 640 keV. Nine of our 48 s-wave resonances are not seen by Syme et al. Of these nine resonances four are weak in transmission but are clearly seen in the capture data; their assignment as s-wave resonances is uncertain. The other five are clearly identified as s-wave resonances from the transmission data. Syme et al. report two s-wave resonances not seen in our data; the one at 172 keV is very small and has a large uncertainty; the one at 473.96 keV is interpreted in our data as an $\ell = 2$ resonance at 476.07 keV.

The resonance energies reported in this work are systematically higher than the energies reported by Syme et al. Our reported neutron widths are larger for 29 of the 39 s-wave resonances seen in both data sets. In general the differences between these neutron widths are larger than the sum of the given statistical uncertainties.

The resonance parameters of the $\ell > 0$ resonances reported by Syme et al. (SYM77) were obtained through an area analysis (Atta-Harvey). The authors found 97 $\ell > 0$ resonances between 10 and 650 keV compared to the 273 that we could see in our transmission data in the same energy interval. In a subsequent analysis

Table 4. The parameters for the *s*-wave resonances reported in Table 2 compared with the results of two previous analyses

Present work			Syme and Bowen (SYM78)		Fröhner (FRO77)	
E_0 (keV)	Γ_n (eV)	Γ_γ (eV)	E_0 (keV)	Γ_n (eV)	E_0 (keV)	Γ_γ (eV)
15.310	1332.1 ± 2.6	0.97 ± 0.30	15.20	1330. ± 120.	15.4	1.46 ± 0.22
36.133	17.78 ± 0.28	1.72 ± 0.03	36.102	17. ± 5.		
63.295	3711. ± 6.	3.5 ± 0.7	63.10	3620. ± 59.	63.0	2.3 ± 0.3
83.391	4.0	1.16 ± 0.04				
108.343	1074.6 ± 3.9	4.8 ± 0.3	108.16	1007. ± 24.	107.7	3.8 ± 0.8
124.001	458.3 ± 2.6	1.56 ± 0.15	123.804	417. ± 13.	124.0	3.5 ± 0.6
137.606	2034. ± 8.	2.9 ± 0.8	137.40	2095. ± 43.	136.8	2.2 ± 0.4
140.288	3054. ± 10.	0.9 ± 0.6	140.08	3048. ± 67.	139.7	2.2 ± 0.5
158.088	5191. ± 12.	3.3 ± 0.8	157.66	4660. ± 86.	159.5	3.0 ± 1.0
168.949	413.6 ± 3.6	1.3 ± 0.2	168.66	300. ± 16.		
			172.00	10. ± 40.		
176.14[a]	4.8	0.56 ± 0.06				
191.896	2465. ± 8.	3.3 ± 0.5	191.54	2050. ± 47.	193.0	3.0 ± 1.0
206.557	7354. ± 15.	6.9 ± 1.0	205.93	5940. ± 110.	207.8	4.5 ± 2.0
211.045	56.9 ± 1.6	0.76 ± 0.06	211.00	15. ± 14.		
233.027	5584. ± 13.	5.3 ± 0.7	232.75	5820. ± 240.	230.4	9. ± 4.
242.36[a]	3.0	0.77 ± 0.12				
245.551	237.6 ± 2.7	0.55	245.02	143. ± 15.		
261.933	14.2 ± 0.8	1.05 ± 0.09				
272.488	5390. ± 13.	5.4 ± 0.6	272.07	4990. ± 110.		
281.599	1947. ± 8.	1.75 ± 0.40	281.06	1610. ± 60.		
285.38[a]	4.0	0.96 ± 0.15				
298.09[a]	4.0	0.56 ± 0.15				
305.405	655.9 ± 4.5	2.8 ± 0.5	304.63	547. ± 31.		
326.025	1582. ± 7.	0.4 ± 0.4	325.29	1580. ± 56.		
335.190	141.5 ± 2.9	2.54 ± 0.13				
349.660	1779. ± 7.	0.8 ± 0.5	349.05	1584. ± 62.		
367.740	125.9 ± 2.1	0.4	366.97	84. ± 2.		
395.027	694. ± 5.	0.5	394.13	600. ± 43.		
417.492	9359. ± 34.	2.6 ± 1.4	417.20	9930. ± 530.		
424.619	7714. ± 29.	3.3 ± 1.8	423.98	9090. ± 360.		
428.049	1084. ± 15.	0.9 ± 0.6	427.175	1590. ± 260.		
455.495	1787. ± 11.		454.43	1560. ± 110.		
462.253	437. ± 5.		461.17	310. ± 40.		
470.409	469. ± 6.		469.40	515. ± 48.		
			473.96	155. ± 29.		
491.810	178.2 ± 4.4					
496.317	1384. ± 10.		495.24	1280. ± 70.		
507.780	1496. ± 10.		506.65	1340. ± 75.		
523.516	1276. ± 9.		522.26	1160. ± 70.		
529.250	195.7 ± 3.7		527.80	300. ± 40.		
541.206	506. ± 7.		539.89	690. ± 50.		
553.713	2390. ± 16.		552.27	2770. ± 150.		
559.725	847. ± 13.		558.17	1260. ± 110.		
567.740	9092. ± 33.		566.24	7730. ± 260.		
588.830	2284. ± 15.		587.51	2400. ± 140.		
600.622	7845. ± 30.		599.27	6570. ± 430.		
618.202	399. ± 6.		616.50	333. ± 64.		
630.970	155. ± 7.					
636.371	9189. ± 45.		636.18	460. ± 310.		

[a] *s*-wave assignment is uncertain.

(SYM78) they mentioned that 230 $\ell > 0$ resonances were analyzed between 10 keV and 1 MeV but no values were given.

In Table 5 our parameters for $\ell > 0$ resonances are compared with the parameters of Ref. SYM77 up to 120 keV. In this energy range 22 of the 30 $\ell > 0$ resonances seen in our transmission data are also seen in the Harwell data. On the other hand we could not see in our transmission data the resonance reported by Syme et al. at 96.88 keV, but this resonance is clearly seen in our capture data. To be in agreement with our transmission data the $g\Gamma_n$ of this resonance must be three times smaller than the one given by Syme et al. They also report resonances at 52.26 and 118.07 keV that we do not see in any of our data; the first one is very narrow and has an 85% uncertainty, but the other one should have been seen in our data and was not. This last resonance may correspond to the resonance at 118.5 keV reported by Fröhner from the Karlsruhe capture-data analysis.

For most of their $\ell > 0$ resonances, between 10 and 300 keV, Syme et al. give three different values for $g\Gamma_n$: one for an enriched ^{58}Ni sample and two for two different samples of natural nickel. As they did when comparing their results with values given in an earlier report (MOX73) we compared our $g\Gamma_n$ results with their values obtained for the thick sample of natural nickel if available, otherwise with the value obtained for the isotopic sample. (However, for the resonance at 26.63 keV they chose to compare with Moxon the value obtained for the ^{58}Ni sample even though there were values for the two other samples.) Only eight (out of 22) of the neutron widths of the $\ell > 0$ resonances, seen in the ORELA and Harwell transmission data below 120 keV, agree within the limits of the uncertainties. For the resonance at 32.397 keV the neutron widths obtained by Syme et al. for both samples of natural nickel are three times smaller than our value (5.7 ± 0.9 eV compared to 17.6 ± 0.3 eV), whereas the value given for the ^{58}Ni sample is equal to 15.0 ± 1.2 eV which is in much better agreement with our value of 17.6 eV.

5.2 COMPARISON WITH FRÖHNER'S EVALUATION

The Karlsruhe capture cross section data were analyzed with a multilevel R-matrix code between 10 and 230 keV. Fröhner remarks that above 160 keV the resolution was insufficient for a reliable interpretation of multiplets.

Between 10 and 235 keV we report 14 well-defined s-wave resonances. (The resonance at 176.14 keV in not clear in transmission and its s-wave assignment is uncertain.) In the same energy interval Fröhner reports ten s-wave resonances. Because of our higher resolution we identify only four of their ten s-wave resonances as singlets (at 15.4, 63.0, 136.8 and 159.5 keV) for which the radiation widths can be compared with ours. For the resonance at 63 keV the discrepancy between the two Γ_γ's is slightly larger than the combined uncertainties; otherwise, the agreement is good. The other six s-wave resonances are unresolved multiplets of $\ell = 0$ and $\ell > 0$ resonances. It should be noted that above 150 keV the uncertainties on the energies of the s-wave resonances reported by Fröhner are between 2 and 3 keV.

Table 5. The neutron widths and capture kernels from Table 2 for the $\ell > 0$ resonances below 120 keV compared with the results from two previous analyses.

Present work			Syme et al. (SYM77)		Fröhner (FRO77)	
E_0 (keV)	$g\Gamma_n$ (eV)	$g\Gamma_n\Gamma_\gamma/\Gamma$ (eV)	E_0 (keV)	$g\Gamma_n$ (eV)	E_0 (keV)	$g\Gamma_n\Gamma_\gamma/\Gamma$ (eV)
6.906[a]	0.025	0.024 ± 0.001				
12.641[a]	0.032	0.030 ± 0.002				
13.317	7.43 ± 0.05	0.72 ± 0.01	13.42	4.9 ± 2.5	13.34	0.50 ± 0.08
13.638	2.14 ± 0.06	0.68 ± 0.01	13.63	2.9 ± 1.2	13.68	0.63 ± 0.20
17.232[a]	0.032	0.030 ± 0.004			17.21	0.02 ± 0.01
19.010[a]	0.090	0.077 ± 0.004			19.05	0.08 ± 0.02
20.024	1.39 ± 0.12	0.29 ± 0.01			20.04	0.24 ± 0.05
21.144	4.24 ± 0.24	0.76 ± 0.01			21.15	0.61 ± 0.10
24.762[a]	0.018	0.018 ± 0.001				
26.069[a]	0.42	0.35 ± 0.01			26.08	0.27 ± 0.05
26.643	2.9	0.96 ± 0.01	26.63	1.9 ± 0.5	26.65	0.78 ± 0.15
27.63[a]	0.039	0.036 ± 0.003				
32.268	0.60	0.46 ± 0.01				
32.397	17.61 ± 0.28	1.48 ± 0.02	32.38	5.7 ± 0.9	32.34	1.40 ± 0.25
34.242	1.6	0.77 ± 0.01	34.22	1.8 ± 0.5	34.23	0.70 ± 0.11
35.070[a]	0.021	0.020 ± 0.005				
					36.12	0.99 ± 0.15
39.552	1.1	0.78 ± 0.01	39.54	2.2 ± 0.4	39.55	0.64 ± 0.10
44.013[a]	0.17	0.138 ± 0.004			43.88	0.14 ± 0.03
47.901	9.0 ± 0.6	1.38 ± 0.02	47.88	7.0 ± 0.8	47.81	1.03 ± 0.15
51.906	1.2	0.95 ± 0.01				
52.226	2.0	1.10 ± 0.01	52.20	2.3 ± 0.5	52.01	1.70 ± 0.30
			52.26	0.53 ± 0.45		
54.790[a]	0.67	0.29 ± 0.01			54.64	0.30 ± 0.05
58.700	1.6	0.71 ± 0.02	58.69	1.7 ± 0.6	58.60	0.60 ± 0.09
60.150	32.9 ± 0.7	0.86 ± 0.02	60.12	21.2 ± 3.0	60.10	0.64 ± 0.09
61.791	17.2 ± 0.7	1.68 ± 0.03	61.76	16.1 ± 2.4	61.75	1.11 ± 0.16
66.473[a]	1.4	0.71 ± 0.02			66.40	0.55 ± 0.08
68.673[a]	0.62	0.28 ± 0.02			68.56	0.30 ± 0.05
69.917	7.3 ± 0.6	0.62 ± 0.02	69.89	5.1 ± 1.2	69.81	0.56 ± 0.09
78.087[a]	0.49	0.25 ± 0.14			77.86	0.18 ± 0.05
81.326	2.0	1.29 ± 0.03			81.10	1.08 ± 0.20
82.877	83.0 ± 1.2	2.66 ± 0.04	82.84	63.0 ± 3.0	82.7	2.0 ± 0.5
83.845	31.0 ± 0.9	0.25	83.82	36.4 ± 2.2	83.6	1.5 ± 0.4
83.917	4.6	1.39 ± 0.02				
84.878[a]	0.40	0.20 ± 0.01				
89.984	9.0 ± 0.7	0.75 ± 0.01	89.93	8.8 ± 1.5	89.78	0.69 ± 0.1
92.725[a]	0.49	0.25 ± 0.01			92.35	0.25 ± 0.04
95.680[a]	1.95	1.47 ± 0.03			95.55	1.05 ± 0.15
96.978[a]	1.2	0.64 ± 0.02	96.88	3.7 ± 1.1	97.0	0.66 ± 0.10
97.604	20.0 ± 0.9	0.43 ± 0.02	97.58	11.2 ± 0.7		
101.42	8.7 ± 0.6	1.28 ± 0.03	101.38	3.2 ± 1.0	101.1	0.95 ± 0.24
105.443	19.0 ± 0.9	2.49 ± 0.03	105.38	21.7 ± 3.3	105.3	1.60 ± 0.40
107.12	1.0	0.31 ± 0.03			unresolved from the	
107.760	5.7	1.72 ± 0.04	107.74	7.7 ± 1.9	s-wave res. at 107.7 keV	
110.750	7.9	0.96 ± 0.04	110.67	4.5 ± 1.5	110.7	1.1 ± 0.3
111.490	2.0	0.85 ± 0.04				
116.82[a]	0.22	0.15				
117.879	16.5 ± 1.0	1.15 ± 0.04	117.82	10.1 ± 0.7	117.5	0.75 ± 0.25
			118.07	4.2 ± 1.5	118.5	1.2 ± 0.4
119.800	7.8	2.94 ± 0.04	119.75	6.6 ± 1.2	120.0	2.4 ± 0.8

[a]Resonances seen in capture data only. The values of the neutron widths were chosen to be consistent with the transmission data.

In Table 5 we compare the parameters obtained from our capture data for the $\ell > 0$ resonances with those of Fröhner between 13 and 120 keV. In this energy region we report 46 $\ell > 0$ resonances whereas Fröhner reports only 36. Five of our small resonances were not seen in the Karlsruhe data. Four resonances reported by Fröhner are clearly seen as pairs of resonances in our data, and we identified as an unresolved doublet the resonance seen by Fröhner at 83.6 keV. On Fig. 17 the resonances at 107.12 and 107.76 keV are seen clearly separated from the s-wave resonance whereas these two resonances and the s-wave resonance at 107.7 keV are unresolved in the Karlsruhe data. The resonance reported by Fröhner at 36.12 keV corresponds unmistakably to our small s-wave resonance at 36.13 keV, but the one he reports at 118.5 keV with a capture kernel of 1.2 eV should be seen clearly in our data but is definitely not there. As mentioned earlier, Syme et al. also report a resonance around that energy. Twenty-nine resonances are singlets in both analyses. For these resonances our capture kernels are systematically larger than the ones reported by Fröhner. This difference in the capture kernels is reflected in the average capture cross-section discussed in Section 6.7.

Above 120 keV resonance by resonance comparison is not possible since, up to 230 keV, Fröhner reports only 12 $\ell > 0$ resonances where we have 58.

5.3 COMPARISON WITH WISSHAK'S CAPTURE KERNELS BELOW 30 KEV

The most recent measurements of capture yield in the low-energy region were made by Wisshak et al. (WIS84) using Moxon-Rae detectors and various sample thicknesses. Two methods were used to evaluate the capture kernels. The final values obtained for the first s-wave resonance are $E_o = 15.35$ keV and $\Gamma_\gamma = 1.53 \pm 0.10$ eV. This radiation width is in good agreement with Fröhner's value but 50% larger than ours.

In WIS84 an attempt is made to evaluate the capture kernel for three groups of unresolved $\ell > 0$ resonances below 30 keV. These parameters, ours and those of Fröhner, are compared in Table 6. For the first group around 13.5 keV our value is 11% higher than the value of Wisshak et al., but, as discussed in Section 3.4, a 10% under or overestimation was possible in the calculation of the capture kernels for this group of narrow resonances because of the vicinity of the large s-wave resonance at 15.31 keV. Our parameters are slightly lower (3%) than those of Wisshak et al. for the two other groups. Fröhner's parameters are systematically smaller than ours and Wisshak et al. by as much as 30% for the group around 26 keV.

Table 6. The sums of the capture kernels of the resolved multiplets, below 30 keV, reported in this work and in Fröhner's evaluation compared with the results of Wisshak et al.

	$g\Gamma_n\Gamma_\Gamma/\Gamma$ (eV)		
E (keV)	This work[a]	Fröhner (FRO77)	Wisshak et al. (WIS84)
13.32	0.72 ± 0.07	0.50 ± 0.08	
13.64	0.68 ± 0.07	0.63 ± 0.20	
	1.40 ± 0.10	1.13 ± 0.22	1.26 ± 0.08
19.01	0.077 ± 0.005	0.08 ± 0.02	
20.02	0.29 ± 0.02	0.24 ± 0.05	
21.14	0.76 ± 0.03	0.61 ± 0.10	
	1.13 ± 0.04	0.93 ± 0.11	1.17 ± 0.08
24.76	0.018 ± 0.002		
26.07	0.35 ± 0.02	0.27 ± 0.05	
26.64	0.96 ± 0.04	0.78 ± 0.15	
27.63	0.036 ± 0.004		
	1.36 ± 0.05	1.05 ± 0.16	1.40 ± 0.09

[a] A 10% systematic uncertainty was combined with the statistical uncertainty for the first two resonances, and a 4% systematic uncertainty for the remaining resonances.

5.4 COMPARISION WITH ENDF/B-V RESONANCE PARAMETERS

The resonance parameters for ^{58}Ni in ENDF/B-V (DIV79) are the same as in ENDF/B-IV and ENDF/B-III and are based on an evaluation by Stieglitz et al. (STI73). Thirty s-wave and 36 p-wave resonances were reported between 6 and 650 keV. The radiation widths were set equal to 2.14 eV for all the s-wave resonances and to 0.6 eV for 34 of the 36 $\ell > 0$ resonances which have a $p_{1/2}$ or a $p_{3/2}$ assignment. See Section 6.7 for the comparison of the average capture cross sections calculated with ENDF/B-V and with our data. The new set of resonance parameters given in the present report is a definite improvement over the resonance parameters given in ENDF/B-V.

6. DISCUSSION OF RESULTS

6.1 REDUCED NEUTRON WIDTH DISTRIBUTION OF *S*-WAVE RESONANCES

Sixty-two *s*-wave resonances are reported from 10 to 813 keV. Six of those are weak resonances for which the *s*-wave assignment is uncertain. The distribution of the reduced neutron widths of the *s*-wave resonances is usually assumed to follow a Porter-Thomas distribution (POR56).

The reduced neutron width at 1 eV for *s*-wave resonances is

$$\Gamma_n^0 = \Gamma_n \sqrt{1\text{eV}/E_n} \ ,$$

where E_n is in eV.

The Porter-Thomas density function is:

$$P(x) = (2\pi x)^{-1/2} e^{-x/2} \ ,$$

where $x = \Gamma_n^0/\overline{\Gamma}_n^0$ and $\overline{\Gamma}_n^0$ is the average reduced neutron width.

The distribution of the reduced neutron widths has a mean of 4.2 eV and a standard deviation of 1.7 eV. The histogram giving the normalized reduced neutron widths, $\Gamma_n^0/\overline{\Gamma}_n^0$, for the 62 s-wave resonances found in the region analyzed is shown in Fig. 45 (top). The smooth curve is the Porter-Thomas density function normalized to give the same number of levels under the curve as the observed number of levels in the range of values of x from 0.2 to 4.0 where we assume that no *s*-wave resonance was missed. The normalization factor for this range of values of x is 13.1. In the range of values of x smaller than 0.2 (which correspond to small resonances), this normalized Porter-Thomas distribution is in agreement with the number of levels observed, i.e., 21 levels.

6.2 *S*-WAVE LEVEL SPACINGS

The average level spacing for the *s*-wave resonances, D_o, obtained from the 62 *s*-wave resonances reported in Table 2 and in agreement with the Porter-Thomas distribution, is equal to 12.9 keV. An uncertainty of 0.7 keV on D_o is estimated by taking into consideration the fact that six of these 62 resonances have an uncertain *s*-wave assignment. D_o is given in Table 7 and compared with two values of D_o reported earlier. Syme and Bowen (SYM78) as well as Mughabghab et al. (MUG81) assumed that some weak *s*-wave resonances were missed; their reported values of D_o reflect corrections they made for these missing levels.

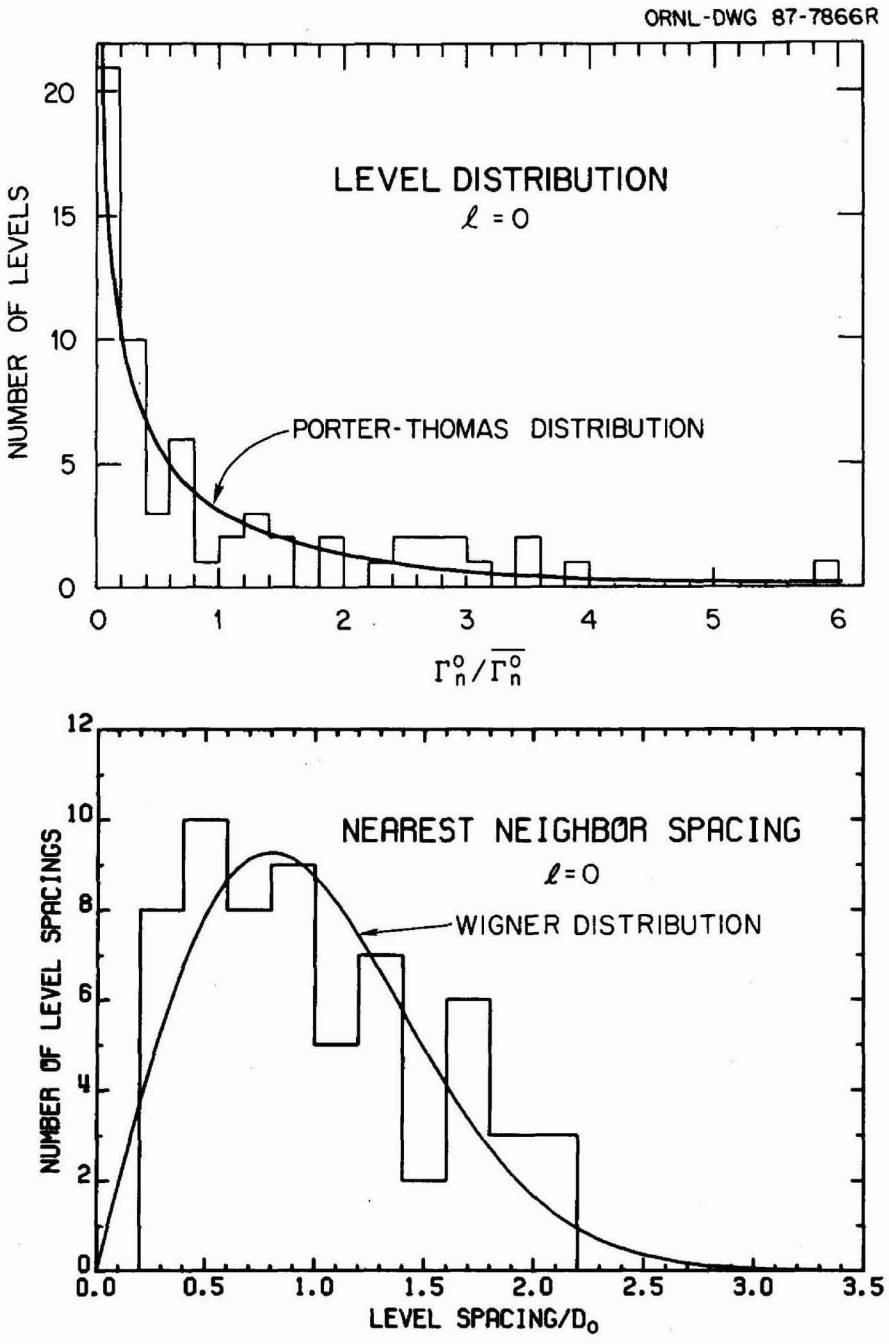

Fig. 45. TOP: The neutron reduced width distribution for the 62 *s*-wave resonances of Table 2. The smooth curve is the Porter-Thomas distribution normalized to the area under the histogram between $\Gamma_n^0/\bar{\Gamma}_n^0 = 0.2$ and 4.0. BOTTOM: The nearest neighbor spacing distribution for the 62 *s*-wave resonances. The smooth curve is the Wigner distribution normalized to the area under the histogram.

Table 7. Statistical resonance parameters for s-wave resonances compared with the results of Syme and Bowen (SYM78) and with the recommended values of Mughabghab et al. (MUG81)

Source	Energy range (keV)	S_o (10^4)	D_o (keV)
Present work	10–813	3.1 ± 0.6	12.9 ± 0.7
Syme and Bowen	10–640	2.9 ± 0.6	14.6 ± 0.4
Mughabghab et al.	10–650	2.8 ± 0.6	13.7 ± 2.0

The distribution of the s-wave nearest neighbor spacings is compared to the Wigner distribution (WIG57) on Fig. 45 (bottom). The Wigner density function is:

$$P(x) = 1/2\pi x e^{-1/4\pi x^2}$$

where $x = d_o/D_o$. d_o is the spacing between neighboring s-wave levels and D_o is the average level spacing. The Wigner distribution was normalized to the area under the histogram.

The distribution of the s-wave level spacing shown by the histogram on Fig. 45 (bottom) is in reasonable agreement with the Wigner distribution.

6.3 LEVEL DENSITIES

As previously done for the ^{60}Ni analysis (PER83), we now compare the number of levels observed with those predicted by the Gilbert and Cameron model (GIL65) where the Fermi-gas constant, a, and the energy shift parameter, Δ, are treated as free parameters.

Gilbert and Cameron started from a Fermi-gas model of the nucleus which was modified to take into account the pairing energy and possible shell model effects, using an effective excitation energy U instead of the actual excitation energy E. The density of levels of total angular momentum J at an effective excitation energy U is given by

$$\rho(U,J) = \frac{\exp[2\sqrt{aU}]}{12a^{1/4}U^{5/4}} \frac{(2J+1)}{2\sqrt{2}} \times \frac{\exp[-(J+1/2)^2/2\sigma^2]}{\sigma^3} ,$$

where a is the Fermi-gas constant and σ^2 is called the spin cutoff parameter. The effective excitation energy U is related to the actual excitation energy E above the ground state by the relation $U = E - \Delta$.

In the Fermi gas model the spin cutoff parameter σ^2 is given by:

$$\sigma^2 \simeq 0.0888 A^{2/3} \sqrt{aU} \ .$$

This value of σ^2 corresponds approximately to the compound system having a moment of inertia equal to 75% of its rigid moment of inertia.(DIL73)

Calculations were made for the s-wave level density using the 62 s-wave resonances reported in Table 2 between 10 and 813 keV with an uncertainty of four levels, together with the low-lying bound levels of ^{59}Ni taken from the Nuclear Data Sheets (AND83). Above the pairing energy gap in ^{59}Ni the highest level density is observed from 3.46 to 4.2 MeV where there are 24 levels. This region was therefore selected and an uncertainty of four levels was used.

The values of the Fermi-gas constant a and the energy shift parameter Δ were obtained using the computer code LEVDEN (LAR88). LEVDEN is a fitting code that solves Bayes' equation, using as prior values 5 ± 10 MeV^{-1} for the Fermi-gas constant and 0 ± 3 MeV for the energy shift parameter. The code was required to produce 24 ± 4 levels in the excitation energy interval of 3.46 to 4.2 MeV above the ground state of ^{59}Ni and 62 ± 4 s-wave levels in the energy interval of 10 to 813 keV above the neutron binding energy of 9.000 MeV in ^{59}Ni. The number of observed resonances for which ℓ is larger than zero was not used in the fitting process because only 35% of them have a definite spin and parity assignment. The posterior values for the Fermi-gas constant and the energy shift parameter, with their standard deviations, were found to be

$$a = 5.61 \pm 0.21 \text{ MeV}^{-1}$$

$$\Delta = -0.06 \pm 0.39 \text{ MeV}$$

with a correlation coefficient of 0.97. The integral of the theoretical level density formula from 10 to 813 keV for $\ell = 0$ resonances calculated with the above parameter values and their uncertainties is shown by the dashed line on the bottom part of Fig. 46 and is compared with the cumulative sum of the observed s-wave resonances.

Of the 415 $\ell > 0$ resonances reported in Table 2, 64% have a definite ℓ-assignment. Therefore, we cannot compare separately the level densities for the $\ell = 1$ and for the $\ell = 2$ resonances with the predictions of the Gilbert and Cameron model. However, assuming that only $\ell = 1$ and $\ell = 2$ resonances were observed in the experiment, we can compare the $\ell > 0$ level density with the prediction for the sum of the $\ell = 1$ and $\ell = 2$ levels using the a and Δ parameters determined above. Such a comparison is shown on the top part of Fig. 46. As was the case for ^{60}Ni, the number of $\ell = 1$ and $\ell = 2$ resonances observed above 150 keV is higher than predicted. However, it is possible that some of the $\ell = 1$ and $\ell = 2$ resonances assigned in the analysis may be $\ell > 2$ resonances. The good agreement with the Gilbert and Cameron formula below 150 keV would then indicate that very few $\ell = 1$ and $\ell = 2$ resonances were missed between 10 and 150 keV.

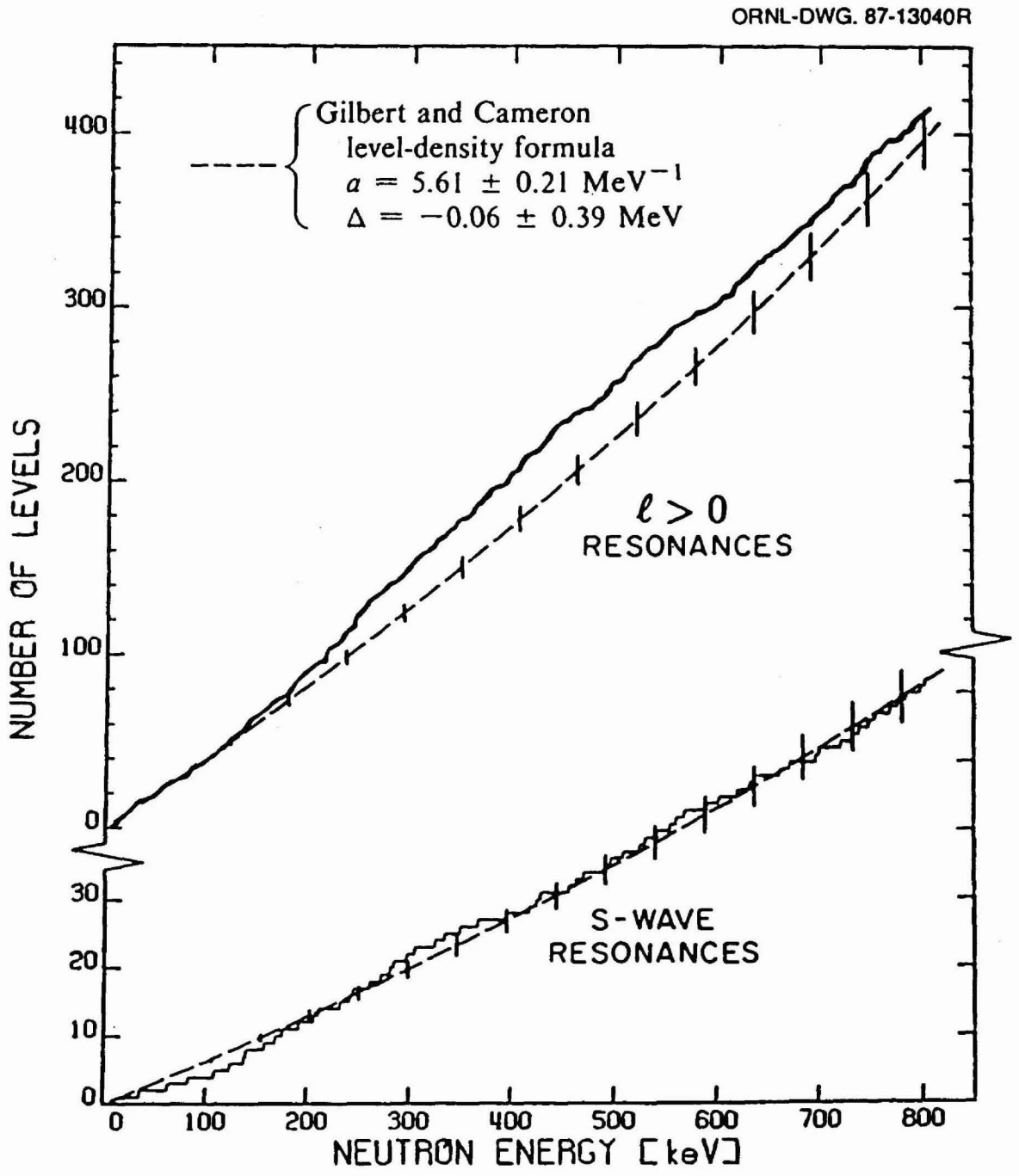

Fig. 46. Cumulative number of resonances for $\ell = 0$ and for $\ell = 0$ as a function of incident neutron energy. The full lines represent the number of observed resonances; the dashed lines are fits to the data using the Fermi-gas model (Gilbert and Cameron formula) as discussed in Sect. 6.3.

6.4 *S*-WAVE STRENGTH FUNCTION AND DOORWAY STATES

The strength function, S_o, is defined as

$$S_o = \frac{\overline{\Gamma}_n^0}{D_o} = \frac{N-1}{N} \frac{\sum_{\lambda=1}^{N} \Gamma_{n,\lambda}^0}{E_N - E_1} \ . \tag{6.4.1}$$

where E_1 is the energy of the first resonance analyzed and E_N the energy of the last one. If one considers the uncertainties in the quantities that appear on the right-hand side of the expression, there is a very small uncertainty in the value of S_o from the analysis of the data. However, as is well known (LYN68), if N levels are drawn randomly from a Porter-Thomas distribution having mean value $\overline{\Gamma}_n^0$, the expectation value in the sum of these N levels is $N\overline{\Gamma}_n^0$ and the variance in this sum is $2N(\overline{\Gamma}_n^0)^2$. Therefore, even though we may have obtained with great accuracy the total strength in the energy interval 0 to 813 keV, there is a relative standard deviation of $\sqrt{2/N}$ or 18% in the numerator of S_o. In comparison the uncertainty in $E_N - E_1$ is small even though one could argue that since the full strength of the first and last resonances is taken in the summation of the reduced neutron widths, half of the average level spacing D_o should be added at each end of the energy interval $E_N - E_1$. The maximum uncertainty on the denominator would still be only 3%. The estimate of the s-wave strength function calculated with relation (6.4.1) is $(3.3 \pm 0.6) \times 10^{-4}$.

An alternative method of obtaining S_o is from the slope of the plot of the cumulative sum of the reduced neutron widths of the observed resonances as a function of the incident energy as shown on Fig. 47. There is no ambiguity in obtaining the s-wave strength function from a staircase plot such as this one since it can be reasonably well approximated by a straight line over the complete energy range analyzed. The value so found is $(3.1 \pm 0.6) \times 10^{-4}$. This value represents a minimal attempt at mitigating the sharpness of the weighting function.

The s-wave neutron strength recommended in Ref. MUG81 for ^{58}Ni in the 10 to 650 keV energy range is $(2.8 \pm 0.6) \times 10^{-4}$. Syme and Bowen (SYM78) reports a value of $(2.9 \pm 0.6) \times 10^{-4}$ from their analysis up to 640 keV. See Table 7.

If one is interested in studying modulations of the strength function in terms of doorway states, it is convenient to average the reduced R function with a Lorentzian weighting function (MAH67). The poles of the Teichman-Wigner reduced R function (TEI52) are necessarily below the energy axis, and we have

$$R(E) = \sum_{\lambda} \frac{\gamma_{n,\lambda}^2}{E_\lambda - E - i\gamma_{e,\lambda}^2/2} \ , \tag{6.4.2}$$

where in our case $\gamma_{e,\lambda}^2$'s are the effective reduced level widths for the eliminated channels: the capture channels. It should be noted that the sum is to be carried over all the poles of the R function, that is to say, it should include the poles outside

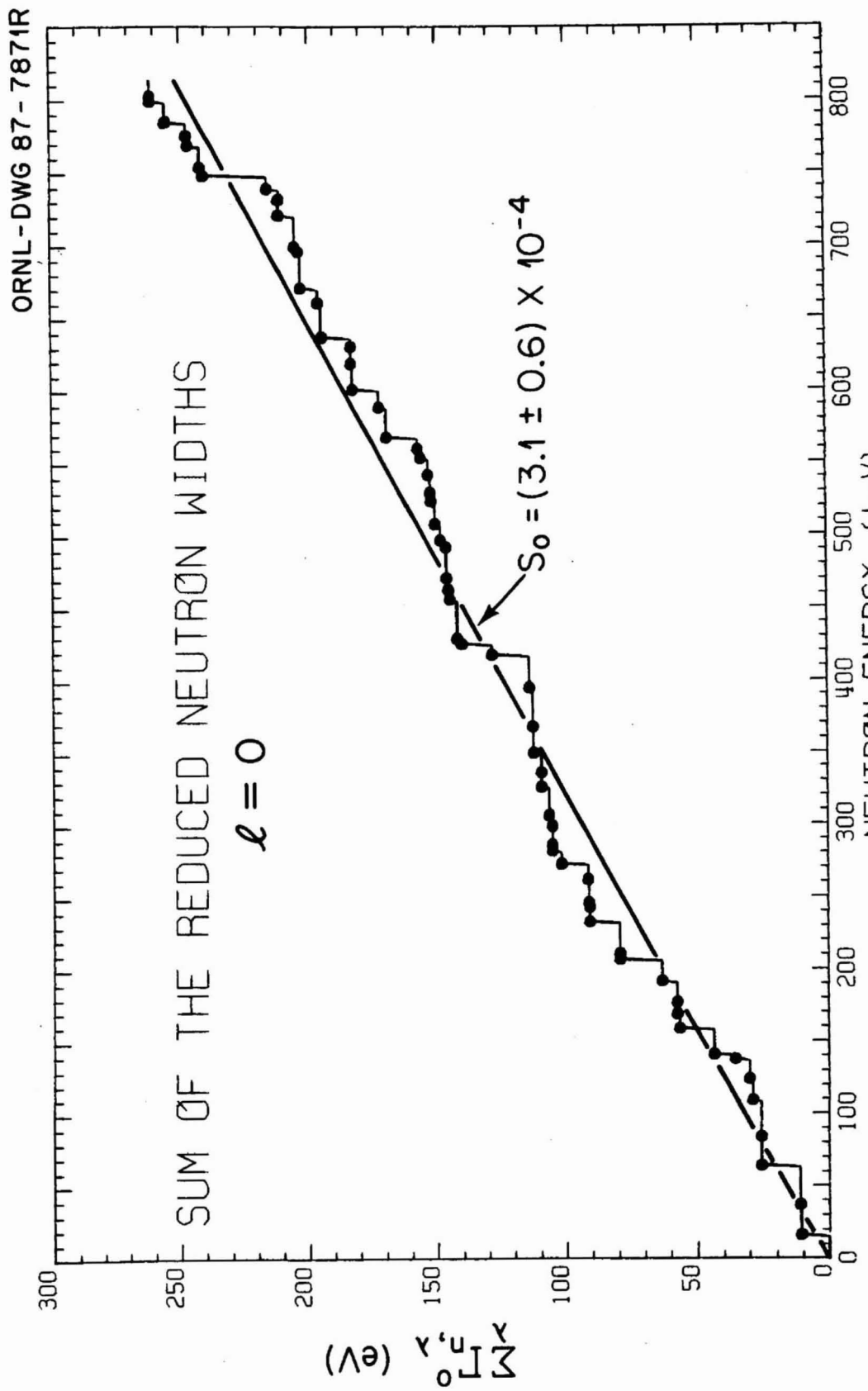

Fig. 47. The sum of the reduced neutron widths for s-wave resonances as a function of incident neutron energy. The strength functions, S_o, is given by the slope of the straight line.

the energy region analyzed. Because the poles of the reduced R function are below the real axis, if one calculates the R function at an energy $E + iI$, where I is a positive number, one is calculating an average value of the R function at the energy E. The amount of averaging that one performs is controlled by the size of I. In the statistical model, one makes I very large compared to the average level spacing in order to completely average over the statistical fluctuations. If the level widths have a Porter-Thomas distribution, I must also be very large in order to effectively average over the fluctuations. The value of the R function at a complex energy $E + iI$ where $I >> \gamma^2_{e,\lambda}$ is usually denoted by

$$R(E + iI) = \overline{R}(E, I) + i\pi S(E, I) \ , \tag{6.4.3}$$

where

$$\overline{R}(E, I) = \sum_{\lambda} \frac{\gamma^2_{n,\lambda}(E_\lambda - E)}{(E_\lambda - E)^2 + I^2} \tag{6.4.4}$$

and

$$S(E, I) = \frac{I}{\pi} \sum_{\lambda} \frac{\gamma^2_{n,\lambda}}{(E_\lambda - E)^2 + I^2} \ . \tag{6.4.5}$$

Because of the factor $E_\lambda - E$ in the numerator, $\overline{R}(E, I)$ is often identified with the contribution of the distant levels, away from the value of E, to the average. The absence of such a factor in the numerator of $S(E, I)$ means that its value at the energy E is more strongly dominated by the levels near the energy E and $S(E, I)$ is often called the Lorentzian averaged strength function.

In Fig. 48, $S(E, I)$ is calculated using $I = 4D_o$; the contributions of the levels inside the energy region analyzed, S_{int}, and those of the levels outside of the energy region, S_{ext}, are shown. It should be noted that the levels outside the energy region analyzed are not "physical levels" in the sense that we expect actual resonances or states to be observed there. These external levels are merely an expansion of the contribution of the levels outside the energy region to the R function inside the energy range analyzed. These contributions must be included in any analysis in order to fit the data but are often not represented by a pole expansion except for a single negative energy resonance.

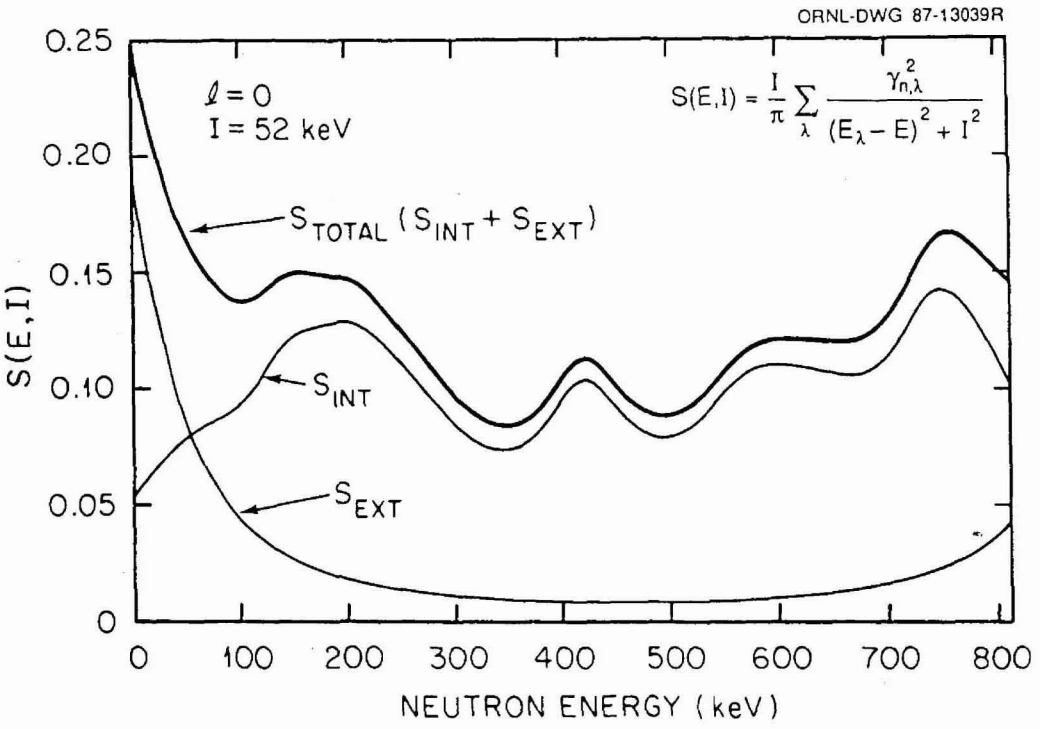

Fig. 48. Lorentz-weighted *s*-wave strength function of the reduced level widths averaged with $I = 52$ keV between 0 and 810 keV. S_{INT} is the contribution of the 62 observed *s*-wave resonances inside the 0- to 810-keV region. S_{EXT} is the contribution of the five outside resonances. S_{TOTAL} is the sum of S_{INT} and S_{EXT}.

Figure 48 displays graphically the modulation of strength of levels in the energy region analyzed. In the case of ^{60}Ni, similar but slightly more pronounced modulations were interpreted as suggestive of possible doorway states. However, such modulations could be due merely to statistical fluctuations in the level widths. In Figure 49(a) we show the staircase plot for the ^{58}Ni data together with four other staircase plots where the reduced level widths were selected randomly from the Porter-Thomas distribution based upon the level widths observed for ^{58}Ni, the energies of the levels being those observed for ^{58}Ni. In Figure 49(b) we show the corresponding Lorentz-weighted *s*-wave strength functions. Since in two of the four cases where the reduced level widths were selected randomly from a Porter-Thomas distribution the modulations in the Lorentz-weighted *s*-wave strength functions are larger than those observed for ^{58}Ni, it does not seem that one should interpret the modulations observed for ^{58}Ni as evidence for possible doorway states.

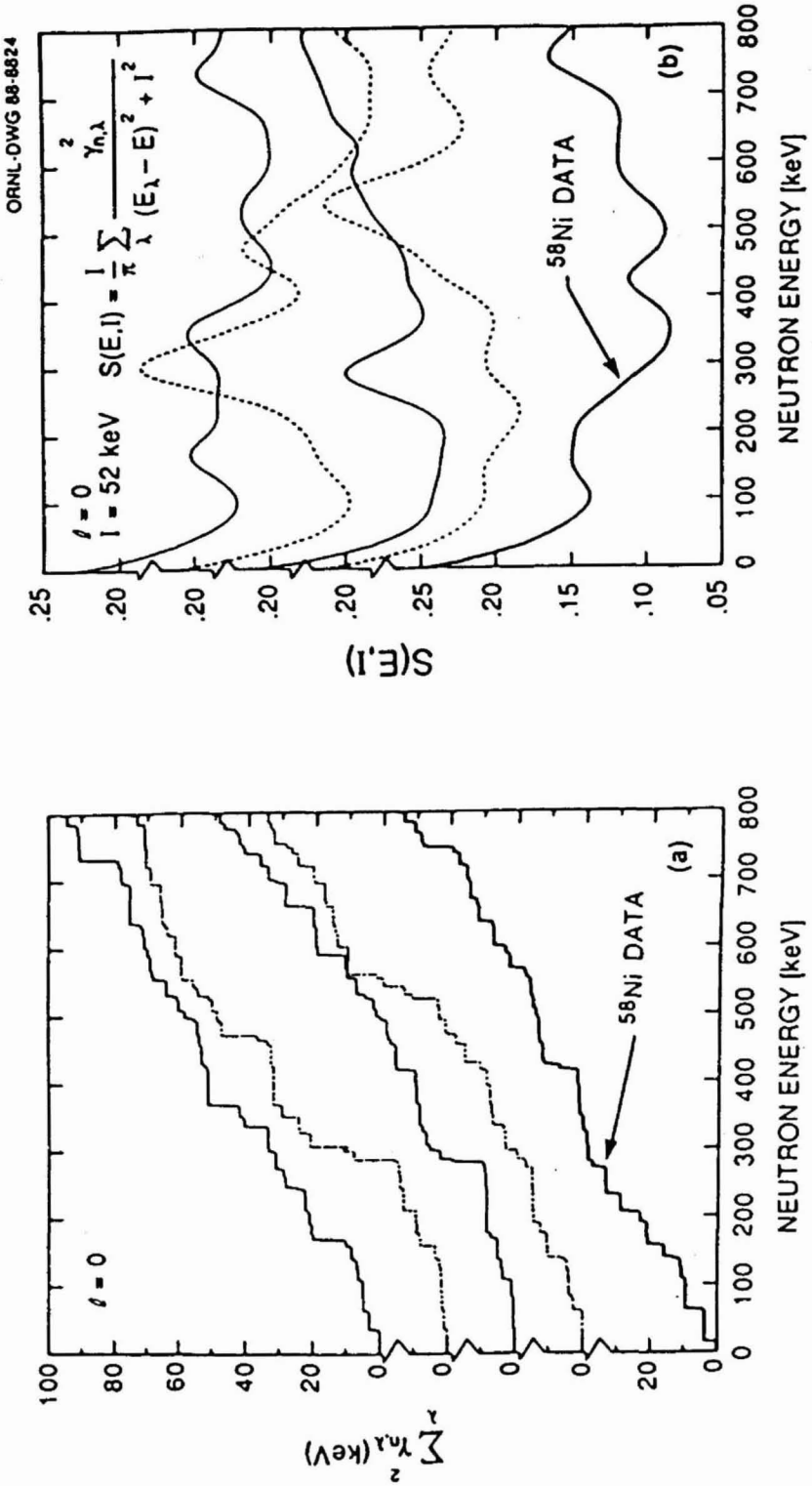

Fig. 49. Comparison of the ^{58}Ni data with results obtained from 4 sets of randomly distributed reduced level widths. (a) The summations of the reduced level widths of the *s*-wave resonances included in the 0- to 800-keV energy region are shown. (b) The Lorentz-weighted strength functions of the reduced level widths are shown in the 0- to 800-keV energy regionb, but all the *s*-wave resonances (including the five fictitious ones) were used in the computation.

6.5 AVERAGE RADIATION WIDTHS

6.5.1 $\ell = 0$ Resonances

Of the 31 s-wave resonances reported between 10 and 450 keV, four are weak resonances in the transmission data. Their s-wave assignment are uncertain; therefore, they were not used in the computation of the s-wave resonance average radiation width.

The mean value of the distribution of the radiation widths of the remaining 27 s-wave resonances is equal to 2.3 eV and the standard deviation of the distribution is 1.7 eV. As indicated by Note 3 in Table 2, 19 of these 27 s-wave resonances had their radiation width corrected for the neutron sensitivity of the detector.

The mean value of the distribution of the s-wave radiation widths for ^{58}Ni (2.3 eV) is considerably larger than the value of 1.3 eV found for ^{60}Ni but is consistent with previous measurement (FRO77).

6.5.2 $\ell > 0$ Resonances

Only the resonances whose angular momentum and spin could be determined through the analysis of the differential elastic-scattering data were used in the computation of the average radiation widths for the $\ell = 1$ and $\ell = 2$ resonances. Of these resonances we eliminated the ones which were part of a multiplet since for these resonances only the sum of the capture areas is well determined, not the capture area of each individual resonance.

The mean value of the distribution of the radiation widths of the p-wave resonances, calculated from the parameters of 39 resonances, is equal to 0.77 eV and the standard deviation is 0.33 eV.

For the d-wave resonances the mean value of the distribution of the radiation widths calculated from the parameters of only nine resonances is equal to 1.3 eV and the standard deviation is 0.5 eV. The mean value of the distribution would be 1.2 eV if the calculation included the 37 resonances for which the $\ell = 2$ assignment is determined but not their spin. The fact that this value of 1.2 eV is close to the one obtained with the nine single resonances for which the spin and parity are known just indicates that the spins we assigned to these 37 resonances based solely on the value of $g\Gamma_\gamma$ are consistent with the little information we have for the d-wave resonances.

6.6 CORRELATION BETWEEN Γ_N^o AND Γ_γ FOR S-WAVE RESONANCES

Because a correlation between the reduced neutron widths and the radiation widths of the s-wave resonances might indicate nonstatistical effects, such correlation coefficients are frequently calculated.

From the analyses of high-resolution ORELA data for medium weight nuclides the correlation coefficients between Γ_n^o and Γ_γ for eight nuclides in the mass region $54 \leq A \leq 68$ were calculated and reported in Ref. PER83.

The correlation coefficient calculated with the parameters of Table 2, for the 31 s-wave resonances between 10 and 450 keV, is 0.69 ± 0.10. If the four small s-wave resonances for which the spin and parity assignment is uncertain are not taken into account the correlation coefficient becomes 0.66 ± 0.11. The value obtained for ^{60}Ni (PER83) was 0.53 ± 0.18. This correlation coefficient was obtained from 30 s-wave resonances observed in the same energy interval of 10 to 450 keV. The uncertainties on the correlation coefficients reflect only the distribution of the widths. The effect on the value of the correlation coefficients of the large uncertainty on the neutron sensitivity coefficient, C, is discussed in Ref. PER83.

For the nine nuclides studied in the mass region $54 \leq A \leq 68$ the values of the correlation coefficients range from 0.33 for ^{59}Co to 0.94 for ^{54}Fe, the average value of these coefficients being 0.56. Therefore, it seems that, in this mass region, there is a significant correlation between the neutron and the radiation widths suggesting nonstatistical effects. It should be noted that in the case of ^{60}Ni the distribution of the s-wave neutron strength was indicative of such nonstatistical effects but those are not as evident in the case of ^{58}Ni.

6.7 AVERAGE AND THERMAL CAPTURE CROSS SECTIONS

The average capture cross sections given in Table 8 in lethargy intervals up to 450 keV were obtained by summing the capture areas of the resonances in each interval including the contributions from the negative energy resonances. The uncertainties include the statistical uncertainties as well as the uncertainties from the correction for the detector neutron sensitivity. The uncertainties in the correction for the detector neutron sensitivity were treated as uncorrelated.

The average capture cross section above 400 keV was obtained from the average capture data in the following manner: from 400 keV to 1400 keV the thick sample data were corrected for sample thickness effects, primarily capture after scattering, using strength functions and averaging over a Porter-Thomas distribution in each energy interval. Average scattering cross sections were computed from the present work up to 800 keV and from the literature up to 1000 keV then extrapolated to 1400 keV. Inelastic scattering to the first 2^+ level begins at a 1480-keV threshold and the detectors responded strongly to the inelastic gamma ray. These sample thickness corrections ranged from 10% to 3% in the 400–1400 keV energy range for the intervals shown.

Table 8. Average capture cross section from this work and from Ref. FRO77. The values obtained from ENDF/B-V, which include a 6-mb smooth background, are also reported.

Energy range (keV)	Average capture cross section (mb)			
	This analysis	Averaged capture data	Fröhner (FRO77)	ENDF/B-V
1.00 – 1.26	14.7 ± 1.9			12.1
1.26 – 1.59	12.1 ± 1.6			11.4
1.59 – 2.00	9.9 ± 1.2			10.9
2.00 – 2.51	8.0 ± 1.0			10.4
2.51 – 3.16	6.4 ± 0.8			10.0
3.16 – 3.98	5.2 ± 0.6			9.7
3.98 – 5.01	4.2 ± 0.5			9.5
5.01 – 6.31	3.5 ± 0.5			9.5
6.31 – 7.94	13.0 ± 1.0		2.6 ± 0.3	18.4
7.94 – 10.00	3.3 ± 0.6		3.3 ± 0.5	11.0
10.00 – 12.59	6.2 ± 1.6		6.6 ± 1.0	16.0
12.59 – 15.85	196. ± 19.		195. ± 25.	196.
15.85 – 20.0	20.9 ± 4.		26.3 ± 3.2	54.
20.0 – 25.1	45.8 ± 1.9		35.2 ± 4.4	35.
25.1 – 31.6	36.3 ± 1.5		26.2 ± 3.9	24.
31.6 – 39.8	78.6 ± 3.2		55.7 ± 5.0	52.
39.8 – 50.1	14.5 ± 0.6		10.6 ± 1.3	20.3
50.1 – 63.1	41.7 ± 2.2		31.4 ± 2.3	14.0
63.1 – 79.4	14.2 ± 1.5		9.8 ± 0.7	9.6
79.4 – 100.0	25.5 ± 1.0		17.3 ± 1.7	6.3
100.0 – 125.9	35.2 ± 1.5		22.0 ± 2.1	12.2
125.9 – 158.5	21.3 ± 1.5		12.6 ± 1.0	11.5
158.5 – 199.5	23.6 ± 1.0		16.5 ± 2.4	9.9
199.5 – 251.2	19.3 ± 0.9		13.1[a] ± 3.3	8.6
251.2 – 316.2	15.5 ± 0.7			7.6
316.2 – 398.1	12.7 ± 0.6			7.6
398.1 – 450.	12.6 ± 0.7	12.2 ± 1.2		7.0
450. – 500.		12.8 ± 1.3		7.6
500. – 600.		12.0 ± 1.2		7.0
600. – 800.		12.2 ± 1.2		
800. – 1000.		11.4 ± 1.1		
1000. – 1200.		12.3 ± 1.2		
1200. – 1400.		14.1 ± 1.4		

[a]This average is calculated in the interval from 199.5 to 231.0 keV.

The average capture cross section obtained from this analysis is shown from 1 keV to 1 MeV on Figs. 50 and 51 by the full line histograms.

The theoretical calculation shown in Fig. 50 was provided by P. G. Young of Los Alamos National Laboratory from the reaction theory code COMNUC (DUN70). Width fluctuation corrections were made using Moldauer's integral method (MOL76) and an approximation from Tepel et al. (TEP74) for the number of degrees of freedom. COMNUC calculates the capture cross section by using transmission coefficients for gamma rays derived from the width of the E1 giant dipole resonance (AXE62). Only E1 transitions were considered and the gamma-ray partial widths are only functions of the gamma-ray energy E_γ, the initial level spin and the final level spin. Level densities and their spin distributions were obtained from the Gilbert-Cameron formula. The parameters of the giant dipole resonance were taken from Ref. BER76. In the case of ^{58}Ni the giant dipole resonance is double humped with one resonance at 16.3 MeV which is 2.44 MeV wide and the other at 18.51 MeV is 6.37 MeV wide; the ratio of the peak cross section for the second resonance to the first resonance being 1.6. The absolute magnitude of the giant dipole resonance was adjusted to yield the experimentally observed value of $2\pi\overline{\Gamma}_{\gamma_o}/D_o$. This model usually predicts the capture cross sections within a factor of 2 (AXE62). In this case the capture cross section was overpredicted, and the theoretical predictions in Fig. 50 were normalized by a factor of 0.65.

The dotted line histogram on Fig. 51 is the average capture cross section obtained from the parameters of Fröhner (FRO77). The results are given in Table 8. From 20 to 231 keV Fröhner's data give systematically smaller values than we obtained from our data.

For comparison with our results, the average capture cross section was calculated with the parameters given in ENDF/B-V, including the tail of the negative energy resonance. Since ENDF/B-V does not have an isotopic evaluation of ^{58}Ni, the resonance parameters were taken from the elemental evaluation of nickel. In ENDF/B the capture cross section is calculated using the resonance parameters to which is added a smooth background. In the evaluation of the elemental nickel, the smooth background is of the order of 6 mb. If this 6-mb background is added to all the isotopes of nickel, we can calculate the ENDF/B-V average capture cross section for ^{58}Ni which is given in the last column of Table 8 and by the dots in Fig. 51.

The first s-wave resonance at 15.31 keV contributes very little (0.19 ± 0.06 b) to the thermal capture cross section of 4.6 ± 0.3 b reported in Ref. MUG81. Summing the contribution of the other 31 s-wave resonances at positive energies up to 450 keV gives only an additional 0.10 b. The difference could be attributed to the direct capture component and to bound levels. Two bound levels are reported in Table 2. Their energy parameters and their neutron widths have been adjusted to properly describe the transmission data above 10 keV; however, their radiation widths were arbitrary but can be chosen so that they generate the 4.3 b of thermal capture cross

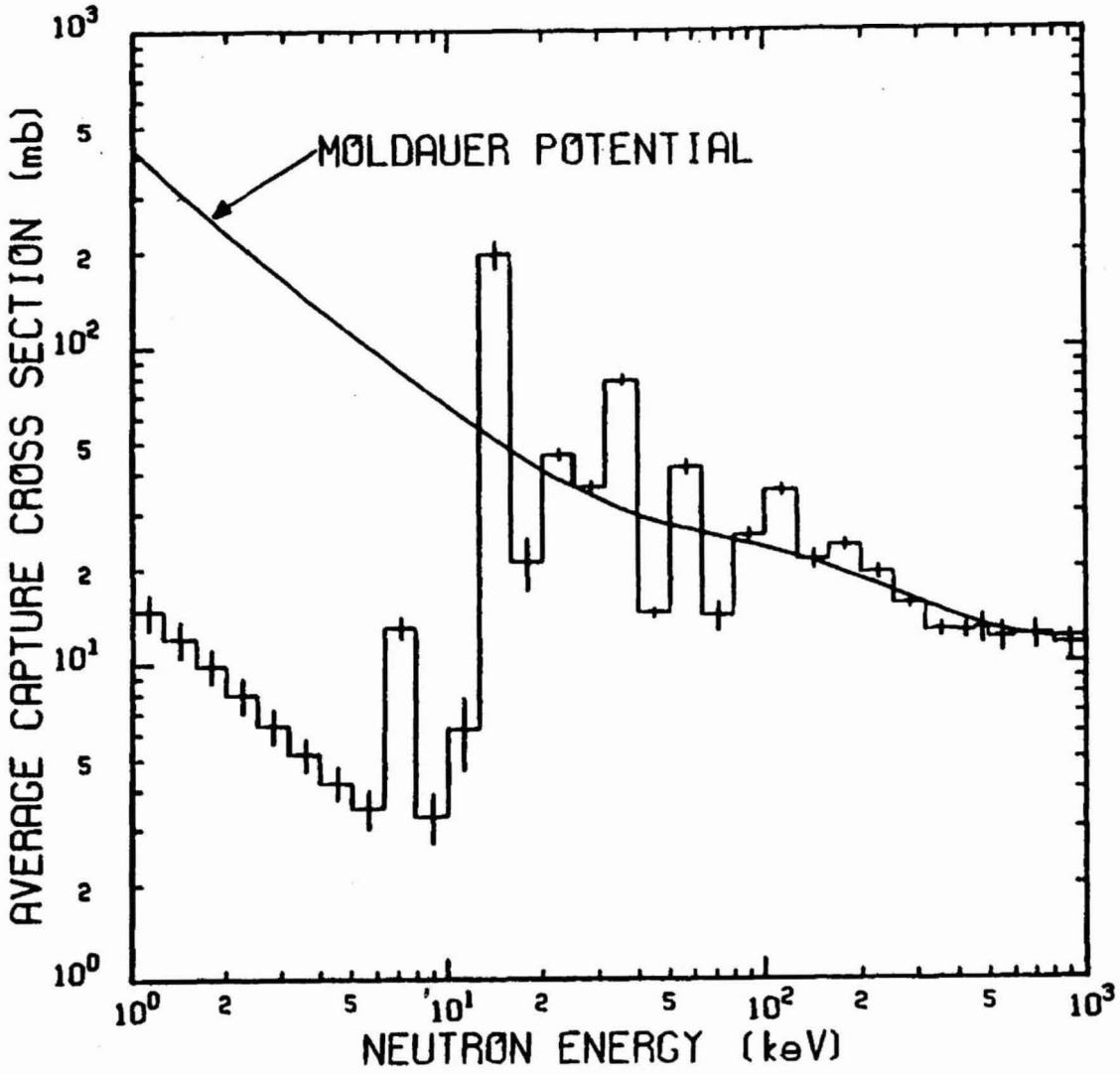

Fig. 50. The average capture cross section from 1 keV to 1 MeV as a function of incident neutron energy. The smooth curve is given by the tail of the double-humped giant dipole E1 normalized by 0.65. See Sect. 6.7 for details.

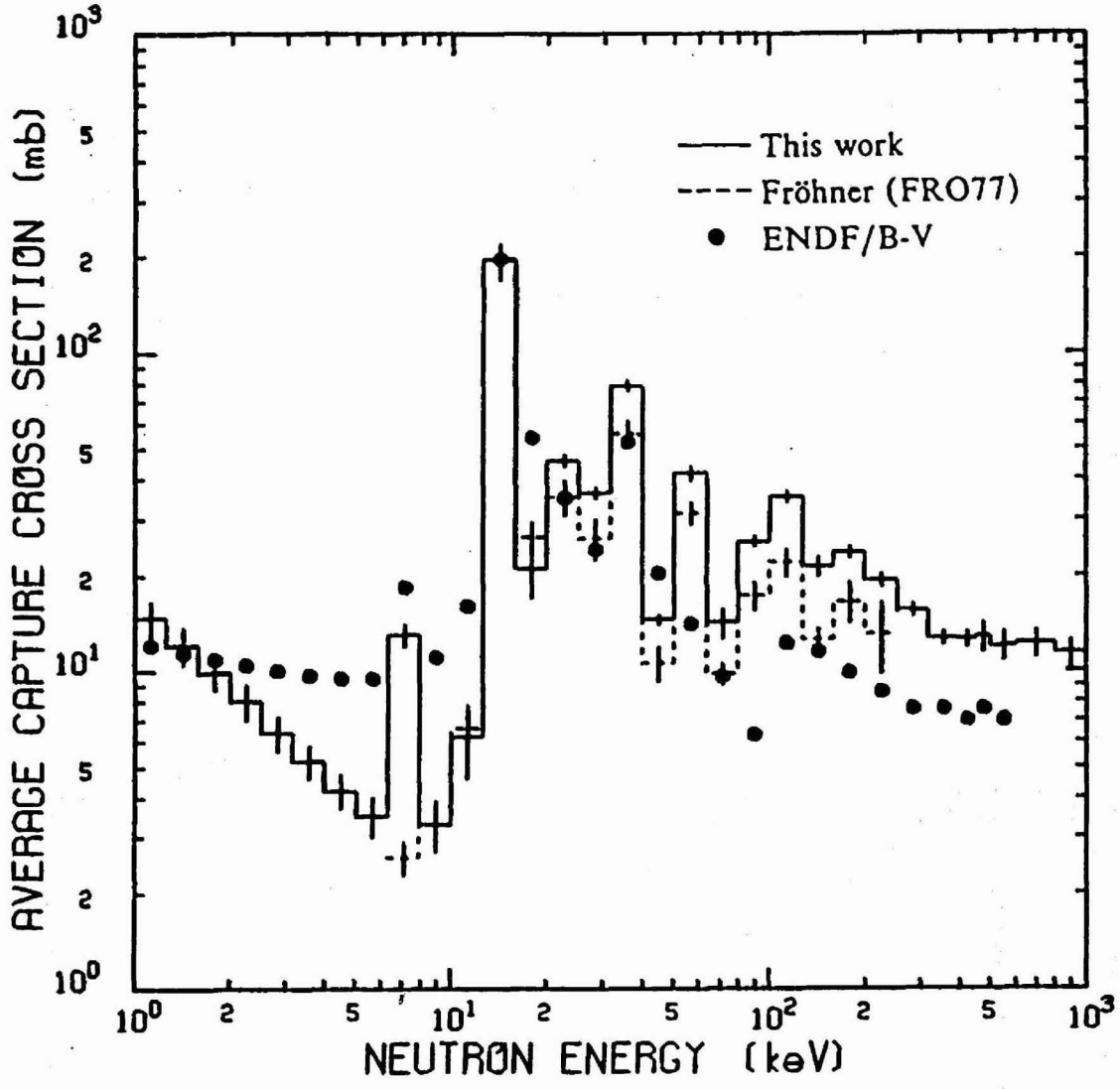

Fig. 51. The average capture cross section from 1 keV to 1 MeV as a function of incident neutron energy. From 1 to 450 keV, the full-line histogram is obtained from our resonance parameters including the tails of the two negative energy resonances; from 450 keV to 1 MeV it is obtained from averaging the capture data. The average capture cross section obtained from the parameters of Ref. FRO77 is shown from 6 to 231 keV by the dotted-line histogram. The dots are the average capture cross section from ENDF/B-V. The 6 mb of smooth background was added to the contribution from the resonances.

section which are missing. A radiation width of 2.0 eV for the resonance at −61.37 keV and of 1.4 eV for the resonance at −4.4 keV generate 4.3 b of thermal capture cross section. These values for the radiation widths are consistent with the average radiation width of 2.1 eV, found for the *s*-wave resonances in the positive energy region, with a standard deviation in the distribution of widths of 1.7 eV.

7. CONCLUSIONS

The work presented in this report considerably extends our knowledge of resonances observed in the interaction of neutrons with ^{58}Ni. Prior to this work only 142 resonances had been observed below 650 keV, whereas we were able to observe 382 up to that energy and 477 up to an energy of 813 keV. Below 450 keV we were able to obtain the neutron widths and capture areas for 264 resonances. The differential cross-section data allowed us to make a definite ℓ-assignment for 64% of the $\ell > 0$ resonances (265 out of 415), but a definite J-assignment could be made only for 35% of the $\ell > 0$ resonances (147 out of 415). Since in this ^{58}Ni data analysis only 24 $\ell > 0$ resonances have a width comparable to or larger than the resolution of the transmission measurements, had the differential cross-section data not been available only very few spin assignments could have been made.

The reduced neutron width distribution of the 61 s-wave resonances reported in this analysis is in good agreement with the Porter-Thomas distribution even though it seems to indicate that about three too many of the very weak resonances have been assigned as s-wave resonances. Therefore, the s-wave level spacing of 13.6 ± 0.7 keV was obtained from 59 rather than 62 s-wave resonances. The distribution of the nearest neighbor spacing is in good agreement with the Wigner distribution. The s-wave strength function is found to be equal to $(3.1 \pm 0.6) \times 10^{-4}$ and the average radiation width to be 2.3 eV. The standard deviation of the distribution of the s-wave radiation widths is 1.7 eV. The correlation coefficient between the reduced neutron widths and the radiation widths of the s-wave resonances is equal to 0.66 ± 0.11 suggesting some nonstatistical effects. These nonstatistical effects do not show as pronounced modulations in the Lorentz-weighted strength function of the reduced level widths as one might have expected if they were associated with doorway states.

The average radiation widths for the p- and d-wave resonances were also calculated and are equal to 0.77 eV for the p-wave and 1.3 eV for the d-wave. The standard deviations of their distributions are 0.33 eV and 0.5 eV respectively.

The results reported in this paper could be significantly improved with higher resolution in the capture data, with a correct weighting function for high energy gamma rays and with a more accurate treatment of the multiple scattering in the capture data analysis.

The extension of our knowledge of the resonances to higher energy is of significant importance in reactor calculations since it eliminates the need to deal with a very approximate unresolved resonance formalism.

Following completion of the work presented in this report a request was made (LAR88A), for ENDF/B-VI evaluation purposes, to extend the transmission data analysis below 10 keV in order to obtain a set of resonance parameters which will

correctly predict the known thermal scattering and capture cross sections while retaining the quality of the fit at higher energies. This would eliminate the need for any background cross-section contribution below 813 keV. The transmission data below 10 keV could not be fitted by only adjusting the parameters of the negative energy resonances and of the large *s*-wave resonances. A satisfactory fit down to 100 eV could only be obtained by renormalizing the data acquired with the 78-m flight path in addition to adjusting the negative energy and some of the large *s*-wave resonances. In the analysis presented in this report the need for such a renormalization was only apparent below 14 keV (Figs. 5 and 6). The implications of renormalizing these data are being investigated but it appears that the resulting parameter adjustments will be small and will not change significantly the conclusions reached in this report. Results of the analysis, extending down to 100 eV, will be published elsewhere.

8. REFERENCES

ALL77 B. J. Allen, A. R. de L. Musgrove, R. L. Macklin, and R. R. Winters, in *Neutron Data of Structural Materials for Fast Reactors, Geel, 1977*, edited by K. H. Bockhoff (Pergamon, New York, 1979), p. 506.

AND83 P. Anderson, L. P. Ekstrom, and J. Lyttkens, *Nucl. Data Sh.* **39**, 641 (1983).

AXE62 P. Axel, *Phys. Rev.* **126**, 671 (1962).

BEE84 H. Beer, G. Walter, R. L. Macklin, and P. J. Patchett, *Phys. Rev.* **C30**, 464 (1984).

BER76 B. L. Berman, *Atlas of Photo Neutron Cross Sections Obtained with Monoenergetic Photons*, UCRL-78482, 1976.

BET69 N. A. Betz, J. W. Reynolds, and G. G. Slaughter, p. 218 in *Proceedings of the Conference on Computer Systems in Experimental Nuclear Physics, Skytop, Pennsylvania, 1969*, Columbia University Report No. CONF-690301.

BLA52 J. M. Blatt and L. C. Biedenharn, *Rev. Mod. Phys.* **24**, 258 (1952).

COC83 C. Coceva, R. Simonini and D. K. Olsen, "Calculation of the ORELA Neutron Moderator Spectrum and Resolution Function," *Nucl. Inst. Meth.* **211**, 459 (1983).

DIL73 W. Dilg, W. Schantl, H. Vonach, and M. Uhl, *Nucl. Phys.* **A217**, 269 (1973).

DIV79 M. Divadeenam, *Ni Elemental Neutron Induced Reaction Cross-Section Evaluation*, BNL-NCS-51326, Brookhaven National Laboratory, 1979.

DUN70 C. L. Dunford, *A Unified Model for Analysis of Compound Nuclear Reactions*, AI-AEC-12931, 1970.

ERN70 A. Ernst, F. H. Fröhner, and D. Kompe, *Proc. Int. Conf. on Nuclear Data for Reactors, Helsinki, 1970*, Vol. 1, p. 633 (IAEA, Vienna, 1970).

FRO77 F. Fröhner, in *Neutron Data of Structural Materials for Fast Reactors, Geel, 1977*, edited by K. H. Böckhoff (Pergamon, New York, 1979), p. 138.

GAR78 J. B. Garg, R. L. Macklin, and J. Halperin, *Phys. Rev. C* **18**, 2079 (1978).

GAY88 D. B. Gayther, J. E. Jolly, and R. B. Thom, "Determination of the Parameters of the 1.15 keV Resonance in ^{56}Fe by Prompt Gamma-Ray Detection," International Conference on Nuclear Data for Science and Technology, May 30-June 3, 1988, Mito, Japan (to be published).

GIL65 A. Gilbert and A. G. W. Cameron, *Can. J. Phys.* **43**, 1446 (1965).

HIL85 N. W. Hill, J. A. Harvey, D. J. Horen, G. L. Morgan, and R. R. Winters, *IEEE Transactions on Nuclear Science*, Vol. NS-32, No. 1 (1985).

HOR86 D. J. Horen, C. H. Johnson, J. L. Fowler, A. D. MacKellar, and B. Castel, *Phys. Rev. C* **34**, 429 (1986).

KIK85 Yasuyuki Kikuchi and Nobuo Sekine, *J. Nucl. Sci. Technol.* **22**(5), 337 (1985).

LAR76 D. C. Larson, C. H. Johnson, J. A. Harvey, and N. W. Hill, *Measurement of the Neutron Total Cross Section of Fluorine from 5 eV to 20 MeV*, ORNL/TM-5612, Oak Ridge National Laboratory, 1976.

LAR80 N. M. Larson and F. G. Perey, *Users Guide for SAMMY: A Computer Model for Multilevel R-Matrix Fits to Neutron Data Using Bayes' Equations*, ORNL/TM-7485, Oak Ridge National Laboratory, 1980; *Updated Users' Guide for SAMMY*, ORNL/TM-9179, Oak Ridge National Laboratory, 1984, and ORNL/TM-9179/R1, 1985.

LAR83 D. C. Larson, N. M. Larson, J. A. Harvey, N. W. Hill, and C. H. Johnson, *Application of New Techniques to ORELA Neutron Transmission Measurements and Their Uncertainty Analysis: The Case of Natural Nickel from 2 keV to 20 MeV*, ORNL/TM-8203, Oak Ridge National Laboratory, 1983.

LAR84 D. C. Larson, N. M. Larson, and J. A. Harvey, *ORELA Flight Path 1: Determinations of Its Effective Length vs Energy, Experimental Energies, and Energy Resolution Function and Their Uncertainties*, ORNL/TM-8880, Oak Ridge National Laboratory, June 1984.

LAR85 D. C. Larson, N. M. Larson, J. A. Harvey, F. G. Perey, D. E. Pierce, and R. H. Seals, *Laser Measurements of Distances from the ORELA Neutron Target to Experiment Stations along Flight Paths 1 and 6*, ORNL/TM-9097, Oak Ridge National Laboratory, March 1985.

LAR88 N. M. Larson, D. C. Larson, C. M. Perey, and F. G. Perey, *LEVDEN: A Level Density Code Using the Fermi-gas Model*, ORNL/TM-10843 (in progress).

LAR88A D. C. Larson, private communication.

LER75 C. Le Rigoleur, private communication (1975).

LYN68 J. E. Lynn, *The Theory of Neutron Resonance Reactions*, (Clarendon, Oxford), 1968.

MAC71 R. L. Macklin, N. W. Hill, and B. J. Allen, *Nucl. Instrum. Methods*, **96**, 509 (1971).

MAC71A R. L. Macklin and B. J. Allen, *Nucl. Instrum. Methods* **91**, 565 (1971).

MAC76 R. L. Macklin, *Nucl. Sci. Eng.* **59**, 12 (1976).

MAC79 R. L. Macklin, J. Halperin, and R. R. Winters, *Nucl. Instrum. Methods* **164**, 213 (1979).

MAC83 R. L. Macklin, D. M. Drake, and E. D. Arthur, *Nucl. Sci. Eng.* **84**, 98 (1983).

MAC84 R. L. Macklin, *Nucl. Sci. Eng.* **86**, 362 (1984).

MAC87 R. L. Macklin, *Nucl. Sci. Eng.* **95**, 200 (1987).

MAH67 C. Mahaux and H. A. Weidenmuller, *Nucl. Phys.* **A91**, 241 (1967); W. M. MacDonald and A. Z. Mekjian, *Phys. Rev.* **160**, 730 (1967); A. K. Kerman and A. F. R. de Toledo Pize, *Ann. Phys. (N.Y.)* **48**, 173 (1968).

MOL76 P. A. Moldauer, *Phys. Rev. C* **14**, 764 (1976).

MOX73 M. C. Moxon, *Neutron Cross Sections of Natural Nickel and Its Isotopes Below a Neutron Energy of 600 KeV*, Report AERE R7568 (1973).

MUG81 S. F. Mughabghab, M. Divadeenam, and N. E. Holden, *Neutron Cross Sections, Vol. 1: Neutron Resonance Parameters and Thermal Cross Sections*, (Academic, New York, 1981), p. 28-2.

PER77 F. G. Perey, G. T. Chapman, W. E. Kinney, and C. M. Perey in *Neutron Data of Structural Materials for Fast Reactors, Geel, 1977*, edited by K. H. Böckhoff (Pergamon, New York, 1979), p. 530.

PER82 C. M. Perey, J. A. Harvey, R. L. Macklin, R. R. Winters, and F. G. Perey, *Neutron Transmission and Capture Measurements and Analysis of ^{60}Ni from 1 to 450 keV*, ORNL-5893, Oak Ridge National Laboratory, 1982.

PER83 C. M. Perey, J. A. Harvey, R. L. Macklin, F. G. Perey, and R. R. Winters, *Phys. Rev. C* **27**, 2556 (1983).

PER83A F. G. Perey, Code RFUNCR, unpublished, 1983.

PER85 C. M. Perey, F. G. Perey, J. A. Harvey, N. W. Hill, and R. L. Macklin, p. 1639 in *Nuclear Data for Basic and Applied Science, Santa Fe, 1985*,

edited by P. G. Young et al. (Gordon and Breach, Science Publishers, Inc., 1986), Vol. 2.

PER88 F. G. Perey, J. O. Johnson, T. A. Gabriel, R. L. Macklin, and R. R. Winters, "Responses of C_6D_6 and C_6F_6 Gamma Ray Detectors," International Conference on Nuclear Data for Science and Technology, May 30–June 3, 1988, Mito, Japan (to be published).

POR56 C. E. Porter and R. G. Thomas, *Phys. Rev.* **104**, 483 (1956).

REI58 C. W. Reich and M. S. Moore, *Phys. Rev.* **111**, 929 (1958).

SOW88 M. Sowerby and F. Corvi, "Matters Related to the NEANDC Task Forces on ^{238}U and ^{56}Fe Resonances," International Conference on Nuclear Data for Science and Technology, May 30–June 3, 1988, Mito, Japan (to be published).

STI73 R. G. Stieglitz, J. T. Reynolds, C. J. Slavik, and C. R. Lubitz, *Evaluated Neutron Cross Sections for Chromium, Iron, and Nickel*, Knolls Atomic Power Laboratory Report No. KAPL-M-7156, 1973.

SYM77 D. B. Syme, P. H. Bowen, and A. D. Gadd, in *Neutron Data of Structural Materials for Fast Reactors, Geel, 1977*, edited by K. H. Böckhoff (Pergamon, New York, 1979), p. 703.

SYM78 D. B. Syme and P. H. Bowen, in *Neutron Physics and Nuclear Data for Reactors, Harwell, 1978*, (OECD, Paris, 1978), p. 319.

TEI52 T. Teichmann and E. P. Wigner, *Phys. Rev.* **87**, 123 (1952).

TEP74 J. W. Tepel, H. M. Hofmann, and H. A. Weidenmüller, *Phys. Lett.* **49B**, 1 (1974).

WIG57 E. P. Wigner, *Proceedings of the Gatlinburg Conference on Neutron Time-of-Flight Methods*, Oak Ridge National Laboratory Report ORNL-2309 (1957), p. 57.

WIS84 K. Wisshak, F. Käppeler, G. Reffo, and F. Fabbri, *Nucl. Sci. Eng.* **86**, 168 (1984).

INTERNAL DISTRIBUTION

1. B. R. Appleton
2. G. de Saussure
3. J. K. Dickens
4. C. Y. Fu
5–9. J. A. Harvey
10. N. W. Hill
11. D. J. Horen
12. J. K. Ingersoll
13. D. C. Larson
14–18. N. M. Larson
19–23. R. L. Macklin
24. F. C. Maienschein
25. R. W. Peelle
26–30. C. M. Perey
31–35. F. G. Perey
36. R. W. Roussin
37. R. R. Spencer
38. L. W. Weston
39. R. R. Winters
40. J. J. Dorning (consultant)
41. R. M. Haralick (consultant)
42–43. Laboratory Records Department
44. Laboratory Records, ORNL-RC
45. Document Reference Section
46. Central Research Library
47. ORNL Patent Section

EXTERNAL DISTRIBUTION

48. Office of Assistant Manager for Energy Research and Development, U.S. Department of Energy, Oak Ridge Operations, P. O. Box 2001, Oak Ridge, TN 37831-8600
49. S. L. Whetstone, Division of Nuclear Physics, ER 23/GTN, U.S. Department of Energy, Washington, DC 20585
50. G. F. Auchampaugh, Los Alamos National Laboratory, MS 442, P-3, Los Alamos, NM 87545
51. H. Beer, Kernforschungszentrum Karlsruhe, Institut für Angewandte Kernphysik, D7500 Karlsruhe 1, Germany
52. A. Brusegan, Bureau Central de Mesures Nucleaires, Steenweg Naar Retie, B-2440, Geel, Belgium
53. R. F. Carlton, Middle Tennessee State University, Physics Department, Box 407, Murfreesboro, TN 37132
54. H. Derrien, Commissariat a l'Energie Atomique, Centre d'Etudes Nucléaires de Cadarache, Boite Postale No. 1, 13115 Saint-Paul-Lez-Durance, France
55. C. Dunford, National Nuclear Data Center, Building 197D, Brookhaven National Laboratory, Upton, NY 11973
56. F. Fröhner, INR, Kernforschungszentrum, Postfach 3640, D-75 Karlsruhe, West Germany
57. D. B. Gayther, Nuclear Physics Division, Atomic Energy Research Establishment, Harwell, Didcot, Oxon, OX11 ORA, United Kingdom
58. Y. Kikuchi, Nuclear Data Center, Department of Physics, Tokai-mura, Ibaraki-ken 319-11, Japan
59. Prof. Claude Mahaux, Institut de Physique, Sart Tilman, 4000 Liege 1, Belgium
60. W. M. Macdonald, Physics Department, University of Maryland, College Park, MD 20740

61. M. C. Moxon, Nuclear Physics Division, Atomic Energy Research Establishment, Harwell, Didcot, Oxon, OX11 ORA, United Kingdom
62. D. L. Smith, Applied Physics, D314, Argonne National Laboratory, 9700 S. Cass Avenue, Argonne, IL 60439
63. M. G. Sowerby, Nuclear Physics Division, Bldg. 418, Atomic Energy Research Establishment, Harwell, Didcot, Oxon, OX11 ORA, United Kingdom
64. D. B. Syme, Nuclear Physics Division, Atomic Energy Research Establishment, Harwell, Didcot, Oxon, OX11 ORA, United Kingdom
65. H. Weigmann, Bureau Central de Mesures Nucleaires, Steenweg Naar Retie, B-2440, Geel, Belgium
66. K. Wisshak, Kernforschungszentrum Karlsruhe GmbH, Postfach 3640, D7500, Karlsruhe 1, Germany
67. P. G. Young, Los Alamos National Laboratory, T-2, MS B243, Los Alamos, NM 87545

68–137. National Nuclear Data Center, ENDF Distribution, Brookhaven National Laboratory, Upton, Long Island, NY 11973

138–147. Office of Scientific and Technical Information, P. O. Box 62, Oak Ridge, TN 37831